8 Strategies and Advances in the Characterisation of Environmental Colloids by Electron Microscopy

DENIS MAVROCORDATOS†

Swiss Federal Institute for Environmental Science and Technology, EAWAG Urban Water Management, 133 Überlandstrasse, CH-8600 Dübendorf, Switzerland

DIDIER PERRET

School of Chemistry and Biochemistry, University of Geneva, 30 quai Ernest Ansermet CH-1211 Geneva 4, Switzerland

GARY G. LEPPARD

National Water Research Institute, 867 Lakeshore Road, PO Box 5050, Burlington, Ontario, Canada L7R 4A6

† Dr Denis Mavrocordatos tragically disappeared in Lake Geneva on 6 December 2003. This chapter is written in his memory by his friends and fellows, holding as much as possible to the spirit of his work in electron microscopy, and relying as much as possible on the chapter structure that he had prepared for this book.

Homme libre, toujours tu chériras la mer!
Charles Baudelaire

Environmental Colloids and Particles. Edited by K. J. Wilkinson and J. R. Lead

1 INTRODUCTION

The significant work of Louis de Broglie in 1923 on wave mechanics established that electrons and other subatomic particles behave like waves. With this insight, Ruska invented transmission electron microscopy (TEM) in 1931, replacing the visible light source of a conventional photon (optical) microscope by a source of focused electrons operated under a vacuum and guided by a series of magnetic lenses. Owing to their intrinsic properties [$\lambda_{\text{electron}} = (\approx 10^{-3}\text{–}10^{-5}) \times \lambda_{\text{visible light}}$], electrons are able to convey information about incident objects with much smaller dimensions than is achievable with visible light. With his microscope, Ruska was able to identify micrometre-sized biological objects with a resolution never before attained. For his seminal work in electron optics that opened the doors to the atomic scale, Ruska finally received the Nobel Prize in 1986, sharing it with Binnig and Rohrer for their invention in the late 1970s of scanning tunnelling microscopy (STM).

The first publications reporting the use of electron microscopy (EM) in the environmental sciences were released long after Ruska's invention, owing to the need for reliable magnetic lenses and appropriate specimen preparation schemes. Soil particles were first described in 1940, airborne particles in 1946 (magnifications up to $2 \times 10^5 \times$), and finally non-living aquatic particles not earlier than the mid-1970s. Since Ruska's time, new opportunities for the observation and characterisation of environmental particles and colloids over a large range of sizes and compositions have arisen, closely matching the successive progress in technological development: scanning-transmission electron microscopy (STEM) in the late 1930s, scanning electron microscopy (SEM) in the early 1950s, high-voltage microscopy, analytical electron microscopy (AEM), X-ray energy-dispersive spectroscopy (X-EDS), electron energy-loss spectroscopy (EELS) and brighter electron sources [LaB_6; field emission gun (FEG)] in the 1960s and 1970s. Although still in their infancy for the study of environmental samples, environmental scanning electron microscopes (ESEM), available in the late 1980s, have finally allowed new possibilities for the observation of (sub-)micrometric entities in their hydrated state [1].

To date, more than 1000 papers have been published on the characterisation of environmental particles and colloids by techniques of electron microscopy. Historically, EM has been exploited for the documentation of the morphotypes, textures and sizes of living and non-living colloidal and particulate entities. Until recently, most studies on electron microscopy were published for merely illustrative purposes, underexploiting the analytical performances of the existing techniques. AEM has now come to maturity, and sensational electron micrographs are frequently supplemented by quantitative measurements aimed at demonstrating the presence of well-characterised species down to the nanometre scale, or even to assess relationships between the formation or existence of specific types of particles or colloids at the microscopic scale and the evolution of their natural macroscopic milieu. Indeed, the detailed characteristics, activities and behaviours of particles and colloids in natural systems must still be better understood in order to model their life cycle and impact, and to design more cost-effective treatment facilities when dealing with problems of pollution control.

Hydrated colloids provide a nanoscale medium into and on to which dissolved contaminants and nutrients can move from the bulk liquid, without significant gravitational settling [2]. At the nanoscale, large numbers of small colloids and suspended macromolecules are likely to influence water quality and particle separation processes. New nanoscale observations should contribute to our understanding of the environmental cycling of chemicals [2–5], aggregation processes [6,7], the interactions of natural organic matter with microorganisms [8] and the deposition from solution of nanoscale mineral aggregates on to microbial cell surfaces [9–15].

Electron optical analyses which correlate morphological data with data from both physical and molecular probes will further facilitate the development of colloid 'speciation' at the nanoscale. Such nanoscale data are already leading to improved characterisations of the following particles and phenomena:

1. contaminant and biogeochemical transport agents in surface waters [3–5, 15–19];
2. specific events in the biogenesis of minerals by bacteria [9–11,14,20,21];
3. immobilisation sites at molecular and nanoscale ranges for heavy metals in lacustrine sediments [13,22] and wastewater flocs [23];

4. pollutant source associated with trace element carriers which are discharged into aquatic ecosystems by combined sewer overflows [3];
5. colloidal promoters of biofouling in membrane filters used for water purification [24];
6. colloidal flocculants used in water treatment [25].

For heterogeneous aggregation processes, new speciation information should allow one to determine the extent to which colloids are major contributors to:

1. engineered aggregation processes;
2. contaminant binding in water treatment facilities;
3. biofouling of immersed surfaces; and
4. the transfer of toxic chemicals to environmental sinks.

Also, a better understanding of mineral nucleation on organic templates might yield a list of characteristics which could become very helpful in the search for biosignatures in ancient environments on Earth and other planets [11].

Correlated multi-method interdisciplinary approaches to water analysis, which include AEM and which use independent methods to provide chemical, biological and environmental context for electron optical observations, are increasingly likely to yield practical information on both nano- and microparticle activities [4,5,13,15,20,22,23,26–28]. Confocal laser scanning microscopy (CLSM), used correlatively with TEM and Scaning-transmission X-ray microscopy (STXM) is contributing to this multi-method interdisciplinary approach [27]; see also Chapter 10, covering confocal laser scanning microscopy.

Over the last decade, TEM has improved drastically and its adaptation for the characterisation of colloidal particles has progressed well. The technique is now considered to be reliable, quantitative and efficient among water scientists [4,12,28–38]. TEM is a remarkable tool and an essential technique for the morphological characterisation of fine hydrated colloids and particles, as it allows the direct observation of individual entities as well as aggregates at the nanometre to micrometre scale, yielding descriptions of size, shape, native associations and internal differentiation on a 'per colloid' basis. The technique complements other more conventional techniques used for sizing, which usually address average signals recorded at the level of the bulk suspension. When utilised under appropriate conditions, *e.g.* in conjunction with accessory techniques and with optimised specimen preparation, TEM may give clues and yield information on the *in situ* processes leading to the formation, transport, function and behaviour of colloids and their aggregates in situations involving complex and heterogeneous species, with an unprecedented level of accuracy [4,6,13,19,23,29–31,33,36,39–41]. Nevertheless, TEM should not be the technique of choice when only simple, rapid, qualitative or semi-quantitative assessments of colloid characteristics are required, because the TEM approach, from sampling to data analysis, is costly and time consuming and requires skilled and experienced staff.

The major accessory techniques applicable to preselected individual colloids are: X-ray energy-dispersive spectroscopy (X-EDS), selected-area electron diffraction (SAED), electron energy-loss spectroscopy (EELS), energy-filtered TEM (EF-TEM), and electron-opaque selective probes. Figure 1a schematises the construction and function of transmission and scanning electron microscopes. The electron–matter interactions within the specimen that give rise to the spectrometric signals used in AEM are shown in Figure 1b.

Detailed discussions of electron optics and the physics of electron microscopy can be found elsewhere [42–50]. Used correlatively in parallel and used in conjunction with the ever-improving atomic force microscopy (AFM), these accessory techniques provide a powerful suite of AEM techniques for studying hydrated environmental particles [4–6,12,15,33,37,41,51,52].

The characterisation of airborne colloids and aerosols, combustion and fly-ash particles, ambient air and vehicle emission particles in the 10 nm–10 μm range also benefits from combined analytical protocols, mostly TEM–X-EDS or SEM–X-EDS, but sometimes TEM–EELS and TEM–SAED, with other micrometric (AFM), semi-micrometric

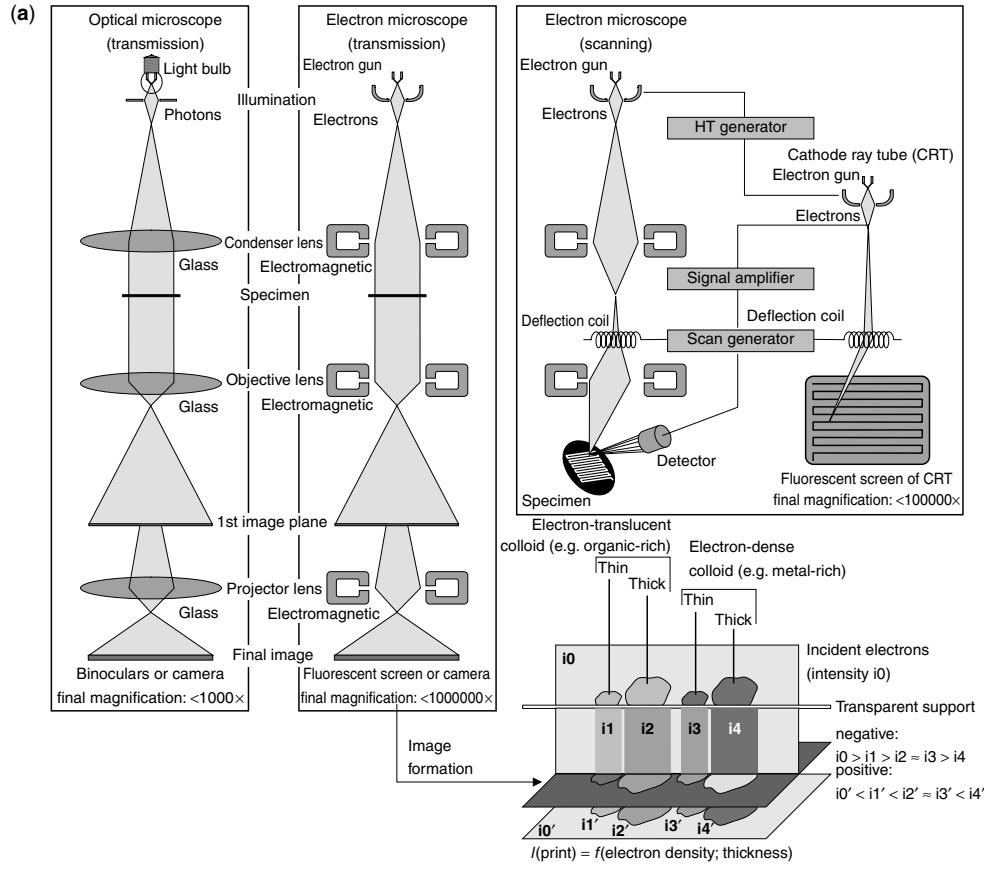

Figure 1. **(a)** Comparison of an optical microscope (left) and a transmission electron microscope (middle), showing the similarities in their construction, and a scanning electron microscope (right). The scheme below the TEM instrument shows that the final image from a mixture of colloids is a complex function of the composition of colloids and their thickness. For example, a 'thick' organic-rich entity may appear with the same grey level as a 'thin' metal-rich entity. (**b**) Analytical electron microscopy can be performed in the transmission electron microscope mostly by means of X-EDS (X-ray energy-dispersive spectroscopy; measurement of the X-rays emitted during the electronic rearrangement of a target element when one of its electrons is ejected by the incident electron beam), or EELS (electron energy-loss spectrometry; measurement of the energy being lost by the incident electron beam during an inelastic event with a target element)

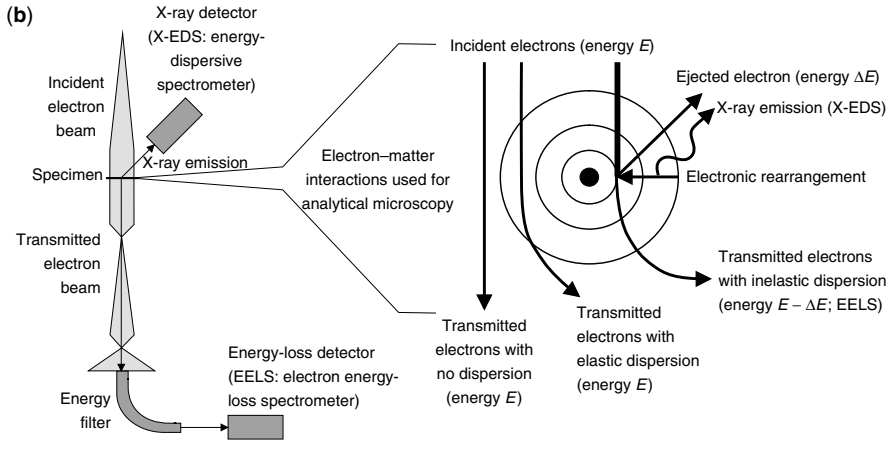

Figure 1. (*continued*)

[proton-induced X-ray emission (PIXE)] or bulk [X-ray fluorescence (XRF), X-ray diffraction (XRD), inductively coupled plasma atomic emission spectroscopy (ICP-AES) or mass spectrometry (ICP-MS), *etc.*] analytical devices [53–67]. Because of the weak hydration state of these 'dry' particles, specimen preparation is usually less sophisticated than is necessary for aquatic entities.

2 SAMPLING OF ENVIRONMENTAL COLLOIDS FOR ELECTRON MICROSCOPIC INVESTIGATION

Particulate matter consists of living entities (bacteria, algae, fungi, protozoa) and non-living ones (refractory macromolecular organics, viruses, recognisable cell fragments, crystalline or amorphous mineral phases). Its unbiased investigation by electron microscopy in either a hydrated or dry state requires a blend of dedicated sample collection schemes and specimen preparation techniques. Figure 2 highlights the most appropriate approaches to be used, from specimen preparation to particle characterisation.

Whatever investigations are to be performed on a given type of sample, it must be kept in mind that every step of the protocol should be designed to avoid artefacts due to alteration of the native physicochemical characteristics of the sample (*e.g.* precipitation, coagulation or dissolution due to variations in particle concentration, ionic strength, pH, redox potential, temperature or uncontrolled dehydration of the sample).

The sections below discuss the specific measures that have to be taken when aerosol and atmospheric colloids, soil and sediment colloids, or aquatic colloids are to be investigated. Indeed, sampling of suspended matter should take into account the nature of the medium in which these colloids are dispersed. It must be borne in mind, however, that each particular situation usually requires optimisation of the generic procedure if satisfactory results are to be obtained.

2.1 SAMPLING OF AEROSOLS AND ATMOSPHERIC COLLOIDS

Atmospheric particles are probably the most straightforward to sample, as a variety of collectors, in which particulate material can be size fractionated, have been devised

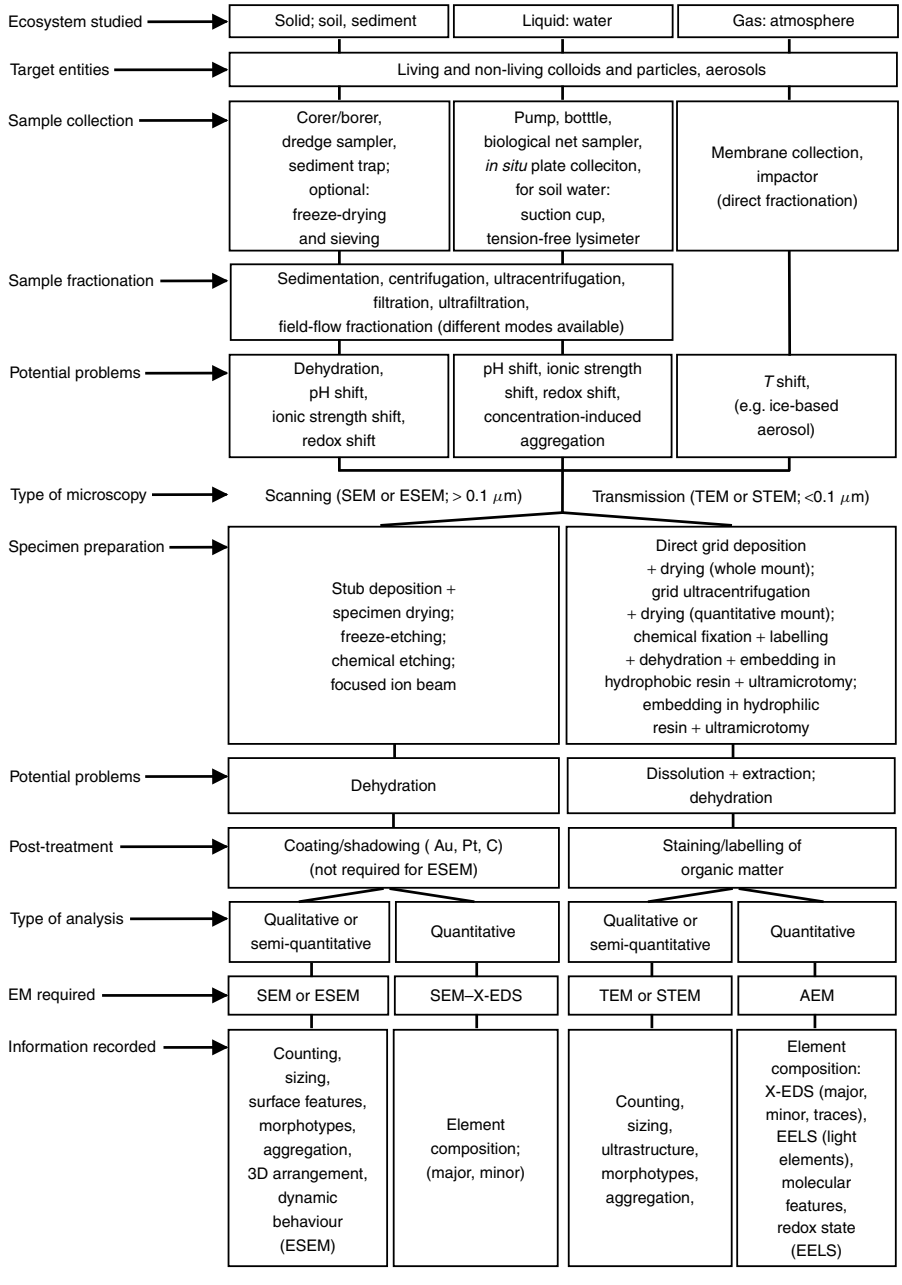

Figure 2. Overview of the recommended approaches, crucial steps and possible artefacts relevant to the physicochemical characterisation of particulate material in environmental systems by electron microscopies. This scheme does not take into account precautions required for conventional bulk physicochemical analyses

and optimised over the past half century or more. Sampling of aerosol particles, unlike aquatic ones, is less sensitive to physicochemical changes, although biased size fractionation may occur owing to particle hydrophilicity/hydrophobicity or surface charges. For instance, filtration of aerosols may be just as problematic for air as for water samples. The most commonly used procedures are briefly summarised below; critical discussions of the collection and characterisation of atmospheric particles have been published elsewhere [68–74].

For indoor particles (*e.g.* asbestos fibres, industrial particles, soot or combustion smoke of health concern), direct sampling by air pumping through collecting membranes (smooth/flat neutron-impacted Nuclepore-type filters) without size fractionation is the optimal sampling method [71,75]. Outdoor atmospheric or plume particles can be size fractionated and collected by cascade impactors, charged-particle collectors, thermal precipitators, filters or nephelometers [67,76–80]. Particles have to be transferred by contact from the sampling device to the specimen holder, be it a stub for SEM or a grid for TEM.

The collection of aerosols requires special procedures that are aimed at maintaining the original temperature and hydration status of the sample. This is especially important for studies involving wet or frozen entities for which the mechanisms of cloud or ice formation are driven by the complex interaction of water, inorganic condensation nuclei, dissolved salts and organics acting as hygroscopic agents [81–86]. In these cases, microscopic examination of specimens with a cold stage should be carried out with minimal delay. TEM (for the smallest colloids) and SEM (for larger particles) in imaging or element analysis modes are used indiscriminately for the characterisation of atmospheric entities. ESEM, which allows imaging under various conditions of temperature, hydration and pressure, and which also allows energy-dispersive spectroscopy, is especially useful for water-containing particles larger than 50 nm [71,87].

2.2 SAMPLING OF SOIL AND SEDIMENT COLLOIDS

Soil and sediment colloids have been the subject of numerous publications concerned with the identification of the phases which constitute the soil or the sediment matrix, and with the formation of soils or sediments and their stratification. To a lesser extent, scientists have examined the role of colloids as scavengers and contaminant carriers. For these reasons, sampling and specimen preparation protocols for soil or sediment particles are usually less sophisticated than protocols for aquatic particles, provided that one considers soil and sediment particles as static entities having a limited mobility in their surrounding water. A detailed discussion of the collection and characterisation of soil particles is given elsewhere [88].

While the majority of soil samples are characterised by slow reactivities and thus require fewer precautions, hydromorphic soils subjected to rapid hydration and dehydration are highly sensitive to redox changes and must be sampled with care in order to avoid precipitation of dissolved species (*e.g.* Fe^{2+} and Mn^{2+}) through accidental aeration. Otherwise, soils are usually dried, sieved and ground before being resuspended in an electrolyte for the selective isolation of various constituents (*e.g.* organic matter, clay, silt, and sand) by sedimentation or centrifugation. These approaches are, however, not recommended for the identification of trace metals, as drastic morphological and compositional modifications can be expected at each step of the protocol. Because of their size, soil particulates

are most frequently analysed by SEM, but the ultrastructural analysis of clay micelles or other finely divided components (*e.g.* iron oxides and humic substances) requires TEM examination [89–105].

The particulate phases in hydrated sediments represent an intermediate situation between soil particles and suspended aquatic particles. Except for deeply buried, highly consolidated sediments, the water content of sediments is large and their reactivity is comparable to, or even larger than, that of hydromorphic soils. Sediments are sampled by means of vertical corers, from which the different season- or event-dependent strata must be subsampled by slicing in a glove-box under controlled atmosphere. Textural analysis of sediment particles can be performed by SEM [106], but more detailed investigations will require dilution of the samples in an electrolyte of composition similar to the interstitial water, prior to specimen preparation for TEM.

2.3 SAMPLING OF AQUATIC COLLOIDS

The study of suspended solids, whether as individual particles or as aggregations of particles, encompasses a wide variety of matrices (marine and fresh waters, surface and ground waters, gravitational and capillary water of soils, engineered particles in water treatment facilities, *etc.*), particle types and sizes (nanometre to millimetre, living, non-living, organic, organomineral and mineral), and phenomena (structure–composition–function relationships, contaminant transport, mechanisms of formation and dissolution, *etc.*). The sampling of aquatic particles is thus a complex task which requires systematic adaptation of generic protocols to the specific type of material under investigation. However, the most relevant investigations usually employ correlative EM techniques, namely the use of scanning and transmission electron microscopes to examine in parallel whole mounts and resin-embedded specimens (see below), to embrace the broadest and most accurate physicochemical fingerprints of particles.

Sampling and handling of natural waters for TEM must be performed with the greatest care in order to avoid physical, chemical and microbial alteration of the native state of colloids and particles. As much as possible, the partial pressure of dissolved gases (*e.g.* low O_2 in anoxic waters or high CO_2 in carbonated ground waters) should be maintained in order to avoid redox or pH drifts during sample storage. Temperature is also an important parameter that should be kept constant, whenever feasible.

Furthermore, preservatives (*e.g.* acids, organic solvents, NaN_3 or $HgCl_2$) must not be added to the samples, as they may produce artefacts owing to coagulation and sedimentation, or dissolution of colloids, photosynthetic activity, or microbial production of extracellular polymeric substances [40]. When visually identifiable, particulates larger than several tens of micrometers should be discarded from the sample, either by gentle sieving (*e.g.* with a 50–100 μm nylon mesh), by flotation (for light organic debris) or by brief sedimentation/centrifugation (for dense mineral debris).

To avoid rapid modification of the physicochemical and microbiological characteristics of natural water samples due to dissolution, precipitation, coagulation, sedimentation, microbial growth or shifts in chemical equilibria affecting colloids and particles brought about by changes in temperature, pH, depth, dissolved O_2 or CO_2, light, and convection, aquatic samples should be processed for EM without delay (in <1 day), as is also the case for conventional bulk chemical analyses. Prefractionation of aquatic particles and

colloids to divide them into narrower classes can be performed by gravitational sedimentation in thermostated columns, by single or cascade centrifugation/ultracentrifugation or by single or cascade filtration/ultrafiltration. Samples treated by either fractionation approach are subject to artefacts, but these can be minimised by careful control of conditions. For example, centrifugation must be performed with relatively dilute suspensions to avoid problems of differential settling. Similarly, tangential-flow filtration at low flow-rates usually yields no, or less, polarisation concentration and membrane clogging than uncontrolled/unstirred cross-flow filtration. Centrifugation and filtration are usually performed to eliminate the fractions containing the largest particles, although they may be used instead to collect appreciable amounts of particulate material from waters with low concentrations of suspended solids (*e.g.* ground water or pristine waters), with possible biases caused by apparent coagulation of particles. It is clear that the structural features of physically unstable, well-hydrated aggregates of colloids in their native state can be altered by treatments and apparatus so as to confound analysis [107]. However, exquisite attention to the details of sample preparation can overcome even the most subtle of artefacts.

Particulate material can also be sampled from natural waters by direct collection on vertical or horizontal plates (Teflon, glass, plastics) inserted for periods of a few days to weeks in the water column [108]. Horizontal plates collect sedimenting particles without the drawbacks of conventional sediment traps (shifts in biological activity and redox conditions due to the absence of mixing at the bottom of the trap); vertical plates selectively collect those entities exhibiting a certain affinity for the plate (*e.g.* adhering bacteria, polysaccharides, humic substances and iron and manganese oxyhydroxides).

Particles suspended in soil water require different sampling approaches, depending on the type of water to be sampled [93,97,109]. Gravitational water is better collected by means of tension-free lysimeters; as these devices integrate the sampled water over time, the particles should be recovered without delay to avoid modifications in their size distribution or chemistry. It must be stressed however, that tension-free lysimeters may exhibit fairly low collection efficiencies (as low as 10% of the gravitational water, depending on soil texture and porosity). On the other hand, the capillary water of soils can be recovered by means of suction cups made of a porous material (ceramic or plastic), which are inserted in the soil and connected to a syringe or pump. Owing to their porosity (*ca.* 10–100 μm), these devices inevitably fractionate the particulate matter, and tend to clog with time. In addition, the nature of the porous material may result in selective adsorption of colloids.

3 SPECIMEN PREPARATION

This section will be confined to colloids and particles suspended in an aquatic medium, whatever their origin (soil, sediment or natural waters). After appropriate sampling, suspensions of particulate and colloidal material have to be converted to specimens for SEM or TEM investigation. Consider on the one hand a natural aquatic system containing living entities, such as bacteria, algae, fungi and protozoa, and non-living ones such as viruses, debris and macromolecular aggregates in their native medium (freshwater or saline, environmentally stressed or not, in still or running water, oxic or anoxic, *etc.*). The suspension may contain 10^8–10^{13} entities dm^{-3} over a 1–10^5 nm range, with a broad diversity of

morphotypes (*e.g.* fibrillar or compact, ill-defined and amorphous or crystalline). Be that as it may, however, conventional EM requires that the particulates of interest be analysed under high vacuum, i.e. in the absence of water.

The criteria for a successful and accurate TEM study is its ability to overcome this dilemma, transforming a given volume containing billions of entities into an unbiased specimen of colloids and aggregates evenly dispersed on a small supporting grid (3.05 mm diameter). Under controlled and appropriate conditions, the characterisation of *ca.* 100–1000 entities (individual colloids and aggregates) per grid can be expected to yield statistically relevant results, which can then be quantitatively extrapolated back to the original suspension.

Specimen preparation for SEM [43,47] requires the collection of particles on stubs (either directly or after precollection on Nuclepore-type membranes), followed by coating, most frequently with an Au or Pt film (for imaging) or a C film (for analysis). On the other hand, specimens for ESEM require no prior coating or treatment, but the spatial resolution of ESEM is usually limited when operated in wet mode (*ca.* 30–100 nm) [110]. The maximum achievable resolution that one can expect for SEM of complex heterogeneous environmental particles is *ca.* 10–50 nm, even for high-intensity FEG-SEM.

For morphological and sizing aims, the most useful TEM grids are made of 200-mesh Cu (square holes: *ca.* 80×80 μm) with alpha-numeric labels (Figure 3). More exotic (and expensive) grids (*e.g.* Be, Au or Pt) should be reserved for AEM (*e.g.* element analysis by energy-dispersive spectrometry, TEM–X-EDS). To ensure the most transparent and stable support possible, TEM grids must be coated with a flexible ultra-thin (10–50 nm) supporting film of Formvar or Parlodion for strength, then carbon-sputtered (3–10 nm) for thermal and electrical conductivity. When ultrastructural analysis is required, the plastic film can be dissolved, at the expense of specimen strength.

The choice of the grid type and supporting film is critical for analytical TEM/STEM (AEM in X-EDS or EELS modes). It is important to bear in mind that the X-rays produced by the analyte under the focused electron beam are emitted in a spherical region of the sample and will induce secondary X-rays of the materials they hit (*e.g.* the supporting grid or the pole pieces of the EM column). These secondary X-rays may be emitted in the direction of the detector, generating artefact peaks.

While Formvar- or Parlodion-coated, carbon-sputtered copper grids are the best choice from the standpoint of price and ease of operation for imaging purposes, element analysis requires supporting materials which will not mask the elements of interest. For example, gold grids are preferred for the X-EDS analysis of trace transition metals.

For the identification of carbon-rich entities prepared as whole mounts or quantitative mounts (i.e. without resin embedding), the supporting film should be substituted by a carbon-free 5–15 nm SiO film (not useful for Si-rich entities) or Be film (expensive). Large-scale entities (*e.g.* 3D networks or organic–mineral mixtures) can be collected on holey or Quantifoil (supporting film with controlled and repetitive holes) or lacey carbon films for the analysis of their unsupported portions (Figure 3), with the risk of a weaker mechanical and electrical stability under the electron beam. Whichever grid is used, the alpha-numeric styles are generally preferred in order to keep track of the particles of interest over time.

Depending on the information to be extracted, different methods are available for the optimal specimen preparation for TEM investigation: ultramicrotomy (preparation

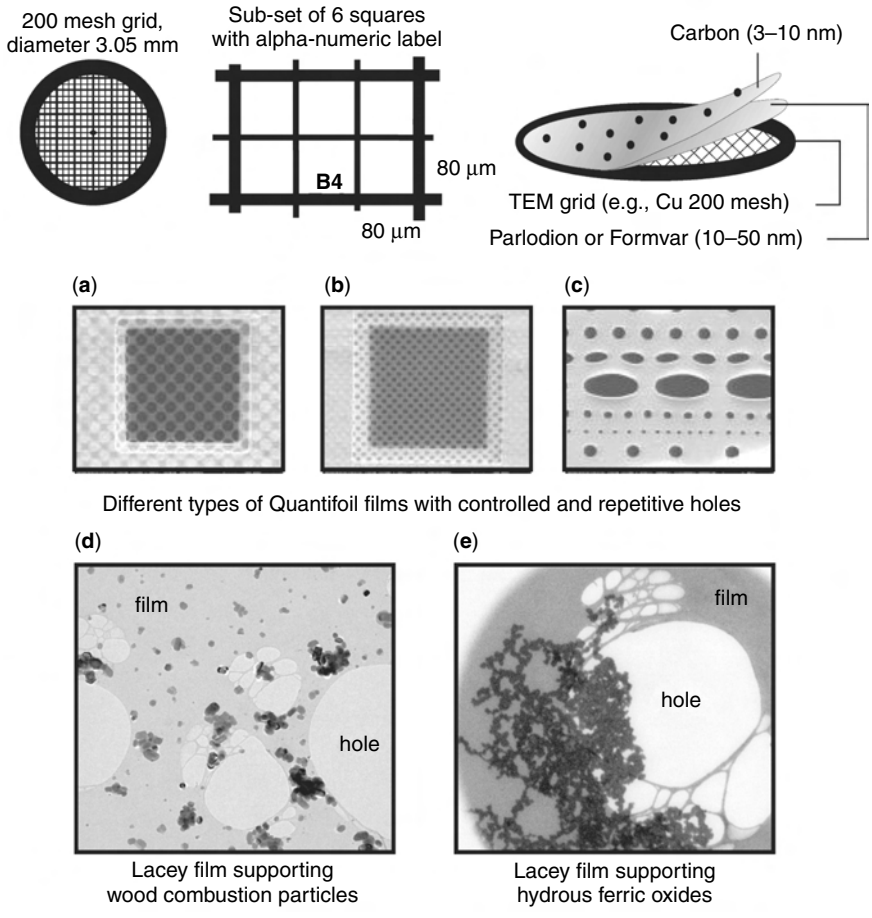

Figure 3. Specimen grids used to collect colloids and particles for TEM investigation. Supporting films with holes [*e.g.* Quantifoil with repetitive holes, micrographs (**a**)–(**c**), or lacey films, micrographs (**d**) and (**e**)] are recommended when supporting film-free element analysis of entities larger than the hole size (*e.g.* aggregates or fibrillar material) is required. In micrograph (**d**), wood combustion particles are too small to be analysed without a contribution from the supporting film; in micrograph (**e**), the aggregate of hydrous ferric oxides is large enough to cover the unsupported portion of the film and is thus prone to film-free element analysis

of ultra-thin sections of colloids embedded in plastic resin), preparation of whole mounts (deposition of the suspension on TEM grids), ultracentrifugation (direct and quantitative collection of colloids on grids), freeze-etching or vitrification (direct fixation of colloidal material at low temperature) and focused ion beam milling (microsectioning of material in the electron microscope). These techniques are described in full below.

3.1 ULTRAMICROTOMY

Ultrastructural investigations require the preparation of ultra-thin sections (*ca.* 50–100 nm), while thicker sections (which are much easier to obtain but should not exceed

150–200 nm) are amenable to element analysis, even when performing EELS, which theoretically requires the thinnest possible specimens.

For the extraction of ultrastructural information (in particular from bacteria, algae and three-dimensional networks of polymers in organic flocs), large entities (i.e. >1 μm) should be examined by TEM after preparation of thin sections obtained by resin embedding and ultramicrotomy (Figure 4). To avoid artefacts, the choice of an appropriate embedding medium is crucial. A hydrophilic resin (Nanoplast), rather than one of the more conventional hydrophobic ones (*e.g.* Spurr, Epon or Araldite) is appropriate because the latter require stepwise dehydration of the sample in organic solvents (acetone, methanol, ethanol or propylene oxide). These dehydration steps are potentially disturbing, as they may cause dissolution of particulate organic moieties and modifications of the morphology of complex three-dimensional networks containing organic entities. As Nanoplast produces water molecules during the permeation and polymerisation step, it readily infiltrates porous specimens (*e.g.* loose and amorphous colloids) and biological entities (*e.g.* bacteria), maintaining their fine morphological features [111,112].

For aquatic samples rich in microorganisms, one may require additional contrast of the cellular ultrastructure. This can be done as part of a fixation protocol prior to embedding or as part of a counterstaining protocol applied directly to ultrathin sections [113–115]. The most effective 'morphological stains' for microbiota are based on compounds which contain Os, U or Pb, or all three used in sequence [113–117]. Unfortunately, the stain technology that has been well developed for samples embedded in hydrophobic resins is underdeveloped for samples embedded in the hydrophilic Nanoplast resin. One solution to this dilemma is to split the sample and embed it in both kinds of resin [118]. In principle, Nanoplast-embedded specimens yield images in which individual colloids within aggregates retain their true three-dimensional disposition, whilst images of specimens embedded in a hydrophobic resin [117] reveal essential details of microbial ultrastructure.

Ultramicrotomy of the resin-embedded material should be performed exclusively with a diamond knife to overcome the hardness of mineral particles or biogenic minerals such as silica frustules, which quickly damage conventional glass knives. Diamond knives must be used with great caution, since they are expensive and can be chipped by hard minerals in the true particle size range. The 'chipping' is related less to particle hardness than to particle size, the result of the very slender shape of the diamond at its cutting edge. Nanoparticles of extremely hard materials are usually not problematic for the diamond knife, although such particles may sometimes 'pop out' of the embedding matrix during cutting, leaving a hole in the ultrathin section.

3.2 WHOLE MOUNTS

TEM offers a broad palette of protocols for specimen preparation. The most important procedures are illustrated schematically in Figure 4. Qualitative investigations are best served by direct deposition of a suspension on TEM grids (whole mounts), followed by evaporation (air drying). This rapid procedure may, nonetheless, induce (a) crystallisation of undesirable electrolytes (*e.g.* salt crystals in marine samples, which can be avoided by rapid rinsing of the grid in ultra-pure water), (b) shrinkage of aggregates of flexible organic materials (*e.g.* extracellular polymeric substances) or (c) coagulation of small colloids.

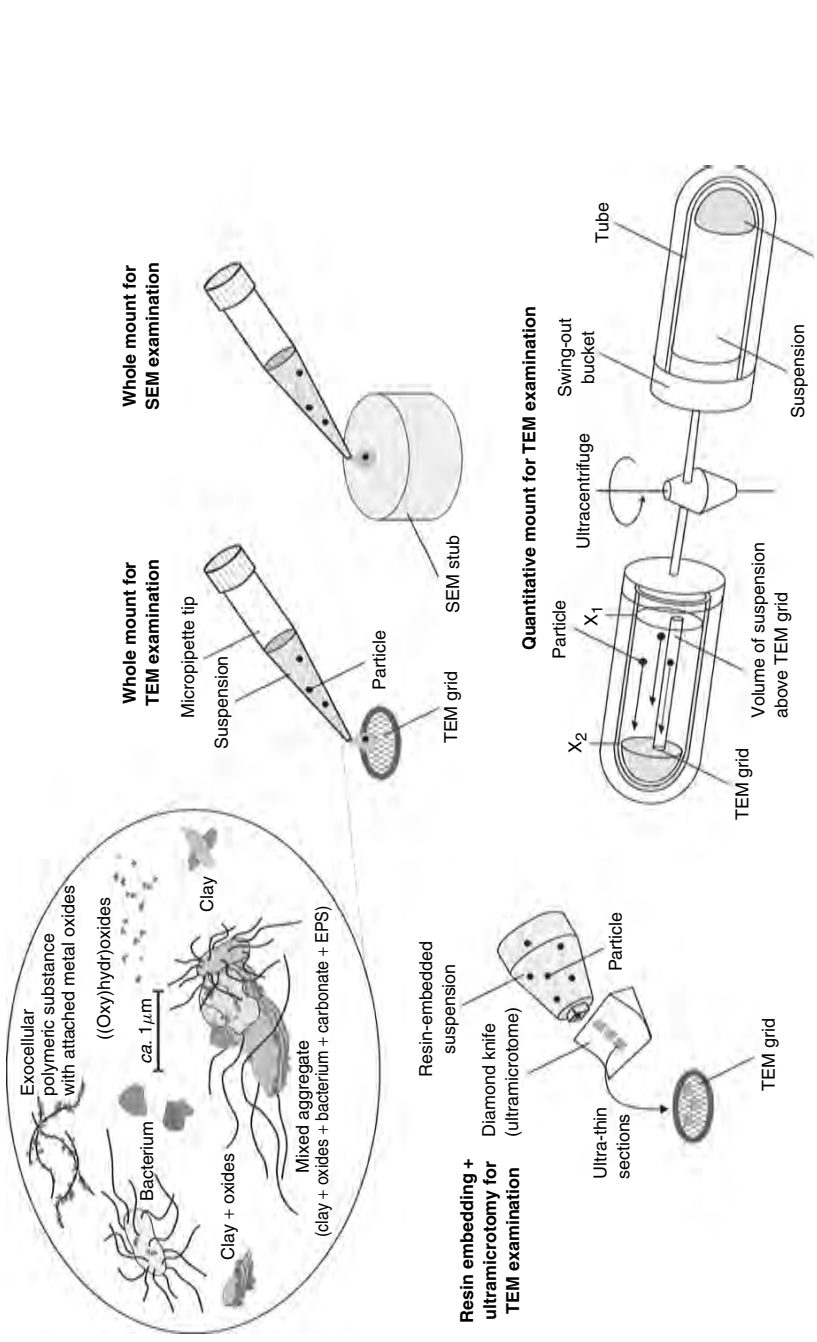

Figure 4. Scheme of the most useful qualitative and quantitative specimen preparation schemes for the SEM/TEM examination of colloids and particles present in aquatic samples. The preparation of whole mounts (on grids for TEM; on stubs for SEM) is the most rapid and easy to perform, but subsequent EM observation is usually biased by artefacts produced due to the evaporation of water from the specimen and support. Resin embedding is time consuming and requires operator skill but is well suited for ultrastructural analysis of specimens rich in biota. Ultracentrifugation is generally the most quantitative approach, as there is a direct relationship between the number of colloids impacted onto the grid and their concentration in the sampled medium

3.3 ULTRACENTRIFUGATION

Whenever quantitative results are expected [*e.g.* particle size distribution (PSD)], colloids and particles must be deposited on the grid in a quantitative way. For this reason, the usual preparation of direct whole mounts is strongly discouraged, as it leads to shrinking and aggregation of entities during dehydration. Probably the most successful approach to prepare specimens for quantitative analysis by TEM is based on their controlled deposition by direct ultracentrifugation of the particles on TEM grids [31,94]. This procedure (Figure 4) yields quantitative whole mounts with evenly distributed particles. For a given suspension, the final coverage of the grid can be fine-tuned by varying the centrifuged volume, allowing a fairly accurate estimation of the particle concentration in the initial sample, while avoiding the excessively high concentration of particles that is commonly seen in whole mounts. Entities sensitive to dehydration or redox modifications can be post-protected by horizontally spinning an ultrathin film of hydrophilic Nanoplast resin. Indeed, the preparation of quantitative mounts can be coupled to sequential fractionation schemes to narrow further the number of particle types that are collected on the grids.

For this specimen preparation scheme, TEM grids are fixed with a light adhesive (one contact point at the periphery of the grid is sufficient), carbon side up, on the flat surface of a hemispherical plug which is inserted in a centrifuge tube (the plug having been moulded from epoxy resin to fit the tubes). A known volume of suspension is poured in the tube, which is then mounted in the swing-out bucket of an ultracentrifuge rotor. The duration and the speed of the centrifugation, together with the optimal volume of the suspension to be centrifuged, rely on the types of colloids to be collected and on the initial concentration of particulates in the suspension.

According to Stokes' law, the time t(s) required for a spherical particle of diameter d(cm) and density ρ(g cm^{-3}) to settle from the top x_1 (cm) of the suspension with density ρ_0 (g cm^{-3}) and viscosity η (Pa s) to the surface of the grid x_2 (cm) when subjected to an angular rotation speed ω (rad s^{-1}) is given by

$$t = [18\eta \ln(x_2/x_1)]/[d^2(\rho - \rho_0)\omega^2] \quad (1)$$

For example, an inorganic colloid ($\rho = 2.0$ g cm^{-3}) with $d = 20$ nm would be collected on the TEM grid after *ca.* 1 h of centrifugation at *ca.* 1.25×10^5 g, whereas an equivalent organic colloid ($\rho = 1.1$ g cm^{-3}) would require *ca.* 14 h of centrifugation. On the other hand, a large and dense mineral colloid ($d = 450$ nm; $\rho = 2.0$ g cm^{-3}) would reach the TEM grid after merely 0.5 h at *ca.* 520 g. Strictly, however, these approximations apply only to ideal rigid spherical colloids; most natural colloids (*e.g.* tabular clay crystals or fibrillar polysaccharides) deviate very far from this ideal.

The key factor for optimal centrifugation is the fraction of the TEM grid covered with particles. Ideally, a coverage of *ca.* 1–5% will minimise the probability of 'apparent aggregates', i.e. of individual entities occupying the same position on the grid (see sketch in Figure 5). In practice, turbid waters (*e.g.* sediment–water interfaces, wastewaters or waters from eutrophic lakes) require either the centrifugation of a very small volume (i.e. a thin layer of suspension above the grid) or predilution of the suspension with an electrolyte that is as similar as possible to the natural water (*e.g.* ultrafiltered carbonated water of pH 6–8 with ionic strength $I = (1–5) \times 10^{-3}$ mol dm^{-3} for a continental water). In the latter case, however, there is a risk of producing unexpected modifications of the original particle

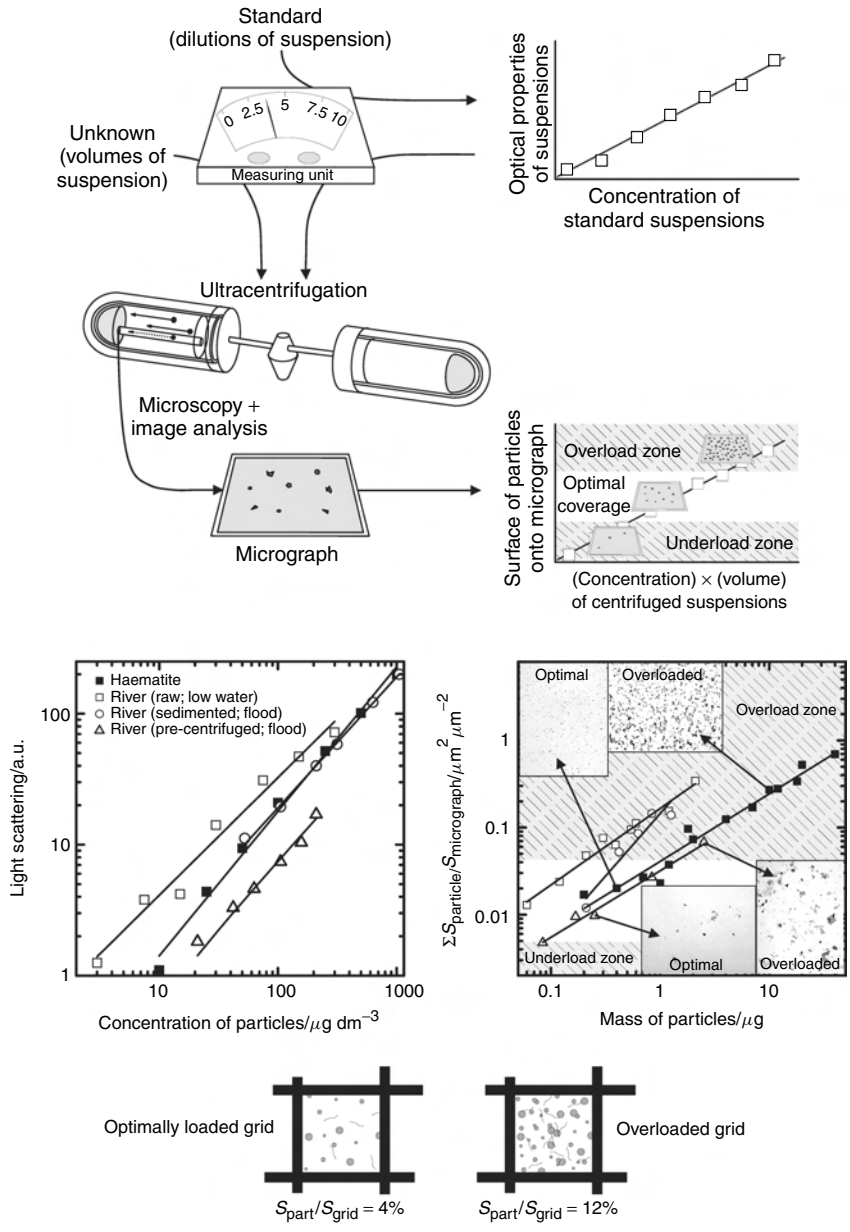

Figure 5. Scheme of a quantitative specimen preparation by the direct ultracentrifugation of colloids on to TEM grids. Optimal preparation of grids is performed in two steps: precalibration of the method with different dilutions of a standard colloid or of the suspension to be studied (for an optimal guess of the relative colloid concentration in the samples to be studied), followed by ultracentrifugation of the volume-optimised samples to avoid over- or underloading of TEM grids. Examples of optimally covered (few entities, homogeneously spread) and overloaded grids (too many colloids, apparently coagulated) are given for standard colloids (synthetic haematite particles) and for a real suspension (precentrifuged river during a flood event). The ratio of surface of TEM grid covered by colloidal entities to surface of TEM grid visualised determines the optimal coverage range (in general, $\leqslant$10% coverage is a maximum)

size distribution. For unknown samples, the conditions of specimen preparation can be optimised empirically by centrifuging a large set of different volumes and dilutions. On an *ad hoc* basis, the experimenter may measure some optical parameter of the suspension (*e.g.* turbidity, nephelometric data, light scattering or optical density) in order to estimate the concentration of particles, and thus the best combination of centrifugation conditions, to avoid overloaded or underloaded TEM grids [31].

Replicate grids are positioned in the same tube, and suspension volumes between *ca.* 10^{-3} and 3×10^{-2} dm^3 should be centrifuged. Nonetheless, the crucial parameter for optimal grid coverage is the height of the suspension above the grid, not the volume of suspension. Thus, centrifuge tubes of small diameter are preferred for small volumes (i.e. very low heights of suspension). For example, a suspension containing *ca.* 10^{11} particles dm^{-3} will result in *ca.* 6400 particles spread over a TEM grid square (80×80 μm) when a 1 cm high suspension is centrifuged.

For specific purposes, the direct ultracentrifugation of colloids on to TEM grids can be performed with appropriately selected sequences of increasing centrifugal forces and durations, new grids being inserted in the tube at each step. In such cases, the suspension is depleted in particles with high density and size, and the recovered TEM grids exhibit increasing proportions of colloids with low density and size. This specimen preparation scheme can also be performed for the AFM study of aquatic colloids and particles (see Chapter 9).

Labile specimens, i.e. ones prepared from redox-sensitive waters or from samples containing flexible fibrils that may shrink during dehydration, can be protected after centrifugation with an ultrathin film of TEM-transparent hydrophilic Nanoplast [35]. The resin is spun over a grid placed on a horizontal rotating disc. Particulate entities are then embedded during a controlled polymerisation. Rigid, resistant specimens (*e.g.* silica particles) are simply air-dried prior to TEM examination; in this case, shrinking and aggregation of colloids are not observed, as the entities are firmly fixed to the supporting grid by the centrifugal force.

3.4 CRYOTECHNIQUES: FREEZE-ETCHING AND VITRIFICATION

Cryotechniques offer an alternative preparatory technology that complements chemical fixation and embedding, producing aggregates whose 3D relationships are spatially 'fixed' by physical means (*e.g.* vitrification). The cryotechnique that most faithfully preserves the original structure is freeze-etching, which consists of freezing an hydrated sample rapidly enough to vitrify it (i.e. ultra-fast freezing of the suspension to obtain colloids embedded in vitreous water), mechanically generating a fracture plane through it and then making a metallic replica of the fracture surface, while maintaining the vitrified sample below the recrystallisation temperature. The product of the freeze-etch technique is a replica which presents a topographical image of a colloid or aggregate, untouched by chemical agents and amenable to analysis by TEM. In any case, given the complexity (i.e. need for dedicated technical skills) and cost of freeze-etching, well developed by cell biologists for analyses of intracellular structure, it has been essentially unexploited by scientists who examine hydrated colloids despite its potential as a confirmatory technique [29].

Indeed, vitrification should be the best specimen preparation scheme [119–125]. Unfortunately, this technique is not adapted to colloids and particles because of the fairly high

cost and need for dedicated technical skills. In addition, the large differences in thermal conductivities between particulate material and the surrounding water matrix make it difficult to obtain purely vitrified colloid–water interfaces for entities larger than several nanometres, thus resulting in local crystallisation of ice and damage to the morphology of colloids.

3.5 FOCUSED ION BEAM SECTIONING

Focused ion beam (FIB) sectioning, an emerging technique for the microscopic analysis of environmental samples, was described in the late 1980s for the preparation of specimens from semiconductor devices [126]. The technique is highly versatile, because it provides the user with the ability to control visually, in real time, a preselected portion of a massive environmental sample (*e.g.* a bacterial mat, a large aggregate, a filtration membrane, a fraction of soil, a specimen preembedded in resin) that is to be transformed into a thin (or even ultrathin) section for TEM observation. The FIB approach consists in cross-sectioning a sample in a dedicated SEM equipped with a beam of charged elements (*e.g.* Ga^+, Ne^+ or Ar^+ ions at energies down to 100 eV) that are focused to a small spot size (typically 10 nm) and rastered across the sample. The thin section that is produced can be transfered by micromanipulator to a TEM grid for examination at high resolution (Figure 6).

FIB milling can be applied to hard (*e.g.* materials science [127]) and soft (*e.g.* biological [128, 129]) samples, and even to complex materials that include hard and soft counterparts (*e.g.* [130]). Very limited beam damage is reported, even for high-resolution

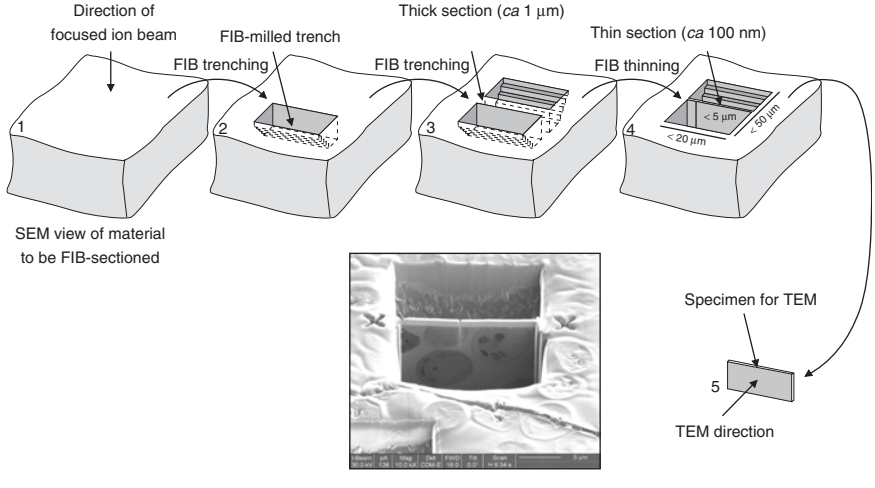

Figure 6. Scheme of the steps required for the preparation of a thin section for TEM examination in an SEM equipped with an FIB. A cross-section is milled by the ion beam on the sample surface; a similar cross-section is then milled in the vicinity in order to produce a preliminary thick section, which is ion-thinned from both sides until it becomes electron transparent. The thin section is finally cut free and removed for TEM investigation. The whole process is monitored in the SEM. The micrograph shown is a typical example of the operator's control over the preparation and thinning of a FIB section of algae; cross-sections of cells are visible at the freshly milled surface of the thin section; the layer above the specimen is a protective platinum coating

TEM, provided that the energy and the incidence angle of the beam are carefully controlled [131–133]. FIB sections of material of known composition and controlled thickness can be prepared and used to standardise the TEM–X-EDS signals [134]. For a review of the technique and details related to FIB, the reader is referred to a special publication on ion beams [135] and references therein.

3.6 STAINING AND LABELLING OF ORGANIC-RICH COLLOIDS

Staining procedures designed for biological or medical applications can be applied to environmental specimens (in particular in soils, sediments and natural waters) either to enhance the contrast of poorly electron-opaque organic material (salts of heavy elements, amongst which the most commonly employed are uranyl acetate, lead citrate, phosphotungstate, and Alcian Blue; see Figure 7) or to stain extracellular polymeric substances selectively [136–138]. For instance, Thiéry [139,140] described an elegant multi-step reaction with silver proteinate yielding nanometre-sized Ag grains on polysaccharides embedded in a Spurr resin (Figure 7). This selective identification method was

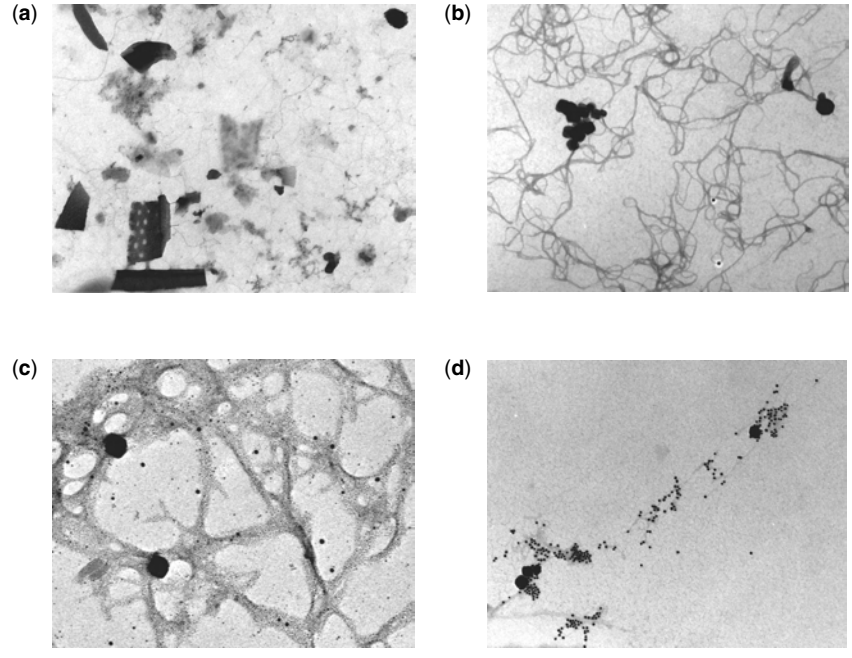

Figure 7. Examples of natural and synthetic polysaccharides. (**a**) Unstained heterogeneous lacustrine sample (Paul Lake, USA); the barely visible exocellular polymeric substances are 'naturally stained' by the major ions (mostly Ca^{2+}) present in the system. (**b**) Mixture of alginates (produced by *Macrocystis pyrifera*) and 50 nm haematite nanoparticles; the polysaccharides were post-stained with uranyl acetate (i.e. after deposition of colloids on the grid and recovery of the latter), and appear as uniformly dark. (**c**) Mixture of xanthans (produced by *Xanthomonas campestris*) and haematite; the polysaccharides were selectively post-labelled by reaction with silver proteinate, and appear as dark networks carrying small black dots (Ag grains). (**d**) Xanthans were specifically post-labelled by reaction with a lectin–gold conjugate (lectin: UEA_1 *Ulex europaeus*); the 10 nm black spheres are the gold colloids. All specimens were prepared by quantitative ultracentrifugation

later applied to soil extracellular polymeric substances (EPS) that cement clay particles together [141] and to bacterially produced polysaccharides in freshwaters [5,142].

At present, it is not easy to identify clearly colloidal and macromolecular humic/fulvic substances, which constitute an important proportion of natural organic materials. On the other hand, highly sophisticated labelling techniques using ultraspecific markers {*e.g.* gold–lectin conjugates that bind specifically to given carbohydrate moieties of polysaccharides (Figure 7) [143–158]} that were developed for the study of macromolecules in plants, animals and fungi should, in the near future, prove to be extremely useful for distinguishing similar natural organic macromolecules (*e.g.* neutral vs acidic polysaccharidic moieties produced by bacteria and algae) in aquatic samples.

The development of ultraspecific markers for TEM is progressing so well that it is now possible to label individual protein species selectively within a microdomain inside an individual bacterial cell [159] and specific polysaccharide molecules within the mucilage matrix of a biofilm [27,160].

In many environmental situations, colloidal organic matter is naturally stained by the major ions present in the electrolyte and therefore requires no staining for simple visualisation purposes. It must be noted, however, that most existing staining protocols were not designed for environmental specimens (whole mounts or resin-embedded ones) and necessitate careful optimisation before they can be used on a routine basis.

3.7 POTENTIAL ARTEFACTS RELATED TO SPECIMEN PREPARATION

Protocols recommended for obtaining ultrathin sections and optimally prepared whole mounts have been discussed elsewhere [35,118], as have procedures for analysing the three-dimensional architecture of readily deformed water-rich flocs [161,162]. The principal artefacts to consider in the production of sections and whole mounts for analysis are those caused by dehydration and shrinkage, extraction being a potential but soluble problem in the case of sections. These artefacts are well understood and readily minimised for many kinds of samples [29,30,40]. AEM (TEM, STEM–X-EDS, EELS, EF-TEM) techniques and rationales for the selection of representative images as related to the artefact problem have been treated at some length in the literature [4,23].

For the optimal preparation of native wet colloids prior to AEM analyses, a detailed treatment of the detection, assessment and minimisation of artefacts was given by Leppard and Buffle [40]. Artefacts include those inherent in preparatory protocols and those created before analysis (*e.g.* sample mishandling at time of sampling, unnecessary fractionation, alteration during storage, exposure to chemical agents that cause perturbation and excessive preconcentration). Leppard and Buffle [40] recommend (i) avoiding sample storage, (ii) minimising the number of steps in water sample preparation, (iii) paying exquisite attention to detail in the use of any fractionation procedure and (iv) adapting the prefractionation steps (if necessary) to take account of particle size polydispersity.

4 MORPHOMETRIC ANALYSIS OF PARTICLES AND COLLOIDS

Over recent decades, the investigation of environmental samples by EM was traditionally performed for merely illustrative purposes, although the spatial resolving power and analytical capabilities of modern electron microscopes presented unique features with the

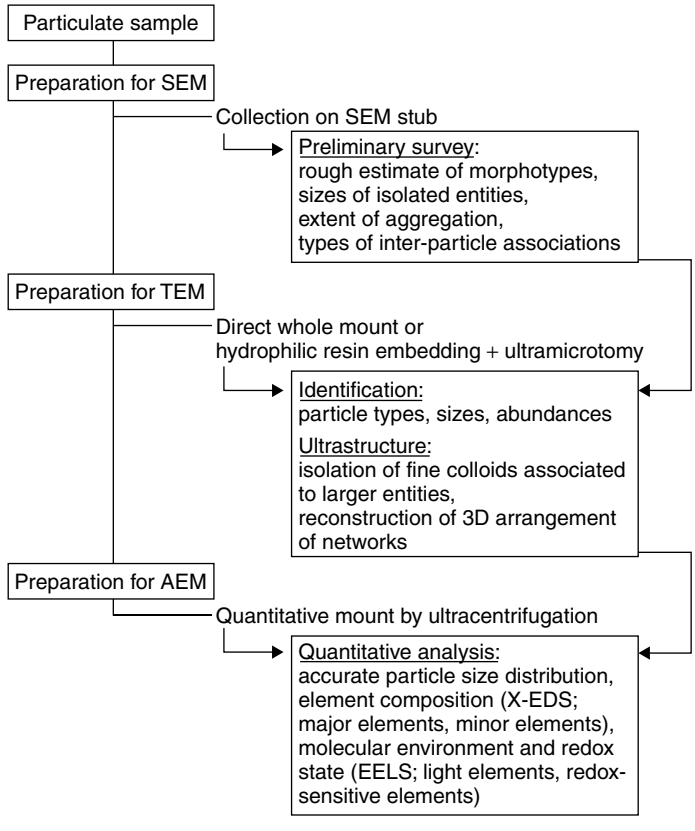

Figure 8. Idealised correlative electron microscopic procedure for the examination and physicochemical characterisation of environmental colloids and particles. Examples of micrographs, spectra and plots can be found in the other figures

potential to supply qualitative and quantitative methods for providing unequivocal answers to complex problems in which colloids and particles play a central role.

Although the qualitative and quantitative aspects of this sort of investigation are discussed separately in the following sections, they should be considered as being intimately interrelated within the framework of every correlative electron microscopic investigation, as illustrated in an idealised hypothetical investigation outlined in Figure 8.

4.1 QUALITATIVE OBSERVATIONS

SEM and ESEM are particularly well suited for the imaging and quantification of surface and textural features of large particulate entities (*ca.* >1 μm) and for a rough estimate of the particle size distribution. Qualitative three-dimensional morphological information is readily extracted from SEM, operated in either the secondary electron mode or backscattered electron mode. The extent of aggregation among particles (provided that the aggregation is not an artefact produced by overloaded specimen stubs) can be documented

with a resolution down to *ca.* 50 nm without difficulty. Because of its ease of operation, SEM should be selected for the routine gross-scale survey of samples, in particular for atmospheric and soil particles. Preliminary qualitative surveys should help the operator to focus on either the general trends (*e.g.* major classes of particle types, sizes or associations) or the significant specificities of the sample (*e.g.* characteristic aggregation between two types of particles or prevalence of a narrow size class for a given type of entity). On the other hand, ESEM is useful for looking at wetting and drying processes involving highly flexible organic polymers and aggregates, eventually avoiding perturbation of their structure, as can be the case for microscopy performed under high vacuum. Under controlled conditions, it is even possible to determine particle size distributions, fractal dimensions and element maps by ESEM [110].

When carried out in the context of conventional bulk experiments and analyses employed in research on ecosystems, qualitative SEM/ESEM may yield significant supplementary information, affording increased understanding of the ecosystems. For example, visualisation of the microscopic features of humic and fulvic substances, as affected by changes in the pH or ionic strength of the surrounding milieu, has contributed greatly to our knowledge of conformational changes in these dominant organic substances in soils. Thus, humic colloids with shapes from spheroids to flexible extended fibrils or densely networked three-dimensional systems have been observed [163–167]. Similarly, the systematic SEM–X-EDS identification of the general features of particles transported through a complex peat–river–karst–spring aquifer has highlighted the ubiquity of a well defined Fe–Ca–C-rich class of globules and the role of humic substances in their formation and behaviour [4,168,169]. In a similar manner, the role of associations between clays and fibrillar polysaccharide networks on the stabilisation of soil structures has been assessed mainly by means of SEM. Nonetheless, such investigations require careful specimen preparation techniques (*e.g.* freeze-drying instead of air-drying) to minimise artefactual changes in conformation which may occur at any step of the preparation.

Accurate qualitative or semi-quantitative investigations on colloidal entities (*ca.* <500 nm) are better performed by means of TEM or STEM, with a resolving power down to the nanometre scale even for complex heterogeneous entities (a claimed sub-ångstrom resolution being achievable using TEM with aberration-corrected electron optics [170–172]). Whole mounts and quantitative mounts (Figure 4) are appropriate for semi-routine TEM investigations on colloidal entities, provided that TEM grids are not too densely covered with large particles and aggregates. In addition, inorganic entities can be verified for their potential crystallinity (Figure 9) by qualitative electron diffraction, either in selected area mode or in convergent beam mode. This is particularly useful for ill-defined particles (*e.g.* ferrihydrites or partly amorphous oxides) that may reveal locally ordered domains of their atoms, or to distinguish between particles exhibiting approximately the same morphology and composition but representing different stages of ageing.

Ultrastructural TEM characterisation of ultrathin resin sections is recommended for the detection of structures such as microscopic mineral deposits on bacterial cells, which would be obscured by the thickness-related opacity of bacteria prepared as whole mounts. This method is also recommended for the study of complex large-scale networks of fibrillar extracellular polymers, which retain their natural conformation when embedded in an appropriate resin. The reconstruction of their three-dimensional architecture is

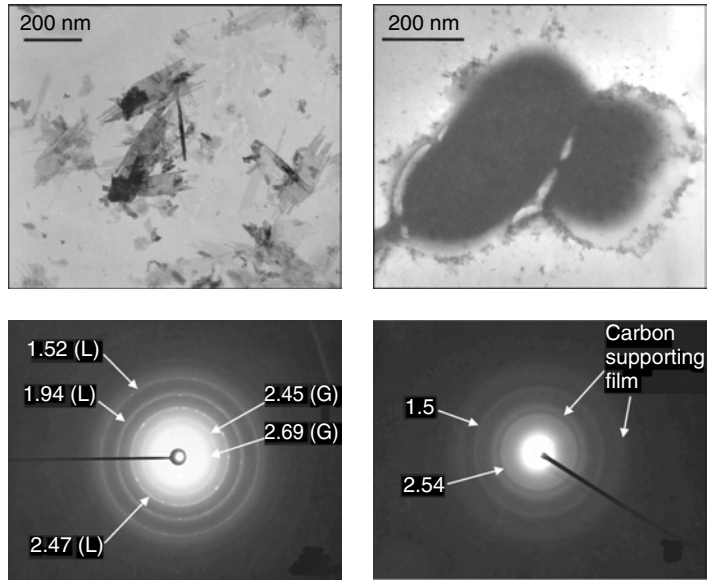

Figure 9. Examples of electron diffraction patterns (SAED) obtained on an abiotic mixture of goethite (G) and lepidocrocite (L) (left side), and on hydrous ferric oxides formed in the presence of *Bacillus subtilis* (right side). The *d*-spacings are given in Å. Whereas goethite and lepidocrocite are highly diffractive, the biotic hydrous ferric oxide can be identified as a two-line ferrihydrite [287]

theoretically achievable by imaging successive serial sections, but this requires tedious and extensive image analysis.

4.2 QUANTITATIVE ANALYSIS AND PARTICLE SIZE DISTRIBUTION

Automated particle detection systems have been described [66,173–182], but their use is rather limited. This discussion will therefore focus on the conventional use of TEM for the recording of micrographs which are later processed by image analysis to extract information on particle size distributions (PSDs) and other useful morphological parameters.

Quantitative PSDs (either for all types of particles and aggregates present in the specimen or for a specific type of particle identified either by morphological criteria or by routine X-EDS element mapping) must be performed on quantitative whole mounts. High-quality micrographs can then be digitised for mathematical morphometry using image analysis software. The accurate determination of the PSD of atmospheric, aquatic, soil or sediment entities may yield information on the processes driving their behaviour (*e.g.* formation, dissolution, coagulation and sedimentation). It is also possible to estimate the mechanisms of colloid aggregation by measuring the fractal dimension of the aggregates. Provided that micrographs are obtained under carefully controlled conditions of illumination, estimates on the volume of non-spherical particles of known composition can also be obtained by image analysis (thickness-dependent opacity of the particles).

Owing to the physicochemical processes involved, such as the formation, coagulation and sedimentation of particulate material in aquatic systems, PSDs usually appear to

follow some kind of power law (*e.g.* Pareto's distribution; [183]), *e.g.*

$$\mathrm{d}(N_{\mathrm{part}})/\mathrm{d}(d_{\mathrm{part}}) = a d_{\mathrm{part}}^{-b} \tag{2}$$

where $\mathrm{d}(N_{\mathrm{part}})$ is the number of particles in a given interval of particle sizes $\mathrm{d}(d_{\mathrm{part}})$, and a and b are characteristic constants of the system. The constants can be linked to the colloidal transformation process in the water column (Figure 10).

In other words, the number of particles tends to decrease when their size becomes larger. This consideration must be kept in mind when dealing with TEM, as the human eye is a subjective tool. The experimenter can easily miss significant numbers of small colloids when they are in the presence of much larger, more conspicuous entities, such as diatoms, algae, clusters of bacteria and mineral particles which obviously monopolise the attention of the observer. To avoid such biases, TEM sessions for the determination of PSD must always be planned in a rigorous, systematic and objective way.

As a first step, TEM grids should be previsualised at very low magnification in order to control the quality of the sample preparation protocol. At nominal magnifications $<10^3\times$ (i.e. magnifications corresponding to the image projected on the fluorescent screen of the TEM, not taking into account further magnification when a digital camera is installed), only large particles (>1 μm) are identifiable; they should be evenly distributed on the grid.

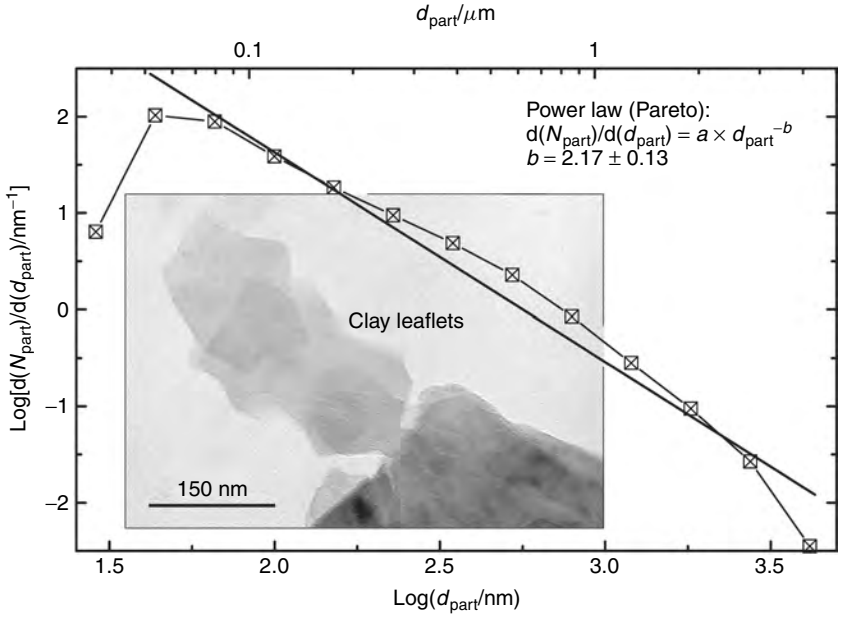

Figure 10. Example of a particle size distribution (PSD) obtained on colloids in a deep marl ground water. Colloids, as small as 30 nm, consist mainly of clays (see micrograph) in roughly equal proportions of chlorite, illite and smectite. The low concentration of colloids (<0.5 mg dm^{-3}) and the reducing conditions ($E_h = -310$ mV) required careful sampling and specimen preparation; approximately 9600 individual colloids were analysed to yield an unbiased PSD, the slope of which ($b = 2.2$) indicated that clay entities were subjected to elimination from the ground water by orthokinetic coagulation

As the recovery of TEM grids following centrifugation requires considerable skill, broken portions of the supporting film are not uncommon. Nonetheless, they do not impair further observations, as they are discarded from the set of 2–3 potentially interesting zones (i.e. assemblies of 2 × 3 squares with alpha-numeric label). A rapid previsualisation of a replicate grid can ascertain whether the centrifugation step was performed under optimal conditions.

In a second step the zones of interest have to be accurately surveyed at higher magnification in order to record micrographs of the colloidal and particulate entities. A nominal magnification factor of *ca.* $(2.5–5) \times 10^4\times$ is a good compromise to avoid underestimation of very small colloids (at $5 \times 10^4\times$, entities <20 nm appear as <1 mm) or very large particles (at $5 \times 10^4\times$, entities >2–5 μm cannot be entirely recorded). Nonetheless, even at this magnification, huge numbers of micrographs can be generated (at $5 \times 10^4\times$, $>10^3$ micrographs of a single grid square could be recorded).

Surveys of the zones to be micrographed can be performed either randomly or statistically. The random survey consists of recording micrographs at different randomly selected positions of the zone. This procedure is recommended when colloids exhibit a fairly narrow PSD and are homogeneously distributed on the supporting film. The statistical approach consists of recording micrographs at predetermined nodes of an imaginary grid; this approach ensures less bias in the selection of micrographs.

As far as possible, the recording of micrographs, either on negatives or with a digital camera, should be performed under reproducible conditions. Experimental parameters of the TEM, such as apertures, magnification, beam current, beam spreading and homogeneity, underfocus, exposure time and development process (for negatives), should be kept constant in order to guarantee that identical electron densities (i.e. similar types of materials for a given particulate size) in the specimen will translate into identical grey levels from micrograph to micrograph. Of course, additional magnification factors from the fluorescent screen to the camera must be taken into account, and digital micrographs should be recorded in TIFF format to avoid loss of data during handling of the files.

4.3 IMAGE ANALYSIS

Once recorded, micrographs are generally processed by means of image analysis. There are a number of software programs available for image treatment (*e.g.* Photoshop with dedicated plug-ins and macros for PC, or the shareware NIH-Image for Mac), but the professional (and usually expensive) ones dedicated to image analysis are recommended, as they are fitted with a number of routines and macros relevant for mathematical morphometry, i.e. the recognition of objects and their characterisation [184–203]. Digital archiving of micrographs is convenient, as it allows storage of keywords and other relevant information for further retrieval [204].

Micrographs recorded on negatives must be digitised at a high resolution (*e.g.* 1000 pixels per inch, to record subtle details) prior to image analysis. For example, for a TEM magnification of $5 \times 10^4\times$ on the negative, the diameter of a 10 nm colloid translates into 20 pixels at a resolution of 1000 pixels per inch. Transfer from the negative to the final print is not recommended, as it may induce distortions in the palette of grey levels, the dynamic properties (i.e. the ability to separate shades of very dark or very light greys) of the final print being much narrower than those of the original negative.

Although digitised micrographs may be binarised by selecting a threshold range (meaning that shades of grey are converted to black and white pixels, where certain grey levels

are considered as objects and others as background), it is recommended to work directly on the original files, in order to extract relevant information on the grey levels of each entity.

Figure 11 shows a simplified sketch of the steps that must be taken before measurements are started. Specific digital filters (*e.g.* shade correction or differential contrast enhancement) can, under certain circumstances, correct variations in the background (as, for instance, when one side of the micrograph is dimmer) when micrographs are obtained in an inhomogeneous electron beam.

After such preliminary corrections, a threshold has to be imposed on micrographs or regions of interest (ROIs) to limit the morphometric analysis to the colloids and particles of interest. Accurate scaling (in X, Y and Z if required) of the micrographs must also be applied in order to measure morphometric parameters in real sizes. Of course, these crucial preliminary operations must be performed and adjusted with care on each micrograph or ROI, but the procedure should be facilitated when all micrographs are recorded under constant conditions.

It must be emphasised that Z calibrations are possible only for clearly identifiable colloids and particles of simple morphology. For instance, spheroids (*e.g.* crystalline iron or manganese oxides), tabular entities (*e.g.* clay leaflets) or fibrillar entities (*e.g.* extracellular polymeric substances) and their aggregates are predisposed to Z calibration. In contrast, the Z calibration of ill-shaped entities and multi-type aggregates or very thick objects cannot be extracted from grey levels, which are a complex function of thickness and electron density.

Among parameters of interest for particle sizing, the following should be measured for each entity: area, minimum and maximum diameter, perimeter and grey levels. Other derived parameters, such as mean diameter, centre of gravity, radius of gyration, mean grey value, equivalent circle diameter [$\mathrm{ECD} = 2(\mathrm{area}/\pi)^{0.5}$], shape factor ($\mathrm{SF} = 4\pi \times \mathrm{area/perimeter}^2$; $0 \leqslant \mathrm{SF} \leqslant 1$) and volume (provided that the grey levels can be accurately calibrated in units of thickness), are easily calculated for an exhaustive description of the morphology of an entity. As a rule, particles on the border of the ROI and also particles with holes in them should be excluded from the analysis to avoid biases in the final description of the morphological characteristics of a population.

Of course, the determination of a PSD is not feasible in every circumstance. For instance, the mean size of an entity with a shape factor $\mathrm{SF} \ll 1$ (*e.g.* fibrillar material or an irregular aggregate or ill-defined porous colloid; see examples in Figure 12) may have no physical meaning. For such entities, the determination of other parameters, in particular their minimum and maximum diameter or shape factor, is more relevant.

Under optimal conditions (i.e. when assemblages of colloids in the specimen present a realistic picture of assemblages in the initial suspension), information on the degree of coagulation and the processes leading to aggregation may also be extracted. For instance, discrimination between reaction-limited and diffusion-limited colloid aggregation [205–217] can be highlighted for colloidal systems by means of their fractal dimension, *Df*:

$$V_{\mathrm{aggr}} \propto (RG_{\mathrm{aggr}}/r_{\mathrm{unit}})^{Df} \tag{3}$$

where V_{aggr} and RG_{aggr} are the volume and radius of gyration of the aggregate, respectively, r_{unit} is the radius of the elementary colloids within the aggregate and *Df* is the computed fractal dimension.

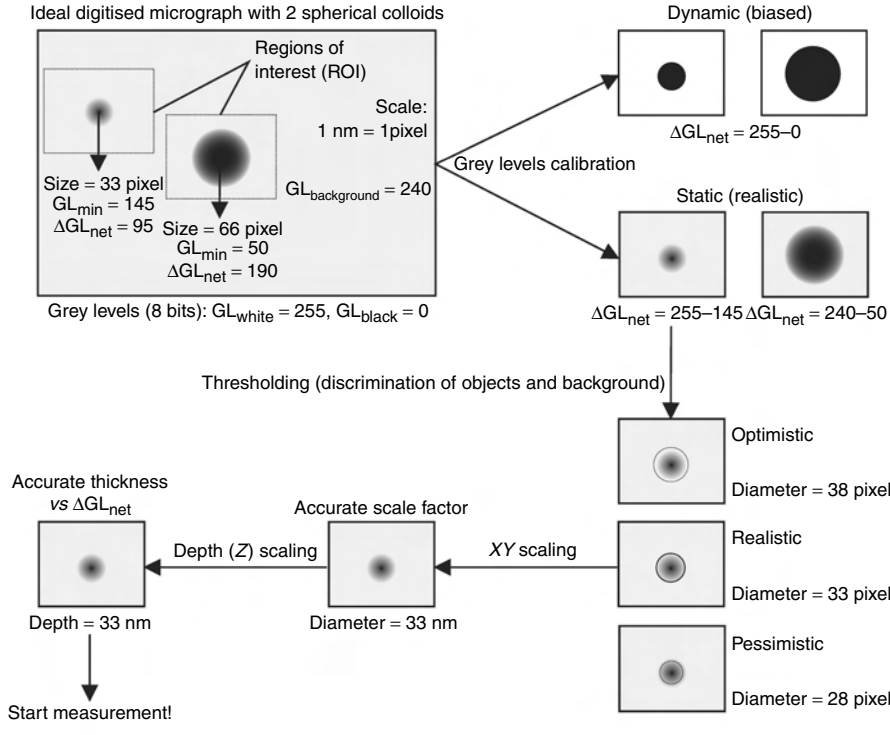

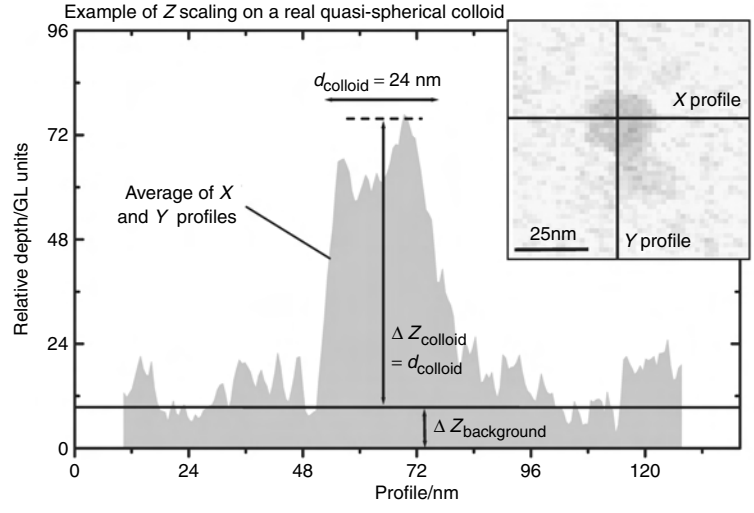

Figure 11. Steps required prior to the morphometric analysis of colloids. The schematised micrograph contains ideally spherical and homogeneous colloids. An accurate grey-level calibration and thresholding is a prerequisite to the least unbiased determination of the colloidal characteristics. An example of the calibration of the thickness of colloids (Z calibration) as a function of their grey levels is given in the bottom graph for a real quasi-spherical colloid (inset). Knowing the size of the colloid and by assuming a spherical shape, one can convert the grey values into real thicknesses

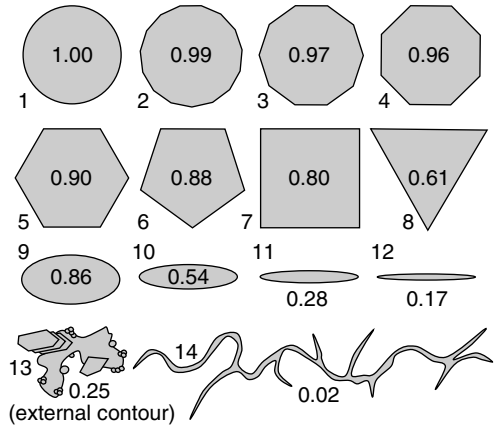

Figure 12. Examples of the variation of the shape factor ($SF = 4\pi \times \text{area/perimeter}^2$) of geometric objects. Whereas the SF is close to 1 for objects with a high symmetry (objects 1–8), it decreases rapidly for elongated objects (9–12), aggregates (object 13) and fibrillar material (object 14)

Similarly, orthokinetic and perikinetic aggregation of colloids can be differentiated by means of a PSD expressed in terms of the Pareto power law (Figure 10 [183,218]).

For quantifying individual native colloid 'species' (as defined by a combination of size and compositional and morphological criteria), a practical electron-optical technology is now available [31], for use in combination with the quantitative ultracentrifugation of colloids on to TEM grids. User-friendly image analysis has become available [219] to facilitate TEM-based colloid quantification efforts.

Computerised image analysis has become a powerful means for extracting quantitative data from EM-based information, and there are many parameters whereby valuable information on environmental particles can be acquired that is not measurable with bulk techniques [29]. For example, with a representative specimen, size distributions of nanoscale particles from a heterogeneous suspension, which are not measurable when bulk techniques are used, can be quantified in a statistically meaningful manner. Such measurements can be evaluated with respect to bulk measurements when the particle population is homogeneous. Recent advances in the analysis of many kinds of particles are relevant to the image analysis of nano- and microparticles.

The accurate determination of the particle size distribution of colloidal entities may yield information on the processes driving their behaviour in the environment (*e.g.* formation, dissolution, coagulation and sedimentation). For instance, Couture *et al.* [220] performed image analysis on *ca.* 9000 individual colloids collected under state-of-the-art conditions from a deep ground water of a potential site for the repository of nuclear wastes in Switzerland. It was demonstrated that clay minerals (mainly chlorite, illite, and smectite with *ca.* 30–4000 nm mean size) were subject to elimination from the waters by orthokinetic (fluid shear-induced) coagulation (slope of the particle size distribution being expressed as a Pareto power law: $b = -2.2$; Figure 10).

In addition, the aggregation regime of particles can be determined. The fractal dimension of an aggregate as determined by image analysis [221–224] provides information about the mechanisms of aggregation. According to Lin *et al.* [206] and Jullien [225],

$Df \approx 1.8$ corresponds to an aggregation controlled by Brownian motion [diffusion-limited colloid aggregation (DLCA)], whereas when $Df \approx 2.1$, owing to electrostatic repulsions, the aggregation rate is limited by the low collision efficiency between colloidal entities [reaction-limited colloid aggregation (RLCA)]. Such calculations have been used by Fatin-Rouge *et al.* [226] to determine the aggregation mechanism of nanoparticles analysed by TEM. In the same manner, Mavrocordatos *et al.* [58] showed that the *Df* of wood combustion particles could be determined by AFM. Results obtained on 1200 particles correlated very significantly with data obtained by STEM–X-EDS, scanning mobility particle sizer (SMPS) and bulk chemical analyses, and were coherent with previous work on combustion particles.

5 ELEMENT ANALYSIS OF PARTICLES AND COLLOIDS

Quantitative investigations of natural particulate matter entail special requirements. First, the specimen must be representative of the original medium. For example, all particle types initially present in the natural sample must be present in the proper proportions, unless the sample has intentionally undergone controlled fractionation to remove certain particle classes. The aggregates present in the specimen must not be artefactual expressions of an overloaded TEM grid or of a sample whose conditions of handling and preparation favoured coagulation of existing entities or precipitation of dissolved species. In that respect, the preparation of quantitative whole mounts (see Figure 5) by direct ultracentrifugation of suspended particles on to TEM grids is the most appropriate approach for quantitative measurements, provided that it is performed without delay. Most samples extracted from natural waters, sediments or soils can be prepared in this manner. In addition, quantitative investigations need to be performed on a statistically significant number of entities in order to yield sound measurements. Depending on the expected confidence of the final results and on the type of suspension (*e.g.* fairly homogeneous classes of colloids vs highly heterogeneous samples), the measurements of size and composition should be performed on a sufficiently large sampling of particles, i.e. between 10^2 (for simple suspensions) and 10^4 entities (for heterogeneous suspensions; Figure 13).

Characteristic X-ray fluorescence (X-EDS analysis) and energy-loss (EELS analysis) features of environmentally relevant elements are given in Figure 14. When dealing with element composition, the measured X-EDS peak intensities must be calibrated against representative standards. These standards may have to be synthesised in the laboratory under the conditions encountered in the ecosystem under investigation, because the mechanisms of X-ray production are influenced by the matrix of the sample material. Standardless analysis [49] is feasible in X-EDS (Figure 15), but it requires accurate measurement of element- and microscope-related parameters. A guide to obtaining quantitative X-EDS results from ultrathin sections of resin-embedded particles has been provided by Russ [227]. For EELS analysis, relative quantification (i.e. the ratio of one element to another one in the particle of interest) is readily obtained by calculation without the need for standards.

5.1 ENERGY-DISPERSIVE SPECTROSCOPY (X-EDS) AND RELATED TECHNIQUES

Over the past two decades, the clever and non-artefactual determination of the composition of environmental particles and colloids by X-EDS has transformed EM into a unique and

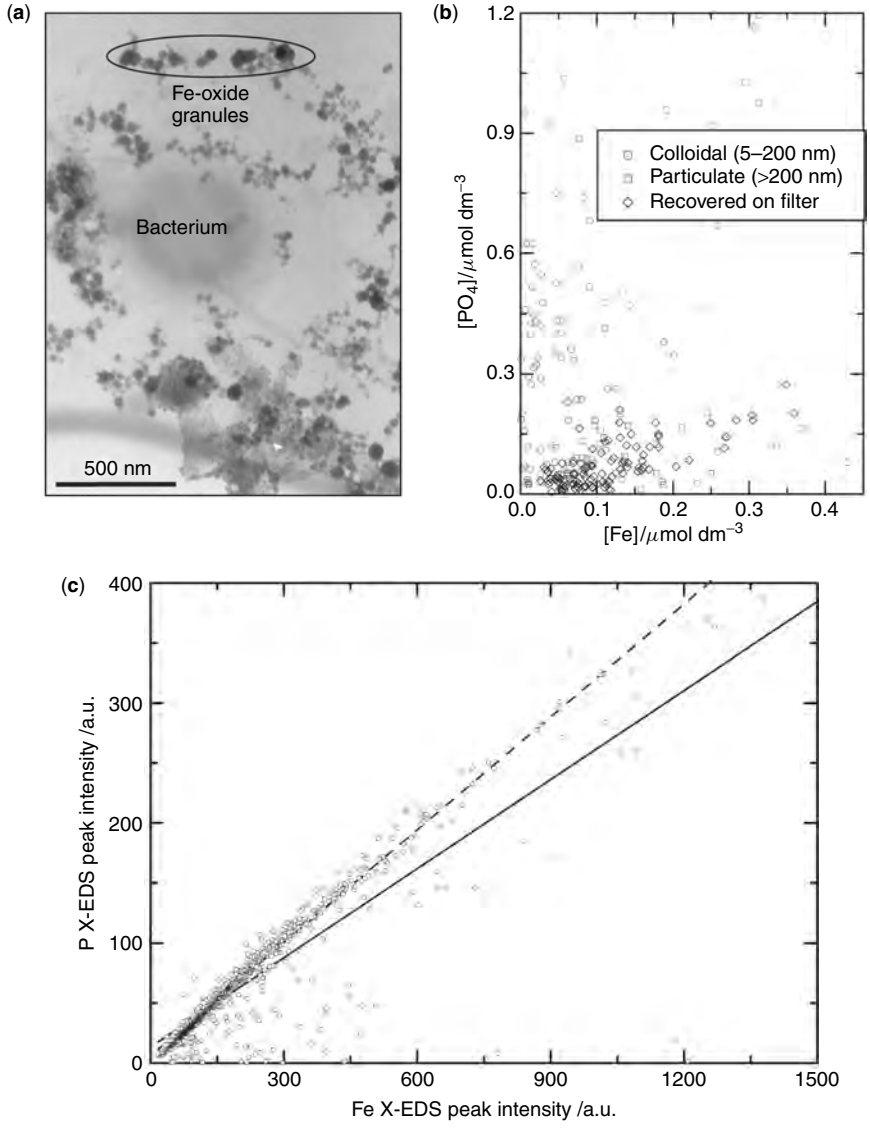

Figure 13. The stoichiometric nature of the association between iron and phosphorus in iron-rich nanogranules isolated from a large lake [234] cannot be expressed in terms of bulk chemical analyses, but requires the TEM–X-EDS analysis on a large set of individual entities. (**a**) Ubiquitous assemblage of Fe-rich nanogranules attached to polysaccharides of biotic origin. (**b**) Bulk chemical analyses of Fe_{tot} and PO_{4tot} in different size fractions of the lake column (obtained by filtration and ultrafiltration). Because of the high heterogeneity of particle types in the water samples, there is no apparent correlation between the two elements, suggesting that phosphorus is not specifically bound to Fe-rich particles. (**c**) TEM–X-EDS analysis of 1096 individual Fe-rich granules (probe size: 50–400 nm). Owing to the visual 'separation' that can be applied during TEM analysis (i.e. only particles exhibiting specific morphological characteristics are analysed by X-EDS), the strong correlation between the two elements indicates that phosphorus is indeed stoichiometrically bound to Fe-rich granules (after conversion of X-EDS peak intensities into element concentrations, $[Fe_{part}]/[P_{part}] = 0.5 \pm 0.04$ for 90% of the granules)

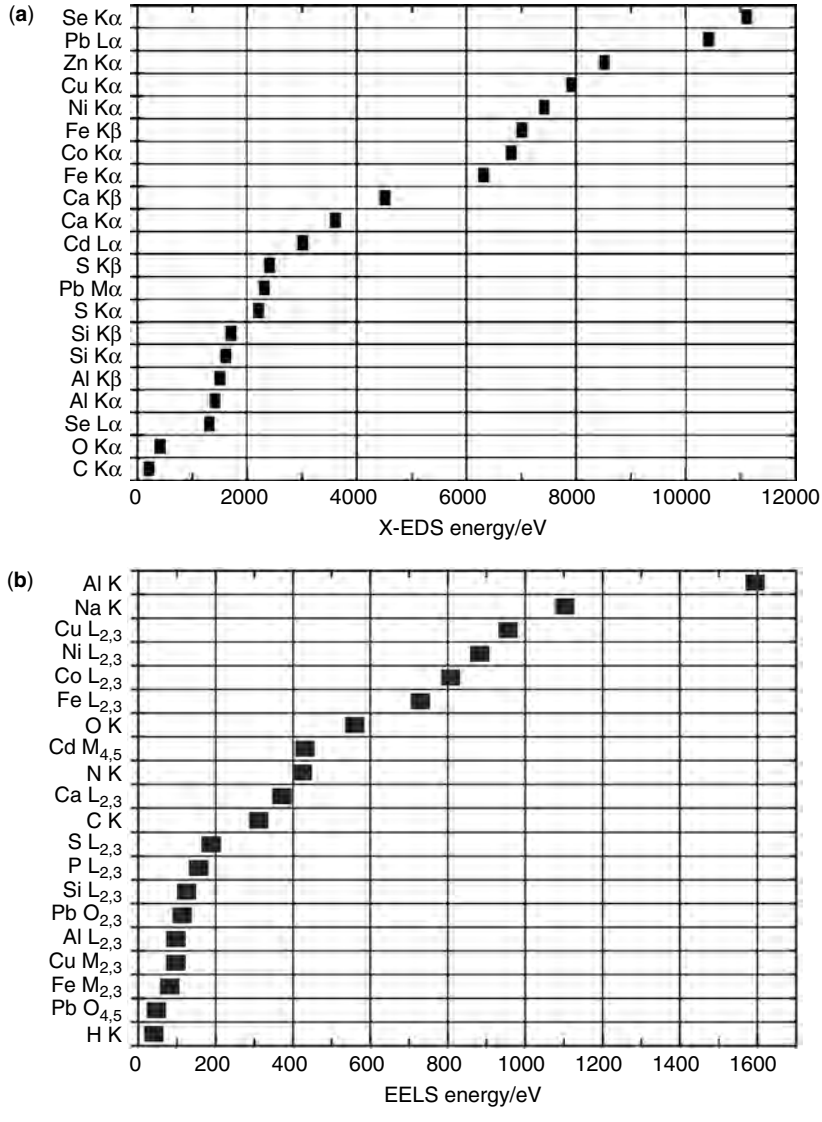

Figure 14. Energies of X-EDS peaks (**a**) and EELS edges (**b**) of some of the most relevant environmental elements; only the most prominent peaks and edges are shown

powerful analytical tool [42,44,45,50,228–233]. Under optimal conditions employing an X-EDS detector equipped with an ultrathin window (and with a parallel beam using the nano mode, if available on the apparatus), even carbon can be quantified, and the detection limits for trace metals can be as low as 500–1000 mg kg^{-1}, even for sub-micrometric particles, provided that the peaks of trace elements of interest are not overlapped by those of other elements (Figure 15).

The X-EDS method is particularly well suited for elements emitting $K\alpha$ peaks in the sensitive 0–10 keV energy range, but L-emitting elements can also be measured in

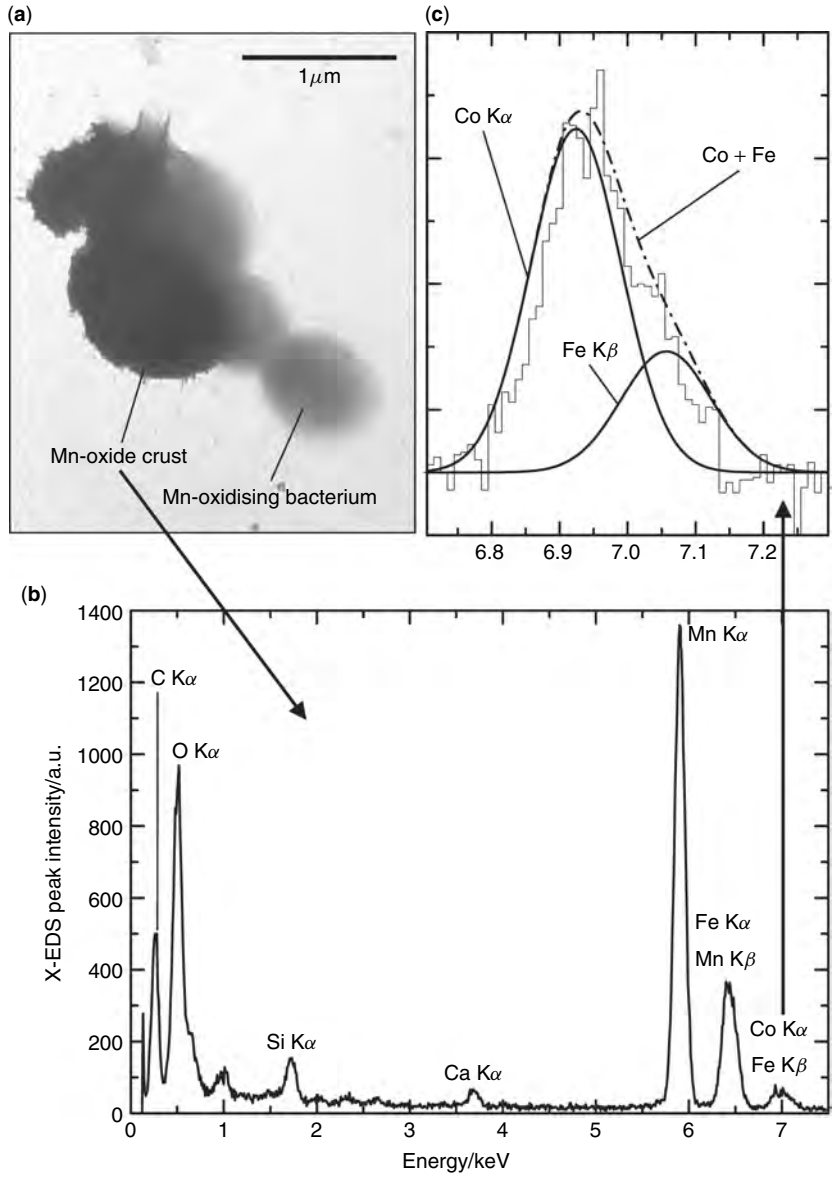

Figure 15. TEM–X-EDS analyses can be performed to highlight the presence of trace elements associated with elements constituting the bulk matrix of the particle of interest. (**a**) Manganese-oxidising bacteria isolated from the oxic–anoxic interface of a small lake [19]. The dark component is a crust of manganese oxide. (**b**) X-EDS spectrum (2 nm spot) of the Mn-rich crust shown in the micrograph. The crust contains mostly $MnO_x(OH)_y$ with impurities of Si, Ca and Fe in non-stoichiometric proportions. The Kα peak of iron (6.398 keV) overlaps the Kβ peak of manganese (6.489 keV). (**c**) A detailed observation of the weak contribution around 7 keV indicates that traces of cobalt (Kα = 6.924 keV) overlap the weak Kβ peak of iron (7.057 keV). Standardless analysis and spectral deconvolution of the Fe Kα + Mn Kβ peaks around 6.4 keV and of the Co Kα + Fe Kβ peaks around 7 keV reveal that the manganese oxide crust contains approximately 2% cobalt

this range, provided that they are not present as trace elements. Quantitative X-EDS analysis is currently an excellent method (and probably the method of choice, provided that the sensitivity is sufficient) for the quasi-routine detection of trace elements bound by particles and the search for stoichiometric relationships between different elements in similar morphotypes [4,34,234].

5.2 ELECTRON ENERGY-LOSS SPECTROSCOPY (EELS) AND RELATED TECHNIQUES

EELS techniques [228,231,232,235–257], employed in either imaging or spectrum modes, are capable of detecting single atoms with energy resolutions as low as 0.2 eV in the useful 0–1000 eV energy range (Figure 14). In comparison, high-resolution X-EDS is achieved at not less than *ca.* 150 eV. This ability has been clearly demonstrated in materials science and even in biological science. Regrettably, however, EELS is not commonly used in environmental science, although several researchers have developed specific methods for the utilisation of EF-TEM and TEM–EELS in the aquatic sciences [19,258,259]. It has to be said, moreover, that the interpretation of spectra is not as clear-cut as in X-EDS, because (i) the technique is best suited for light elements (although transition metals yield valuable spectral information), (ii) the extraction of the EELS K- or L- or even M-edges of elements requires a careful and substantial stripping of the background (in accordance with the power law $I = aE^{-b}$), (iii) the region below *ca.* 100 eV (plasmons region) is difficult to model with accuracy, (iv) there remain uncertainties in the determination of the cross-sections of the M-edges used for absolute quantification purposes and (v) EELS is theoretically best suited for specimens with thicknesses below 20–50 nm. Although it has been demonstrated that the technique can be used to quantify thicker (<500 nm) environmental particles [67], accuracy drops as specimen thickness increases.

In its simplest expression, EELS can be performed in energy-filtered (EF-TEM [33]) or electron spectroscopic imaging (ESI) mode, i.e. to generate element maps, but EELS in spectroscopic mode is better suited for quantitative analysis, with a high energy and lateral resolution (Figure 16).

The main advantage of EELS over X-EDS is its ability to yield molecular information in the form of specific features at and beyond the edges (Figure 17). Energy-loss near-edge structure (ELNES; which extends up to 50–100 eV beyond the edge) is the counterpart of X-ray absorption near-edge structure (XANES) in X-ray spectroscopy. Its features provide qualitative information about the molecular environment of the element giving rise to an EELS edge. For instance, the shape of an EELS–ELNES spectrum is different for aromatic, aliphatic or amorphous organic carbon centres or inorganic carbon centres. EELS spectra acquired with a high energy resolution (<0.5–1 eV) may also reveal the electronic configuration of redox-sensitive elements (*e.g.* Fe^{2+} vs Fe^{3+}, or mixtures of these two oxidation states in the same entity; Mn^{2+} vs Mn^{3+} vs Mn^{4+}; Figure 17). Although exemplary results have already been obtained on pure crystalline iron and manganese minerals, the approach is, as yet, far from routine for complex heterogeneous environmental particles. Similarly, the use of EELS for the redox discrimination of elements of environmental concern such as Cr^{3+}/Cr^{6+}, Cu^{+}/Cu^{2+}, $As^{3-}/As^{3+}/As^{5+}$, $Sb^{3-}/Sb^{3+}/Sb^{5+}$ or $Se^{2-}/Se^{4+}/Se^{6+}$ has not yet been reported.

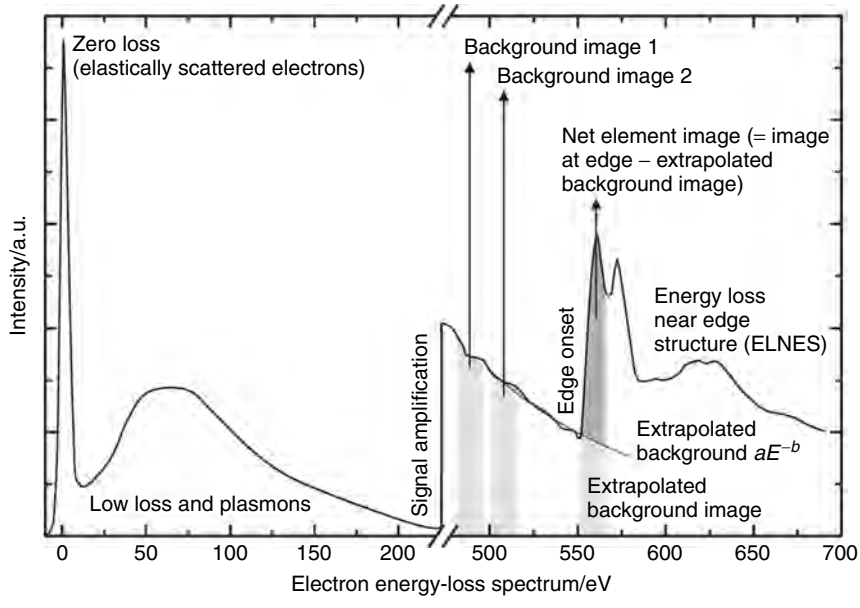

Figure 16. Scheme of a typical EELS spectrum showing several regions of interest. The image that can be obtained at the zero loss is roughly similar to the conventional bright-field image, but with sharper and more contrasted details because aberrations due to inelastically scattered electrons are stripped out. Electron spectroscopic imaging (ESI), i.e. element mapping, requires the recording of two images over a given window at different energies prior to the absorption edge and a third image at the absorption edge of the element of interest. The third image is used to strip the extrapolated background image from the gross image at the edge, and to extract specifically the net image of the element. ESI in the low-loss and plasmons region is feasible, but background extrapolation is more difficult. The ELNES region is used for qualitative molecular information (fingerprint of the molecular environment of the element)

6 APPLICATIONS OF EM AND AEM FOR THE UNDERSTANDING OF PHYSICOCHEMICAL PATHWAYS IN THE ENVIRONMENT

6.1 SELECTED CASE STUDIES RELATING PARTICLE CHARACTERISATION TO CONTAMINANT TRANSPORT

Using a multi-method approach with TEM, Campbell *et al*. [8] demonstrated the accumulation of nanoparticles of natural organic matter on the surfaces of living cells (two algal species and cells isolated from fish gills). Using environmentally relevant pH values and organic matter concentrations, they produced data consistent with the idea that the nanoparticles might exert a *direct* effect on organism physiology at the interface between living cell and aquatic environment. They also presented some interesting and unconventional implications of their findings regarding the interactions of toxic solutes with aquatic biota.

In 1998, Leppard *et al*. [17] isolated microparticles and flocs from the surface waters of Hamilton Harbor (Ontario, Canada) by size class (in ranges from <0.02 to >80 μm), and then analysed each size class for polycyclic aromatic hydrocarbons (PAHs), which presented a serious contamination problem in the harbour. Using TEM, SEM and STEM–

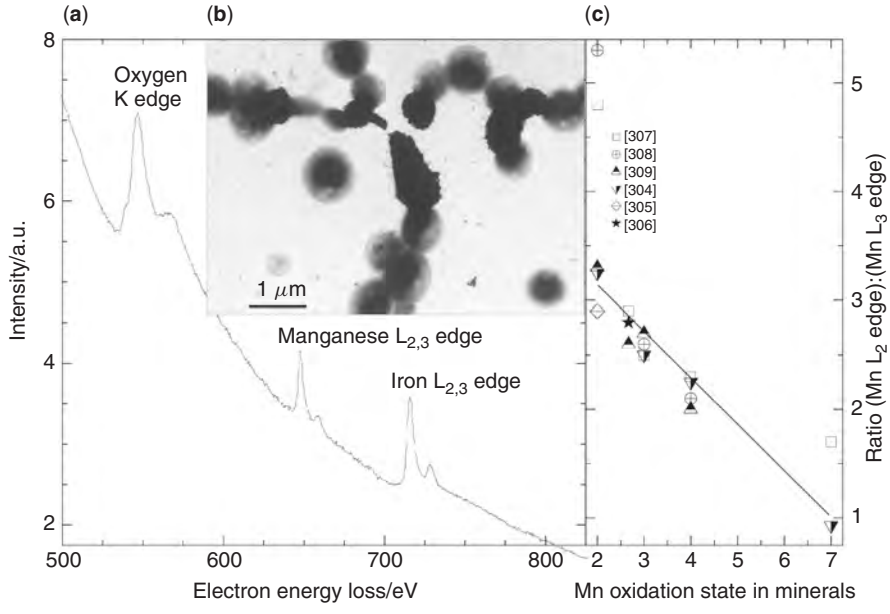

Figure 17. (**a**) EELS spectrum of a complex mixture of manganese oxides and iron oxides at the surface of colonies of Mn-oxidising bacteria (**b**) (see also Figure 15) at the oxicline of a eutrophic lake [19,142]. The presence of iron on the manganese crust is due to aggregation in the water column during sedimentation of the $MnO_x(OH)_y$ bacteria in the Fe-rich layers. The exclusive features of the $L_{2,3}$ absorption edges of the redox-sensitive elements Mn and Fe allow clues on their oxidation states. (**c**) The ratio of the L_2 and L_3 absorption edges of manganese changes with the oxidation state of Mn [304–309]. This ratio is, however, highly dependent on the conditions of specimen preparation and EELS measurement

X-EDS in tandem, they found that the microparticles and flocs consisted mainly of aggregated colloids, among them numerous nanoparticles [260] of minerals (clays, iron oxyhydroxides, manganese-rich colloids and biogenic silica) and organic matter (cell debris, fibrils and humic substances). Heterogeneous porous flocs larger than 20 μm accounted for 98% of phenanthrene binding, 89% of fluoranthene binding and 85% of pyrene binding.

In 2000, Mavrocordatos *et al*. [4] used AEM in an interdisciplinary investigation of individual colloids in successive compartments of a complex peat–karst–spring ecosystem (Vallée-des-Ponts, Switzerland). Their results revealed that globules rich in humic matter (identifiable by their characteristic morphology) formed intimate associations with colloidal iron and then underwent specific physicochemical transformations during their transport through a karstic aquifer, eventually turning into entities with drastically different properties. The investigation focused on the nanoscale characteristics of reactive particulate entities upstream and downstream from the karstic aquifer. The authors pointed out that their analytical approach should have major consequences for estimating the vulnerability of karstic aquifers to pollution events.

Also in 2000, Taillefert *et al*. [5] employed a suite of analytical techniques in conjunction with TEM to study the chemical speciation of iron and lead in the water column of a lake characterised by biogenic meromixis (Paul Lake, MI, USA). The primary goal was

to determine the effect of iron oxyhydroxides and natural organic matter on the speciation of lead, so as to understand better the cycling of lead in a natural lacustrine ecosystem. The results indicated that iron oxyhydroxides and organic fibrils aggregated together to form complex microparticles, which then became enriched in lead. Such a process would not have been accurately described by surface adsorption models.

Previously, Lienemann *et al*. [19,261] showed that sub-micrometre manganese-rich crusts produced by manganese-oxidising bacteria at the oxic–anoxic interface of this highly stratified lake had selectively preconcentrated cobalt ions with respect to the water column. As the manganese-rich and iron-rich layers partially overlapped at depth, classical bulk chemical analyses of the particulate material had to be supplemented by TEM–X-EDS measurements at the 'per particle' level to yield unambiguous insight into the selective scavenging of Pb by particulate iron and of Co by particulate manganese. Their approach, although time consuming, opened up new perspectives for documenting the speciation of toxic trace metals at the solid–solution interface.

6.2 NANO- AND MICROPARTICLES CHARACTERISED BY TEM AND AEM

6.2.1 Humic Substances

Marvin *et al*. [18] described a refined adjustable methodology for fractionating lake water contaminated by PAHs and polychlorinated biphenyls (PCBs), using TEM, STEM–X-EDS and standard images from the literature to characterise the major nano- and microparticles in the fractions richest in PAHs and PCBs. The results showed that the organic contaminants were preferentially associated with fractal aggregates of humic substances. Humic substances have also been shown to influence the formation and behaviour of iron-rich globular colloids [4,34,168,258,262]. Thus, it has been shown that acidic/anoxic peat waters slowly release into the river globule-shaped humic material (<500 nm) and stable complexes of Fe^{2+}, whereupon the Fe^{2+} is oxidised and precipitated at the surfaces of the globules when the pH, O_2 content and ionic strength of the river increase; eventually these particles scavenge quasi-stoichiometric amounts of Ca. Myneni and co-workers [263–265] used high-resolution X-ray spectromicroscopy (in conjunction with standard TEM images from the literature) to demonstrate that macromolecular structures of humic substances vary with the origin of the humic matter, the chemical composition of the ambient solution and the nature of associated minerals. Wilkinson *et al*. [37] characterised humic substances by correlative TEM and AFM, Leppard *et al*. [266] revealed morphological evidence for a fibril-to-humic substance evolution and Senesi [267] explored a fractal approach using TEM images to derive quantitative descriptions of humic substance aggregation patterns and macromolecular morphology.

6.2.2 Polysaccharide Fibrils

Leppard [268,269] provided reviews of multi-method descriptions of polysaccharide fibrils sampled from diverse aquatic ecosystems, which included TEM descriptions of fibril morphotypes and complex aggregates. Wilkinson and co-workers [37,270,271] characterised fibrils using TEM in multi-method investigations, as did Santschi *et al*. [51]. Moreover, Lienemann *et al*. [272] demonstrated a means for the enhanced visualisation of polysaccharides from aqueous suspensions and devised a method for optimal preparation of water samples for TEM examinations of colloids, including fibrils [31].

6.2.3 Iron Oxyhydroxides

Colloidal iron oxyhydroxides and their role in the biogeochemical cycling of various elements have been characterised with the aid of TEM and STEM–X-EDS in a multi-disciplinary, multi-method investigation [4,34,234,273–275]. This major research effort, which was undertaken by different teams working on a wide range of various aquatic environments, led Perret *et al*. [36] to propose a general scheme for the formation of iron oxyhydroxides. They concluded that the various morphotypes of these colloidal species in a given aquifer can be explained and predicted in terms of the physicochemical conditions (pH, ionic strength, oxic/anoxic conditions, presence of humic or fulvic acids or non-humic organic matter, *e.g.* polysaccharides, and concentrations of reacting species) prevailing in the surrounding medium. In addition, this work puts forward a new paradigm for incorporation into geochemical speciation models dealing with surface adsorption. It is generally accepted that natural organic matter has a strong tendency to coat the outer surface of particulate material and to induce globally negative surface charges in water, but a careful EM examination of iron oxyhydroxides revealed that natural organic matter may also act as a heterogeneous template on whose surface the oxidation/precipitation of iron-rich material is favoured.

6.2.4 Viruses and Refractory Cell Debris

Many viruses are readily identified by TEM because of their unique combination of morphology and nanoscale size. This aspect of virology is of paramount interest, since viral populations can numerically dominate natural waters, with a potential as predators to alter the species composition of microbial communities whose individual activities, in turn, dominate aquatic biogeochemistry.

In 1990, Borsheim *et al*. [276] detailed a TEM-based procedure for the enumeration and biomass estimation of aquatic viruses. Proctor and Fuhrman [277–279] extended this work by relating virus population size to bacterial mortality rate. Weinbauer and Peduzzi [280–282] added important details, relating virus morphology to morphological correlations of the infection process. Danovaro *et al*. [283] employed TEM in a multi-method research initiative to determine virus abundance in sediments.

Leppard and co-workers [266,284] have provided TEM descriptions of abundant distinctive cell debris from marine waters and surface/ground waters. The latter study was related to plutonium contamination near a nuclear weapons production facility.

6.2.5 Nanoscale Mineral Agglomerates on Cell Surfaces and on the Surfaces of Extracellular Polymers

The genesis of minerals by bacteria and their extracellular polymers has become a central theme in biogeochemistry. This phenomenon has far-reaching implications and has aroused intense interest among geologists, chemists and microbiologists. A number of advances in our understanding of the microbial biogenesis of minerals which have been made with the aid of TEM and AEM analyses have been reported in the literature [9,11,12,14,15,20,21,285–287].

At present there is keen interest in natural associations of organic fibrils of EPS with other colloids, including iron oxyhydroxides in aquatic environments. Such heterogeneous

associations of abundant nanoparticles with other nanoparticles must be better understood for the sake of improving our understanding of global water processes. It is noteworthy that careful preparation of fragile hydrated specimens is helping to unravel the complexity of interactions between fibrils and other biotic or abiotic entities, such as the abundant ones prevailing in marine snow [31,288] and in wastewater flocs [7,23,118], and elucidate their biogeochemical functions. When the weak electron opacity of organic matter lacking metal-rich markers is an obstacle to its identification by TEM, nanoscale fibrils can still be visualised by means of EF-TEM at the carbon K-edge [272]. In addition, the polysaccharide character of EPS fibrils can be ascertained unambiguously by reaction with specific probes (*e.g.* Ag-proteinate [142], or oligosaccharide-specific lectins labelled with colloidal gold [27]).

For iron oxyhydroxides and their heterogeneous associations, which are virtually ubiquitous in freshwater environments, Perret *et al.* [36] demonstrated specific morphotypes whose structure is mainly a function of (i) the type of macromolecular organic matter present in the water and (ii) the relative concentrations of total iron and natural organic matter (NOM). In the presence of aquagenic EPS, which can form three-dimensional networks of fibrils, Fe–NOM associations tend to lead to the formation of iron oxide nanogranules attached to the surfaces of fibrils, especially when the ionic strength of the ambient water is high and the Fe_{tot}:NOM ratio is low. In contrast, ill-defined Fe–NOM mixtures are favoured at lower ionic strength and high Fe_{tot}:NOM ratios. In the presence of terrestrial humic/fulvic-rich materials, the final Fe–NOM entities are spherical globules made of a C-rich core surrounded by amorphous iron oxyhydroxides. It has also been shown by Lienemann *et al.* [234] that the lacustrine oxidation of Fe(II) may lead to the formation of iron oxyhydroxides which bind phosphates and have a stoichiometric quantity of phosphate and iron, and that this nutrient-scavenging process is an efficient barrier against the upward diffusion of phosphates in the water column of Lake Lugano (Switzerland), a stratified eutrophic lake. In the case of iron–humic complexes formed during the oxygenation of acidic, anoxic Fe(II)-rich peat waters [34], it has been shown by high-resolution TEM–PEELS (EELS in parallel mode) measurements of individual 100 nm globules that the abrupt rise in pH, O_2 and ionic strength in the drainage waters leads to the formation of a compact outer crust of *ca.* 2–4 nm amorphous Fe–Ca-rich granules at the surface of shrunken humic spheroids, the shape of the latter being dictated mostly by pH and ionic strength constraints.

6.3 MICROPARTICLES AS NATURAL AGGREGATES OF NANOPARTICLES

Many of the microparticles found in surface waters and engineered aquatic ecosystems are heterogeneous aggregates of microbes and nanoparticles [7,15,17,18,23,118,162]. A generalised description of colloidal interactions in water (leading potentially to the formation of microparticles) has been published by Buffle *et al.* [6], who demonstrated that the concentration of stable colloids in a given aquatic ecosystem depends on the proportions of three general classes of native colloids (compact inorganic colloids; large rigid biopolymers; and fulvic acids and similar substances). Micelle-like microparticles can form from the self-organisation of dissolved organic matter in river water [289]. For biota-rich flocs, Liao *et al.* [7] proposed a conceptual model of aggregate structure whereby the gel-like matrix consists of two physically distinct regions defined by the arrangement of

nanoscale EPS, which cross-connect individual cells of the microbiota. The physically distinct regions are likely to be differentially affected by agents applied to manipulate floc integrity. AEM and selective extraction methods have revealed heterogeneity in the packing and specific chemical composition of EPS, apparently reflecting floc stability. For marine biota-rich flocs, Heissenberger *et al*. [288] suggested a scheme (based on TEM observations) for the growth and development of marine snow and the occasional subsequent buildup of the economically undesirable mucilage in the water [268]. Heissenberger *et al*. [288] related the growth of suspended marine snow flocs to (i) secretion of nanoscale fibrils by microorganism communities and (ii) a large number of environmental processes that modulate the cross-linking activities of fibrils and the developing flocs.

6.4 SELECTED CASE STUDIES RELATING PARTICLE CHARACTERISATION TO WATER TREATMENT PROBLEMS

Liss *et al*. [118] used TEM and CLSM in parallel to describe the nano- and microscale architecture of engineered flocs sampled from an activated sludge effluent system (Thunder Bay, Ontario, Canada). At a practical resolution of 0.001 μm, they described bacteria and other colloid-sized particles embedded in a complex matrix of extracellular polymeric substances (EPS). This matrix was rich in EPS fibrils (4–6 nm diameter) which (i) acted as bridges between the diverse colloidal particles within a floc and (ii) formed the tenuous boundaries of an extensive intra-floc pore structure. Liss *et al*. [290] then used optical microscopy, TEM, STEM–X-EDS and ESEM to demonstrate correlatively that EPS at the bulk water–floc interface can aggregate so as to form a 'skin' which decreased the surface roughness of the floc. The induced formation of this 'nanoscale skin', which is highly relevant to economically important floc settling problems in water treatment tanks, was achieved by a laboratory manipulation that is potentially capable of being scaled up to an industrial treatment system. Liao *et al*. [7] employed a variety of physicochemical techniques including TEM, to analyse interparticle interactions affecting the stability of sludge flocs sampled from laboratory scale sequencing batch reactors. Focusing on the three-dimensional arrangement and packing of fibrils, they proposed a conceptual model of floc architecture which relates EPS nanoparticles to floc stability in engineered water treatment systems. Since this model was proposed, an interdisciplinary AEM study of contaminated wastewater flocs has demonstrated that various nanoscale flocs immobilise heavy metals differentially [23]. This finding has implications for heavy metal recovery from activated sludge and reuse of the metals.

6.5 CORRELATIVE USE OF TEM WITH AFM AND STXM

Correlative TEM and AFM analyses of aquatic organic nanoparticles (especially aggregated polysaccharides and humic substances) are being conducted to ascertain better the activities and behaviour of organic macromolecules in natural waters. On examining water samples from different marine environments, estuarine and surface and deep waters, Santschi *et al*. [51] found that an important fraction of the colloidal organic matter dispersed in the water consisted of fibrils rich in polysaccharides. Although both techniques were subject to potential artefacts (which could be minimised), the two used in tandem were found to be complementary, especially when used in a multi-method context with standard techniques. Wilkinson *et al*. [266] have developed multi-method approaches to

the characterisation of the supramolecular microscopic structure of humic substances and polysaccharides, whose roles in aquatic biogeochemistry and ecology are largely dependent on their supramolecular structure, and which cannot be determined by bulk chemical methods alone.

Verdugo *et al*. [291] endorsed the correlative use of AFM and TEM to analyse 'oceanic gel phase', polymer gel particles, which are abundant and important in biogeochemical cycling, sedimentation processes, the microbial loop (cycling of elements by microbes), marine carbohydrate chemistry and particle dynamics in the oceans. These gel particles are mainly three-dimensional colloidal networks of biopolymers suspended in sea water, and they range in size from the nanoscale (single macromolecules entwined), to the microscale (networks of colloids), and on to the gross scale (aggregated polymer networks of near millimetre overall size). Regarding the investigation of colloidal environmental particles in general (both aquatic and atmospheric), Mavrocordatos *et al*. [292] discussed the advantages of combining AFM and TEM observations, in a correlative multi-method approach, with data from STEM–X-EDS, TEM–EELS, SEM, FIB and TEM–SAED (selected-area electron diffraction). They provided general guidelines for the effective use of microscopy and presented examples of diverse analyses (including analyses of biofilms, combustion particles, biofouled membranes, biogenic minerals and particle/contaminant associations).

Correlative TEM, STXM and CLSM analyses of colloidal extracellular organic polymeric substances comprising the mucilaginous matrix of a microbial biofilm were described by Lawrence *et al*. [27]. Their goals were to achieve a better understanding of the three-dimensional configurations of the major classes of organic macromolecules within the colloidal matrix structure serving as a habitat for the microbial communities of the biofilms. CLSM and fluorescent probes were used initially on a fresh sample to ascertain the gross architecture of the biofilm matrix and to map out the overall distribution of several abundant extracellular polysaccharides as related to the density and nature of microbe associations. The same fresh sample was subjected to a synchrotron analysis for confirmation of the gross architecture by STXM at a higher spatial resolution; the known abundant macromolecules were used as probes. The different major classes of macromolecules (polysaccharides, proteins, lipids and nucleic acids) were localised and distinguished from each other in a given image, on the basis of their interactions with soft X-rays. Details of the important features were then examined by TEM at much higher resolution, with identification of key nanoscale features.

Chan *et al*. [20] examined the growth of (sub-micrometre) iron oxyhydroxide filaments by combining data from TEM and STXM to yield novel observations of a biological process relevant to biomineralisation. SEM was used for orientation to show fibrils and mineralised filaments protruding from a microbial cell, high-resolution TEM was used to examine nanoscale morphological details within the growing mineralised filaments, and both STXM and X-PEEM (X-ray photoemission electron microscopy) were used to obtain chemical data. Chan *et al*. [20] infer that cells synthesised and then extruded polysaccharide macromolecules in the form of nanoscale-size fibrillar packets (insofar as the smallest diameter was concerned), with the polysaccharide fibrils subsequently localising FeOOH precipitation in proximity to the cell membrane, and thus harnessing a proton gradient for energy production. An organic template coupled to metabolic activity thus generated an iron-rich filament having a specific mineralogy and nanoscale morphology.

Hitchcock *et al.* [293] reviewed the most recent advances in STXM describing instrumentation and acquisition protocols and outlining methods for conversion of image sequences to quantitative maps of chemical components. Moreover, they discuss an example of the correlation of STXM data with CLSM data taken from an identical region of a biofilm. The work also integrated the use of STXM and TEM to characterise selected morphological features of the biofilms with nanoscale resolution (1–3 nm), which is not currently obtainable with STXM [27]. Through the application of adjustable soft X-rays and appropriate analysis of X-ray absorption spectra in the form of NEXAFS image sequences, quantitative chemical mapping at a spatial scale below 50 nm is now achievable [293,294]. To supplement the progress being made with STXM in the analysis of environmental materials, Lerotic and co-workers [295,296] described a method to find natural groupings of spectromicroscopic data without prior knowledge of the spectra of all components. Their approach permits visualisation of nanoscale speciation in complex specimens.

6.6 ACCURATE SELECTION OF TARGET SPECIES AND FINGERPRINTING OF BIOMINERALISATION

Cyanobacteria are important agents of calcite ($CaCO_3$) precipitation in natural waters, but the detailed mechanisms of nucleation of $CaCO_3$ and the influence of abiotic and biotic factors are still debatable. Laboratory experiments employing cultures of specific cyanobacteria under strictly controlled conditions, performed in combination with AEM of selected specimens, may allow an insight into the initial stages of $CaCO_3$ precipitation. Experiments performed by Dittrich and co-workers [297–300] have shown that the picocyanobacterium *Synechococcus* accelerates the nucleation and growth of $CaCO_3$ crystals in waters with low alkalinity (<2 mmol dm^{-3}), high saturation ($[Ca^{2+}][CO_3^{2-}]/K_{sp} = 5–7$) and a high Ca^{2+}/CO_3^{2-} ratio. While SEM reveals that calcite crystals are almost systematically attached to *Synechococcus* (Figure 18a) and even embedded in the cells at later stages of growth (Figure 18b), the FIB preparation of targeted specimens (Figure 18c and d) for TEM observation (Figure 18e) and TEM–EELS fingerprinting (Figure 18f) have proved to be an efficient way to elucidate the chemical bonds at the cell–crystal interface. $CaCO_3$ crystals are intimately bound to the surface of the *Synechococcus* cell, and the cell–crystal interface can be clearly discriminated by EELS owing to the specific features of the EELS near-edge structure of C_{org} (cell fraction; C–C and C=C bonds) and C_{inorg} (crystal fraction; C=O bond). In this example, an ingenious combination of high-resolution AEM techniques (FIB + TEM + EELS) may allow conclusions to be drawn at the molecular level.

6.7 AGGREGATION AND SEDIMENTATION OF ORGANIC MATTER IN LAKE WATER

Natural organic matter (NOM) in lakes strongly influences the fate and behaviour of toxic substances and nutrients. Depending on its nature (*e.g.* whether it is humic matter of terrestrial origin or is made up of non-humic compounds, such as polysaccharides of aquatic origin), NOM will follow different pathways of biophysicochemical transformation that will influence its aggregation and sedimentation properties, which, in turn, will affect

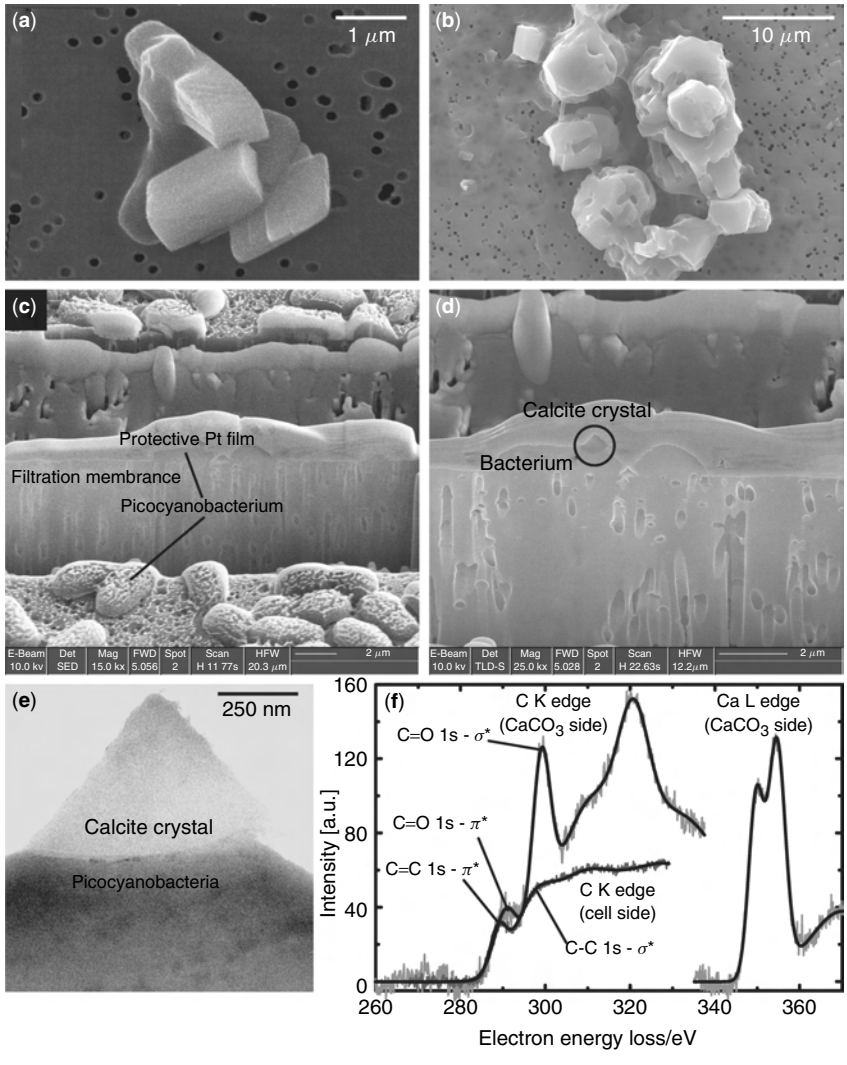

Figure 18. *Synechococcus* picocyanobacteria cells catalyse the growth of calcite crystals onto their surface (**a**) and may even become embedded in calcite at a later stage of precipitation (**b**). (**c**) FIB is used to mill a selected portion of a cell specimen being prepared by filtration on to Nuclepore membranes. The SEM micrograph (**d**) of the FIB-prepared section reveals the presence of a calcite crystal (circle; the layer above the cell–crystal interface is a protective platinum coating). The equivalent TEM micrograph (**e**) highlights the interface between the cell surface and the calcite crystal. (**f**) EELS of the cell and the crystal shown in (**d**) and (**e**), revealing the different patterns of the carbon K-edge for the cell (organic carbon) and the crystal (inorganic carbon)

the distribution of the toxic substances and nutrients it transports. In a survey of the water column of Lake Geneva (Switzerland), Mavrocordatos and Wilkinson [301] distinguished colloidal organic substances from inorganic colloids by their poorly developed electron diffraction patterns, sizes, low electron density and ill-defined shapes when viewed by TEM. The micrographs of organic colloids were digitised, thresholded and binarised with

care to minimise image analysis artefacts. Two mathematical models were applied to calculate the fractal dimension, *Df*, of the resulting objects: the Minkowski model based on the contour of the object (Figure 19a), and the Witten–Sanders model based on the center of mass of the object (Figure 19b).

The absolute values of *Df* were different for the two mathematical operations (Minkowski, $Df = 1.22–1.1$; Witten–Sanders, $Df = 1.9–1.75$), and no clear conclusion

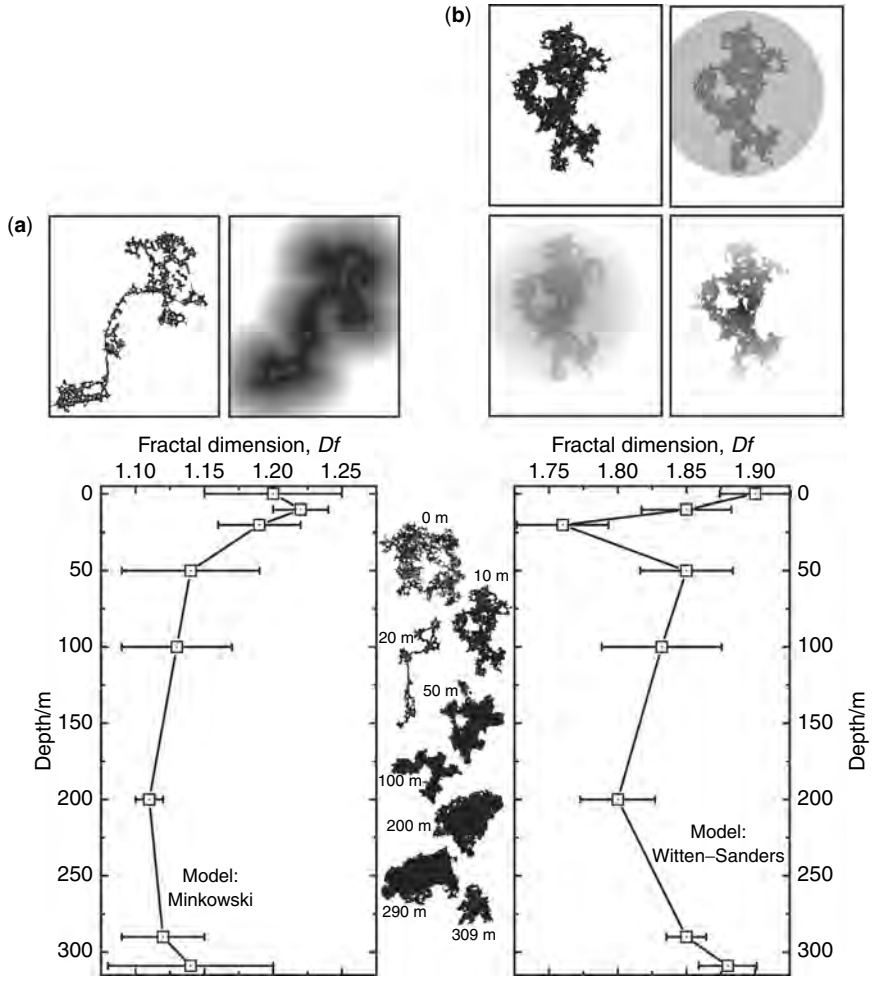

Figure 19. (**a**) The two images at top left show the binarised TEM image of an organic colloid in the water column of a deep lake and the corresponding Euclidean distance map used to calculate the fractal dimension (*Df*) of the colloid by the Minkowski approach, which gives an estimate of the compactness of the object. (**b**) The four images at top right schematise the Witten–Sanders approach, which consists in drawing concentric circles centered on the binarised colloid, to determine the number of intersections between the circles and the object. *Df* is derived from the relationship between the number of intersections and distance. The two profiles at the bottom show the evolution of *Df* with depth in the lake. Typical examples of binarised organic colloids found at different depths are given between the two plots

could be drawn regarding the conditions that typically promote aggregation of NOM in the water column, or whether the phenomenon is diffusion-limited or reaction-limited, owing to the heterogeneous nature of the polysaccharide–humic matter complexes that constituted the colloids. The two models demonstrated a gradual decrease in the fractal dimension of the objects with depth, followed by a weak increase in *Df* at the water–sediment interface, reflecting both compaction of refractory NOM as it settles and heterogeneity of colloidal NOM at the sediment–water interface.

6.8 COPPER SCAVENGING FROM ROOF RUNOFF

Among heavy metal contaminants in the environment, copper is ubiquitous owing to its wide use in human activities. Cu in runoff may originate in large part from corroding copper surfaces on roofs. For example, up to 50% of the Swiss copper load in sewer systems can be related to roof runoff. These potentially dangerous fluxes (Figure 20) can be limited by selective on-site filter/adsorbent systems, consisting of impacted iron oxides (5–500 nm), through which roof runoff is passed. Mavrocordatos *et al*. [302] tested the scavenging efficiency of the iron oxide filter by means of quantitative ultracentrifugation, SEM–FIB sectioning and TEM–EELS identification of the adsorbing material. They observed that up to 95–99% of the copper present in roof runoff was retained by the iron oxide adsorbent. As shown in Figure 20, high-resolution EF-TEM maps of the granular iron oxides revealed that Cu was evenly distributed within the impacted filter/adsorbent particles as a result of their high permeability and surface area (water diffuses through nanochannels in the porous iron oxide). In addition, iron oxides are effective scavengers of heavy metals such as Cu^{2+}, because they have many sites where metal ions can be strongly bound by surface complexation.

Moreover, iron oxides were shown to be surrounded by a relatively thick layer of Cu (up to 20 nm), which may be attributed to a carbonate form, $Cu_2(OH)_2CO_3$, in agreement with the physicochemical conditions of the ambient medium (pH = 7.5) and the EELS correlations between copper and carbon at the nanometre scale. For the sake of fine adjustment of the chemical behaviour of the filter/adsorbent material with respect to copper, Mavrocordatos *et al*. [303] synthesised hydrous ferric oxides and reacted them with solutions containing Cu^{2+} at various concentrations; using a combination of optimal specimen preparation (ultracentrifugation on to holey carbon film) and high-resolution parallel EELS (PEELS; see Figure 20), they were able to demonstrate that EELS yields quantitative information even for trace metals.

7 CONCLUSION

The above selection of applications of analytical electron microscopy in water science exemplifies the progress achieved during the past decade in the development of highly efficient morphological and chemical techniques for characterisation of living and non-living microscopic entities in the natural environment on the micro- and nanometre scales.

Having progressed beyond its infancy, correlative AEM has become part of an integrated characterisation process applicable to raw or treated waters, from initial sampling to final quantitative results. At every step of the complete process, biases have been identified

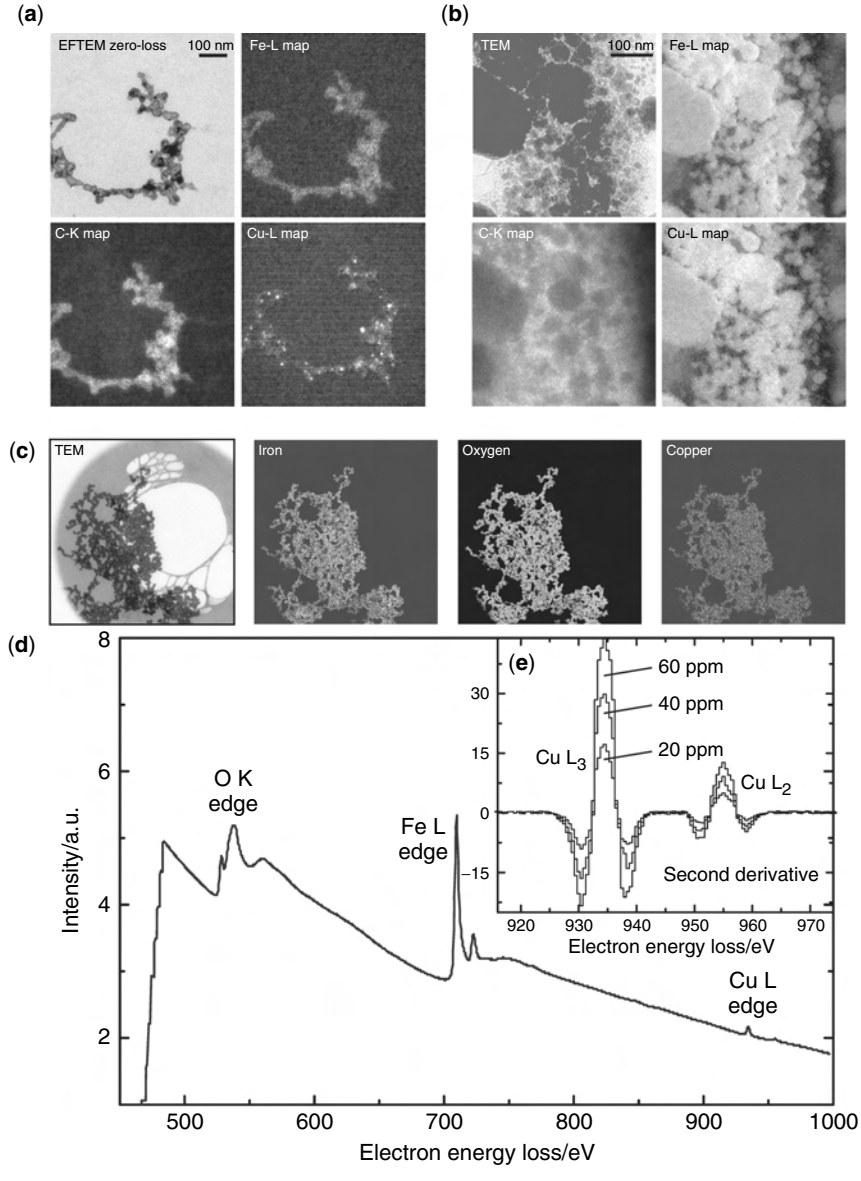

Figure 20. (**a**) Roof runoffs typically transport aggregates containing carbon, iron oxides and traces of copper; EFTEM element maps show that Cu is unevenly distributed in the aggregate and forms individual nanogranules. (**b**) The impacted iron oxide filter/adsorbent retains most of the copper in the runoffs. EFTEM element maps of this FIB section show that Cu is evenly distributed within the filter/absorbent. (**c**) Laboratory experiments on synthetic hydrous ferric oxides (HFO) reacted with copper and mimic the filter/adsorbent. (**d**) The high-resolution EELS spectrum of Cu–HFO indicates the presence of copper, even at relatively high electron energy-losses. (**e**) The inset shows that the intensity of the Cu $L_{2,3}$ edge (second derivative for correct analysis) is directly linked to the concentration of Cu reacted with synthetic HFO

and overcome, while quantitative and representative specimen preparation schemes have been developed. The most suitable techniques of microscopy have been pinpointed and optimised in accordance with the specific requirements of the samples and finally, thanks to the power of image analysis software, representative and quantitative morphological and compositional parameters can be measured.

These days, microscopic techniques are no longer used merely to produce representative qualitative images of particulate matter in natural waters. They are also used very profitably to complement conventional bulk measurements and analyses, producing a wealth of information about variations in physical and chemical properties of sample materials on a microscopic scale, information that is far beyond the reach of the conventional methods.

LIST OF ABBREVIATIONS

AEM	Analytical electron microscopy
AFM	Atomic force microscopy
CLSM	Confocal laser scanning microscopy
Df	Fractal dimension
DLCA	Diffusion-limited colloid aggregation
ECD	Equivalent circle diameter
X-EDS	Energy-dispersive X-ray spectroscopy
EELS	Electron energy-loss spectrometry
EF-TEM	Energy-filtered transmission electron microscopy
ELNES	Energy-loss near-edge structure
EM	Electron microscopy
EPS	Extracellular polymeric substances (exocellular polysaccharides)
ESEM	Environmental scanning electron microscopy
ESI	Electron spectroscopic imaging
FEG	Field emission gun
FIB	Focused ion beam
ICP-AES	Inductively coupled plasma atomic emission spectrometry
ICP-MS	Inductively coupled plasma mass spectrometry
NOM	Natural organic matter
PAH	Polycyclic aromatic hydrocarbon
PCB	Polychlorinated biphenyl
PEELS	Parallel electron energy-loss spectrometry
PIXE	Proton-induced X-ray emission
PSD	Particle size distribution
RG	Radius of gyration
RLCA	Reaction-limited colloid aggregation
ROI	Region of interest
SAED	Selected-area electron diffraction
SEM	Scanning electron microscopy
SF	Shape factor
SMPS	Scanning mobility particle sizer
STEM	Scanning-transmission electron microscopy

STM	Scanning tunnelling microscopy
STXM	Scanning-transmission X-ray microscopy
TEM	Transmission electron microscopy
XANES	X-ray absorption near-edge structure
X-EDS	X-ray energy-dispersive spectroscopy
XRF	X-ray fluorescence
XRD	X-ray diffraction

REFERENCES

1. Doucet, F. J., Maguire, L. and Lead, J. R. (2004). Size fractionation of aquatic colloids and particles by cross-flow filtration: analysis by scanning electron and atomic force microscopy, *Anal. Chim. Acta*, **522**, 59–71.
2. Gustafsson, O. and Gschwend, P. M. (1997). Aquatic colloids: concepts, definitions, and current challenges, *Limnol. Oceanogr.*, **42**, 519–528.
3. El Samrani, A. G., Lartiges, B. S., Ghanbaja, J., Yvon, J. and Kohler, A. (2004). Trace element carriers in combined sewer during dry and wet weather: an electron microscope investigation, *Water Res.*, **38**, 2063–2076.
4. Mavrocordatos, D., Mondi-Couture, C., Atteia, O., Leppard, G. G. and Perret, D. (2000). Formation of a distinct class of Fe–Ca(–C_{org})-rich particles in a complex peat–karst system, *J. Hydrol.*, **237**, 234–247.
5. Taillefert, M., Lienemann, C. P., Gaillard, J. F. and Perret, D. (2000). Speciation, reactivity, and cycling of Fe and Pb in a meromictic lake, *Geochim. Cosmochim. Acta*, **64**, 169–183.
6. Buffle, J., Wilkinson, K. J., Stoll, S., Filella, M. and Zhang, J. (1998). A generalized description of aquatic colloidal interactions: the three-colloidal component approach, *Environ. Sci. Technol.*, **32**, 2887–2899.
7. Liao, B. Q., Allen, D. G., Leppard, G. G., Droppo, I. G. and Liss, S. N. (2002). Interparticle interactions affecting the stability of sludge flocs, *J. Colloid Interface Sci.*, **249**, 372–380.
8. Campbell, P. G. C., Twiss, M. R. and Wilkinson, K. J. (1997). Accumulation of natural organic matter on the surfaces of living cells: implications for the interaction of toxic solutes with aquatic biota, *Can. J. Fish. Aquat. Sci.*, **54**, 2543–2554.
9. Chatellier, X., Fortin, D., West, M. M., Leppard, G. G. and Ferris, F. G. (2001). Effect of the presence of bacterial surfaces during the synthesis of Fe oxides by oxidation of ferrous ions, *Eur. J. Miner.*, **13**, 705–714.
10. Chatellier, X., West, M. G., Rose, J., Fortin, D., Leppard, G. G. and Ferris, F. G. (2004). Characterization of iron-oxides formed by oxidation of ferrous ions in the presence of various bacterial species and inorganic ligands, *Geomicrobiol. J.*, **21**, 99–112.
11. Fortin, D. (2004). Geochemistry: what biogenic minerals tell us, *Science*, **303**, 1618–1619.
12. Jackson, T. A. and Leppard, G. G. (2002). Energy dispersive X-ray microanalysis and its applications in biogeochemical research, *Dev. Soil Sci.*, **28A**, 219–260.
13. Jackson, T. A., West, M. M. and Leppard, G. G. (1999). Accumulation of heavy metals by individually analyzed bacterial cells and associated nonliving material in polluted lake sediments, *Environ. Sci. Technol.*, **33**, 3795–3801.
14. Schultze-Lam, S., Fortin, D., Davis, B. S. and Beveridge, T. J. (1996). Mineralization of bacterial surfaces, *Chem. Geol.*, **132**, 171–181.
15. Webb, S. M., Leppard, G. G. and Gaillard, J. F. (2000). Zinc speciation in a contaminated aquatic environment: characterization of environmental particles by analytical electron microscopy, *Environ. Sci. Technol.*, **34**, 1926–1933.
16. Lartiges, B. S., Deneux-Mustin, S., Villemin, G., Mustin, C., Barres, O., Chamerois, M., Gerard, B. and Babut, M. (2001). Composition, structure and size distribution of suspended particulates from the Rhine River, *Water Res.*, **35**, 808–816.

17. Leppard, G. G., Flannigan, D. T., Mavrocordatos, D., Marvin, C. H., Bryant, D. W. and McCarry, B. E. (1998). Binding of polycyclic aromatic hydrocarbons by size classes of particulate in Hamilton Harbor water, *Environ. Sci. Technol.*, **32**, 3633–3639.
18. Marvin, C. H., Leppard, G. G., West, M. M., Stern, G. A., Boden, A. R. and McCarry, B. E. (2004). Refined tunable methodology for characterization of contaminant–particle relationships in surface water, *J. Environ. Qual.*, **33**, 2132–2140.
19. Lienemann, C. P., Taillefert, M., Perret, D. and Gaillard, J. F. (1997). Association of cobalt and manganese in aquatic systems: chemical and microscopic evidence, *Geochim. Cosmochim. Acta*, **61**, 1437–1446.
20. Chan, C. S., De Stasio, G., Welch, S. A., Girasole, M., Frazer, B. H., Nesterova, M. V., Fakra, S. and Banfield, J. F. (2004). Microbial polysaccharides template assembly of nanocrystal fibers, *Science*, **303**, 1656–1659.
21. Fortin, D., Ferris, F. G. and Beveridge, T. J. (1997). Surface-mediated mineral development by bacteria, *Rev. Miner.*, **35**, 161–180.
22. Leppard, G. G. and Droppo, I. G. (2003). The need and means to characterize sediment structure and behavior prior to the selection and implementation of remediation plans, *Hydrobiologia*, **494**, 313–317.
23. Leppard, G. G., Droppo, I. G., West, M. M. and Liss, S. N. (2003). Compartmentalization of metals within the diverse colloidal matrices comprising activated sludge microbial flocs, *J. Environ. Qual.*, **32**, 2100–2108.
24. Liao, B. Q., Bagley, D. M., Kraemer, H. E., Leppard, G. G. and Liss, S. N. (2004). A review of biofouling and its control in membrane separation bioreactors, *Water Environ. Res.*, **76**, 425–436.
25. He, Q. H., Leppard, G. G., Paige, C. R. and Snodgrass, W. J. (1996). Transmission electron microscopy of a phosphate effect on the colloid structure of iron hydroxide, *Water Res.*, **30**, 1345–1352.
26. Droppo, I. G., Leppard, G. G., Flannigan, D. T. and Liss, S. N. (1997). The freshwater floc: a functional relationship of water and organic and inorganic floc constituents affecting suspended sediment properties, *Water Air Soil Pollut.*, **99**, 43–54.
27. Lawrence, J. R., Swerhone, G. D. W., Leppard, G. G., Araki, T., Zhang, X., West, M. M. and Hitchcock, A. P. (2003). Scanning transmission X-ray, laser scanning, and transmission electron microscopy mapping of the exopolymeric matrix of microbial biofilms, *Appl. Environ. Microbiol.*, **69**, 5543–5554.
28. Perret, D., Newman, M. E., Negre, J. C., Chen, Y. and Buffle, J. (1994). Submicron particles in the Rhine River–I. Physico-chemical characterization, *Water Res.*, **28**, 91–106.
29. Leppard, G. G. (1992). Evaluation of electron microscope techniques for the description of aquatic colloids. In *Environmental Particles*, eds Buffle, J. and van Leeuwen, H. P. IUPAC Series on Analytical and Physical Chemistry of Environmental Systems, Vol.1. Lewis, Boca Raton, FL, pp. 231–289.
30. Leppard, G. G. (1992). Size, morphology and composition of particulates in aquatic ecosystems: solving speciation problems by correlative electron microscopy, *Analyst*, **117**, 595–603.
31. Lienemann, C. P., Heissenberger, A., Leppard, G. G. and Perret, D. (1998). Optimal preparation of water samples for the examination of colloidal material by transmission electron microscopy, *Aquat. Microb. Ecol.*, **14**, 205–213.
32. Mavrocordatos, D. and Perret, D. (1998). Quantitative and qualitative characterization of aquatic iron oxyhydroxide particles by EF-TEM, *J. Microsc.*, **191**, 83–90.
33. Mavrocordatos, D., Lienemann, C. P. and Perret, D. (1994). Energy filtered transmission electron microscopy for the physico-chemical characterization of aquatic submicron colloids, *Mikrochim. Acta*, **117**, 39–47.
34. Mondi, C., Leifer, K., Mavrocordatos, D. and Perret, D. (2002). Analytical electron microscopy as a tool for accessing colloid formation process in natural waters, *J. Microsc.*, **207**, 180–190.
35. Perret, D., Leppard, G. G., Mueller, M., Belzile, N., De Vitre, R. and Buffle, J. (1991). Electron microscopy of aquatic colloids: non-perturbing preparation of specimens in the field, *Water Res.*, **25**, 1333–1343.

36. Perret, D., Gaillard, J. F., Dominik, J. and Atteia, O. (2000). The diversity of natural hydrous iron oxides, *Environ. Sci. Technol.*, **34**, 3540–3546.
37. Wilkinson, K. J., Balnois, E., Leppard, G. G. and Buffle, J. (1999). Characteristic features of the major components of freshwater colloidal organic matter revealed by transmission electron and atomic force microscopy, *Colloids Surf. A*, **155**, 287–310.
38. Xhoffer, C., Wouters, L. and Van Grieken, R. (1992). Characterization of individual particles in the North Sea surface microlayer and underlying seawater: comparison with atmospheric particles, *Environ. Sci. Technol.*, **26**, 2151–2162.
39. Perret, D., Mavrocordatos, D. and Lienemann, C.-P. (1994). Natural microparticles–macromolecules interactions: an EFTEM approach. In *Electron Microscopy 1994, Proc. 13th Int. Congr. Electr. Microsc.*, Paris, 17–22 July 1994, pp. 1277–1278.
40. Leppard, G. G. and Buffle, J. (1998). Aquatic colloids and macromolecules: effects on analysis. In *Encyclopedia of Environmental Analysis and Remediation*, Vol. 1, ed. Meyers, R. A. John Wiley & Sons, Inc., New York, 349–377.
41. Perret, D., Leppard, G. G. and Mavrocordatos, D. (2005). Microscopy: environmental applications. In *Encyclopedia of Analytical Science*, eds Worsfold, P. J., Townsend, A. and Poole, C. F. Elsevier, Oxford, pp. 65–74.
42. Goldstein, J. I. and Yakowitz, H. (1975). *Practical Scanning Electron Microscopy: Electron and Ion Microprobe Analysis*. Plenum Press, New York.
43. Holt, D. B., Muir, M. D., Grant, P. R., and Boswarva, I. M. (1974). *Quantitative Scanning Electron Microscopy*. Academic Press, New York. 570 pp.
44. Kiss, K. (1987). Industrial problem solving with microbeam analysis, *Scanning Microsc.*, **1**, 1515–1538.
45. Murr, L. E. (1991). *Electron and Ion Microscopy and Microanalysis. Principles and Applications, Optical Engineering*. Marcel Dekker, New York.
46. Reimer, L. (1984). Scanning electron microscopy, *Comm. Eur. Commun. Rep.*, EUR8824, 141–168.
47. Wells, O. C., Boyde, A., Lifshin, E. and Rezanowich, A. (1974). *Scanning Electron Microscopy*. McGraw-Hill, New York.
48. Hawkes, P. W., Mulvey, T. and Kazan, B. (2002). *Advances in Imaging and Electron Physics*, Vol. 121. Academic Press, San Diego, CA.
49. Reed, S. J. B. (1993). *Electron Microprobe Analysis*. Cambridge University Press, Cambridge.
50. Rossiter, B. W. and Hamilton, J. F. (1991). *Physical Methods of Chemistry, Vol. 4, Microscopy*. Wiley-Interscience, New York.
51. Santschi, P. H., Balnois, E., Wilkinson, K. J., Zhang, J., Buffle, J. and Guo, L. (1998). Fibrillar polysaccharides in marine macromolecular organic matter as imaged by atomic force microscopy and transmission electron microscopy, *Limnol. Oceanogr.*, **43**, 896–908.
52. Webb, S. M., Gaillard, J. F. and Leppard, G. G. (2000). Analytical electron microscopy characterization of zinc speciation in a contaminated system, *Abstr. 220th ACS Nat. Meet.*, Washington, DC, 20–24 August 2000, ENVR-271.
53. Berube, K. A., Jones, T. P., Williamson, B. J., Winters, C., Morgan, A. J. and Richards, R. J. (1999). Physicochemical characterization of diesel exhaust particles: factors for assessing biological activity, *Atmos. Environ.*, **33**, 1599–1614.
54. Chabas, A. and Lefevre, R. A. (1999). Chemistry and microscopy of atmospheric particulates at Delos (Cyclades, Greece), *Atmos. Environ.*, **34**, 225–238.
55. Conner, T. L., Norris, G. A., Landis, M. S. and Williams, R. W. (2001). Individual particle analysis of indoor, outdoor, and community samples from the 1998 Baltimore particulate matter study, *Atmos. Environ.*, **35**, 3935–3946.
56. Hueglin, C., Gaegauf, C., Kuenzel, S. and Burtscher, H. (1997). Characterization of wood combustion particles: morphology, mobility, and photoelectric activity, *Environ. Sci. Technol.*, **31**, 3439–3447.
57. Kaegi, R. and Holzer, L. (2003). Transfer of a single particle for combined ESEM and TEM analyses, *Atmos. Environ.*, **37**, 4353–4359.
58. Mavrocordatos, D., Kaegi, R. and Schmatloch, V. (2002). Fractal analysis of wood combustion aggregates by contact mode atomic force microscopy, *Atmos. Environ.*, **36**, 5653–5660.

59. Naoe, H. and Okada, K. (2001). Mixing properties of submicrometer aerosol particles in the urban atmosphere – with regard to soot particles, *Atmos. Environ.*, **35**, 5765–5772.
60. Osan, J., Alfoldy, B., Torok, S. and Van Grieken, R. (2002). Characterisation of wood combustion particles using electron probe microanalysis, *Atmos. Environ.*, **36**, 2207–2214.
61. Rietmeijer, F. J. M. and Janeczek, J. (1997). An analytical electron microscope study of airborne industrial particles in Sosnowiec, Poland, *Atmos. Environ.*, **31**, 1941–1951.
62. Shi, J. P., Harrison, R. M. and Brear, F. (1999). Particle size distribution from a modern heavy duty diesel engine, *Sci. Total. Environ.*, **235**, 305–317.
63. Shukla, S., Seal, S., Akesson, J., Oder, R., Carter, R. and Rahman, Z. (2001). Study of mechanism of electroless copper coating of fly-ash cenosphere particles, *Appl. Surf. Sci.*, **181**, 35–50.
64. Watt, J. (1998). Automated characterization of individual carbonaceous fly-ash particles by computer controlled scanning electron microscopy: analytical methods and critical review of alternative techniques, *Water Air Soil Pollut.*, **106**, 309–327.
65. Xhoffer, C., Jacob, W., Buseck, P. R. and Van Grieken, R. (1995). Problems in quantitatively analyzing individual salt aerosol particles using electron energy loss spectroscopy, *Spectrochim. Acta B*, **50**, 1281–1292.
66. Maura de Miranda, R., Andrade, M. d. F., Worobiec, A. and Van Grieken, R. (2002). Characterisation of aerosol particles in the São Paulo Metropolitan Area, *Atmos. Environ.*, **36**, 345–352.
67. Jones, T. P., Williamson, B. J., Berube, K. A. and Richards, R. J. (2001). Microscopy and chemistry of particles collected on TEOM filters: Swansea, south Wales, 1998–1999, *Atmos. Environ.*, **35**, 3573–3583.
68. Bang, J. J. and Murr, L. E. (2002). Collecting and characterizing atmospheric nanoparticles, *J. Miner. Metals Mater. Soc.*, **54**, 28–30.
69. Buffat, P. A. (1999). Electron microscopy for the characterisation of atmospheric particles, *Analusis*, **27**, 340–346.
70. Harrison, R. and Van Grieken, R. (1998). *Atmospheric Particles*. John Wiley & Sons, Inc., New York.
71. Micic, M., Markovic, D., Vukelic, N., Radu, A., Milosevic, B. and Leblanc, R. M. (2000). Environmental scanning electron microscopy study of commonly used filters substrates for the active sampling of atmospheric aerosols, *Fresenius' Environ. Bull.*, **9**, 193–200.
72. Pooley, F. D., de Mille, M. G., (1999). Microscopy and the characterization of particles. In *Particulate Matter: Properties and Effects Upon Health*, eds Maynard, R. L. and Howard, C. V. BIOS Scientific Publishers, Oxford, pp. 19–37.
73. Russel, P. A. (1990). The analysis of anthropogenic atmospheric particulates by electron microscopy, *Microbeam Anal.*, **25**, 445–448.
74. Schlaegle, S. F. and Doerr, A. (2000). Approaches to the collection and analysis of nuisance dust using a combination of old and new sampling methods and analytical techniques. In *Proc. 93rd Air Waste Manag. Ass. Annu. Conf. Exhib.*, Salt Lake City, 18–22 June 2000, pp. 215–223.
75. Ormstad, H., Gaarder, P. I. and Johansen, B. V. (1997). Quantification and characterisation of suspended particulate matter in indoor air, *Sci. Total Environ.*, **193**, 185–196.
76. Ali, A. E. and Bacso, J. (1996). Investigation of different types of filters for atmospheric trace elements analysis by three analytical techniques, *J. Radioanal. Nucl. Chem.*, **209**, 147–155.
77. Eleftheriadis, K. and Colbeck, I. (2000). The fractionation of atmospheric coarse aerosol by a tunnel sampler employing single stage impactors, *J. Aerosol Sci.*, **31**, 321–334.
78. Kronholm, D. F. and Howard, J. B. (2000). Analysis of soot surface growth pathways using published plug-flow reactor data with new particle size distribution measurements and published premixed flame data, *Proc. Combust. Inst.*, **28**, 2555–2561.
79. Lu, R., Turco, R., Stolzenbach, K., Friedlander, S., Xiong, C., Schiff, K., Tiefenthaler, L. and Guangyu, W. (2003). Dry deposition of airborne trace metals on the Los Angeles Basin and adjacent coastal waters, *J. Geophys. Res.*, **108**, AAC11–AAC24.
80. Thurmer, H. and Kersten, N. (2001). Measurement of ultrafine aerosols by a thermal precipitator, *Gefahrstoffe Reinhalt. Luft*, **61**, 275–279.

81. Chen, Y. L., Kreidenweis, S. M., McInnes, L. M., Rogers, D. C. and Demott, P. J. (1998). Single particle analyses of ice nucleating aerosols in the upper troposphere and lower stratosphere, *Geophys. Res. Lett.*, **25**, 1391–1394.
82. Delzeit, L. and Blake, D. (2001). A characterization of crystalline ice nanoclusters using transmission electron microscopy, *J. Geophys. Res.*, **106**, 33371–33379.
83. Okada, K. (1983). Nature of individual hygroscopic particles in the urban atmosphere, *J. Meteorol. Soc. Jpn.*, **61**, 727–736.
84. Posfai, M., Xu, H. F., Anderson, J. R. and Buseck, P. R. (1998). Wet and dry sizes of atmospheric aerosol particles: An AFM–TEM study, *Geophys. Res. Lett.*, **25**, 1907–1910.
85. Rogers, D. C., Demott, P. J. and Kreidenweis, S. M. (2001). Airborne measurements of tropospheric ice-nucleating aerosol particles in the Arctic spring, *J. Geophys. Res.*, **106**, 15053–15063.
86. Rogers, D. C., Demott, P. J., Kreidenweis, S. M. and Chen, Y. L. (2001). A continuous-flow diffusion chamber for airborne measurements of ice nuclei, *J. Atmos. Ocean. Technol.*, **18**, 725–741.
87. Ebert, M., Inerle-Hof, M. and Weinbruch, S. (2002). Environmental scanning electron microscopy as a new technique to determine the hygroscopic behaviour of individual aerosol particles, *Atmos. Environ.*, **36**, 5909–5916.
88. Huang, P. M., Senesi, N. and Buffle, J. (1998). *Structure and Surface Reactions of Soil Particles*. John Wiley & Sons, Ltd, Chichester.
89. Chen, Y. and Schnitzer, M. (1976). Water adsorption on soil humic substances, *Can. J. Soil Sci.*, **56**, 521–524.
90. Chen, Y., Banin, A. and Schnitzer, M. (1976). Use of the scanning electron microscope for structural studies on soils and soil components, *Scanning Electron Microsc.*, **9**, 425–432.
91. Chen, Y. and Schnitzer, M. (1976). Scanning electron microscopy of a humic acid and a fulvic acid and its metal and clay complexes, *Soil Sci. Soc. Am. J.*, **40**, 682–686.
92. Chenu, C., Hassink, J. and Bloem, J. (2001). Short-term changes in the spatial distribution of microorganisms in soil aggregates as affected by glucose addition, *Biol. Fert. Soils*, **34**, 349–356.
93. Keller, C. and Mavrocordatos, D. (1997). Particulate matter and transfer of K, Cu, Al and Fe in the soil solutions of a podzosol: preliminary results on semi-quantitative and qualitative approaches, *Coll. Inst. Nat. Rech. Agron.*, **85**, 373–382.
94. Mavrocordatos, D. and Perret, D. (1995). Non-artifacted specimen preparation for transmission electron microscopy of submicron soil particles, *Comm. Soil Sci. Plant Anal.*, **26**, 2593–2602.
95. Chen, Y. and Banin, A. (1975). Scanning electron microscope (SEM) observations of soil structure changes induced by sodium–calcium exchange in relation to hydraulic conductivity, *Soil Sci.*, **120**, 428–436.
96. Chen, Y. (1998). *Electron Microscopy of Soil Structure and Soil Components*. John Wiley & Sons, Ltd, Chichester.
97. Citeau, L., Lamy, I., van Oort, F. and Elsass, F. (2001). Nature of soils and nature of mobile colloids in gravitational water: a field study, *C. R. Acad. Sci. A*, **332**, 657–663.
98. Golchin, A., Oades, J. M., Skjemstad, J. O. and Clarke, P. (1994). Study of free and occluded particulate organic matter in soils by solid-state C-13 CP/MAS NMR-spectroscopy and scanning electron-microscopy, *Aust. J. Soil Res.*, **32**, 285–309.
99. Huber, K. and Denaix, L. (2000). Genesis and transfer of colloids in gravitational waters of an alpine podzol, *C. R. Acad. Sci. A*, **330**, 251–258.
100. Laird, D. (2001). Nature of clay–humic complexes in an agricultural soil: II. Scanning electron microscopy analysis, *Soil Sci. Soc. Am. J.*, **65**, 1419–1425.
101. Elsass, F., van Oort, F., Le Mot, Y. and Jaunet, A. M. (2002). Identification minéralogique des polluants par microscopies électroniques. In *Les Eléments Traces Métalliques dans les Sols: Approches Fonctionnelles et Spatiales*, eds Baize, D. and Tercé, M. Editions INRA, Versailles, pp. 331–350.
102. Righi, D., Elsass, F. and Lapeyronnie, J. P. (1999). Clay minerals in soils: global characterization by X-ray diffraction in the study of particles with analytical electron microscopy.

In *Structure et Ultrastructure des Sols et des Organismes Vivants*, eds Elsass, F. and Jaunet, A. M. Colloques de l'INRA, Versailles, pp. 79–92.
103. Seaman, J. C. (2000). Thin-foil SEM analysis of soil and groundwater colloids: reducing instrument and operator bias, *Environ. Sci. Technol.*, **34**, 187–191.
104. Southard, R. J., Shainberg, I. and Singer, M. J. (1988). Influence of electrolyte concentration on the micromorphology of artificial depositional crust, *Soil Sci.*, **145**, 278–288.
105. Tiessen, H. and Stewart, J. W. B. (1988). Light and electron microscopy of stained microaggregates – the role of organic matter and microbes in soil aggregation, *Biogeochemistry*, **5**, 312–322.
106. de Boer, D. H. and Crosby, G. (1995). Evaluating the potential of SEM/EDS analysis for fingerprinting suspended sediment derived from two contrasting topsoils, *Catena*, **24**, 243–258.
107. Buffle, J. and Leppard, G. G. (1995). Characterization of aquatic colloids and macromolecules. 2. Key role of physical structures on analytical results, *Environ. Sci. Technol.*, **29**, 2176–2184.
108. Belzile, N., De Vitre, R. R. and Tessier, A. (1989). *In situ* collection of diagenetic iron and manganese oxyhydroxides from natural sediments, *Nature*, **340**, 376–377.
109. Citeau, L., Lamy, I., van Oort, F. and Elsass, F. (2002). Role of colloids in the metal mobilisation in soils: a field study, *Geochim. Cosmochim. Acta*, **66**, A142.
110. Redwood, P. S., Lead, J. R., Harrison, R. M., Jones, I. P. and Stoll, S. (2005). Characterization of humic substances by environmental scanning electron microscopy, *Environ. Sci. Technol.*, **39**, 1962–1966.
111. Froesch, D. and Westphal, C. (1985). Choosing the appropriate section thickness in the melamine embedding technique, *J. Microsc.*, **137**, 177–183.
112. Froesch, D. and Westphal, C. (1989). Melamine resins and their application in electron microscopy, *Electron Microsc. Rev.*, **2**, 231–255.
113. Lewis, P. R. and Knight, D. P. (1992). Introduction to cytochemical staining methods for electron microscopy. In *Cytochemical Staining methods for Electron Microscopy*, eds Lewis, P. R and Knight, D. P. Practical Methods in Electron Microscopy, Vol. 14. Elsevier, Amsterdam, 1–29.
114. Knight, D. and Lewis, P. (1992). General cytochemical methods. In *Cytochemical Staining Methods for Electron Microscopy*, eds Lewis, P. R and Knight, D. P. Practical Methods in Electron Microscopy, Vol. 14. Elsevier, Amsterdam, 79–145.
115. Lewis, P. (1992). Other cytochemical methods for enzymes. In *Cytochemical Staining Methods for Electron Microscopy*, eds Lewis, P. R and Knight, D. P. Practical Methods in Electron Microscopy, Vol. 14. Elsevier, Amsterdam, 237–298.
116. Spurr, A. R. and Galle, P. (1979). Localization of elements in botanical materials by secondary ion mass spectrometry, *Springer Ser. Chem. Phys.*, **9**, 252–255.
117. Spurr, A. R. (1969). A low-viscosity epoxy resin embedding medium for electron microscopy, *J. Ultrastruct. Res.*, **26**, 31–43.
118. Liss, S. N., Droppo, I. G., Flannigan, D. T. and Leppard, G. G. (1996). Floc architecture in wastewater and natural riverine systems, *Environ. Sci. Technol.*, **30**, 680–686.
119. Dubochet, J., Booy, F. P., Freeman, R., Jones, A. V. and Walter, C. A. (1981). Low temperature electron microscopy, *Annu. Rev. Biophys. Bioeng.*, **10**, 133–149.
120. Dubochet, J., Alba, C. M., MacFarlane, D. R., Angell, C. A., Kadiyala, R. K., Adrian, M. and Teixeira, J. (1984). Glass-forming microemulsions: vitrification of simple liquids and electron microscope probing of droplet-packing modes, *J. Phys. Chem.*, **88**, 6727–6732.
121. Dubochet, J. and Lepault, J. (1984). Cryo-electron microscopy of vitrified water, *J. Phys. (Paris)*, **9**, 85–94.
122. Dubochet, J., Bednar, J., Furrer, P. and Stasiak, A. (1994). Cryo-electron microscopy of DNA, *Nucleic Acids Mol. Biol.*, **8**, 41–55.
123. Dubochet, J., Adrian, M. and Vogel, R. H. (1983). Amorphous solid water obtained by vapor condensation or by liquid cooling: a comparison in the electron microscope, *Cryo-Letters*, **4**, 233–240.
124. Dubochet, J. (1987). Life, liquids and cryo-electron microscopy, *Europhys. News*, **18**, 54–56.
125. Dubochet, J., Adrian, M., Dustin, I., Furrer, P. and Stasiak, A. (1992). Cryoelectron microscopy of DNA molecules in solution, *Methods Enzym.*, **211**, 507–518.

126. Kirk, E. C. G., Williams, D. A. and Ahmed, H. (1989). Cross-sectional transmission electron microscopy of precisely selected regions from semiconductor devices, *Inst. Phys. Conf. Ser.*, **100**, 501–506.
127. Phaneuf, M. W., Rowlands, N., Carpenter, G. J. C. and Sundaram, G. (1997). Focused ion beam sample preparation of non-semiconductor materials, *Mater. Res. Soc. Symp. Proc.*, **480**, 39–47.
128. Tanaka, A., Shimizu, T., Kikuchi, M., Kobayashi, Y., Yamashita, T. and Watanabe, H. (1997). Biological effect of penetration controlled irradiation with ion beams. In *Proc. 7th Int. Symp. Adv. Nucl. Energy Res.* JAERI-Conf 97-003, pp. 323–326.
129. Tanaka, A., Watanabe, H., Shimizu, T., Inoue, M., Kikuchi, M., Kobayashi, Y. and Tano, S. (1997). Penetration controlled irradiation with ion beams for biological study, *Nucl. Instrum. Methods Phys. Res. B*, **129**, 42–48.
130. Loos, J., van Duren, J. K. J., Morrissey, F. and Janssen, R. A. J. (2002). The use of the focused ion beam technique to prepare cross-sectional transmission electron microscopy specimen of polymer solar cells deposited on glass, *Polymer*, **43**, 7493–7496.
131. Barna, A., Pecz, B. and Menyhard, M. (1998). Amorphization and surface morphology development at low-energy ion milling, *Ultramicroscopy*, **70**, 161–171.
132. Barna, A., Menyhard, M., Zsolt, G., Koos, A., Zalar, A. and Panjan, P. (2003). Interface broadening due to Ar^+ ion bombardment measured on Co/Cu multilayer at grazing angle of incidence, *J. Vac. Sci. Technol. A*, **21**, 553–557.
133. Barna, A., Menyhard, M., Zalar, A. and Panjan, P. (2005). Ion bombardment induced interface broadening in Co/Cu system as a function of layer thickness, *Appl. Surf. Sci.*, **242**, 375–379.
134. Longo, D. M., Howe, J. M. and Johnson, W. C. (1999). Experimental method for determining Cliff–Lorimer factors in transmission electron microscopy (TEM) utilizing stepped wedge-shaped specimens prepared by focused ion beam (FIB) thinning, *Ultramicroscopy*, **80**, 85–97.
135. Labar, J. L. and Egerton, R. (1999). Special issue on ion beam techniques, *Micron*, **30**, 195–196.
136. Hall, J. L. (1978). *Electron Microscopy and Cytochemistry of Plant Cells*. Elsevier/North-Holland Biomedical Press, Amsterdam.
137. Newman, G. R. and Hobot, J. A. (2001). *Resin Microscopy and On-Section Immunocytochemistry*. Springer, Berlin.
138. Bullock, G. R. and Petrusz, P. (1983). *Techniques in Immunocytochemistry*. Academic Press, London.
139. Thiery, J. P. and Ovtracht, L. (1980). Ultrastructural chemistry on isolated molecules. Technique applied to some biological macromolecules. Study of metachromasy, *C. R. Soc. Biol.*, **174**, 584–597.
140. Thiery, J. P. (1967). Demonstration of polysaccharides in thin sections by electron microscopy, *J. Microsc. (Paris)*, **6**, 987–1018.
141. Chenu, C. (1993). Clay- or sand-polysaccharide associations as models for the interface between microorganisms and soil: water related properties and microstructure, *Geoderma*, **56**, 143–156.
142. Lienemann, C. P. (1997). Associations entre phases minérales de fer et de manganèse, polluants anthropogéniques et biota en milieu lacustre: mise en évidence par microscopie électronique. *Ph.D Thesis*, University of Lausanne.
143. Beesley, J. E. (1987). Colloidal gold. A modern, high resolution immunocytochemical marking system of wide applicability, *Int. Analyst*, **1**, 20–25.
144. Beesley, J. E. and Dougan, G. (1991). Detection of surface antigens by immunogold labeling, In *Microbial Cell Surface Analysis*, Mozes, N. ed., VCH, New York, 151–69.
145. Beesley, J. E. (1992). Preparation of gold probes. In *Immunochemical Protocols, Methods in Molecular Biology*, Vol. 10, ed. Manson M. M. Humana Press, Totowa, NJ, pp. 163–168.
146. Beesley, J. E. (1993). *Immunocytochemistry: a Practical Approach*. Oxford University Press, Oxford.

147. Benhamou, N. and Ouellette, G. B. (1986). Use of pectinases complexes to colloidal gold for the ultrastructural localization of polygalacturonic acids in the cell walls of the fungus *Ascocalyx abietina*, *Histochem. J.*, **18**, 95–104.
148. Benhamou, N., Chamberland, H., Ouellette, G. B. and Pauze, F. J. (1987). Ultrastructural localization of β-(1,4)-D-glucans in two pathogenic fungi and in their host tissues by means of an exoglucanase–gold complex, *Can. J. Microbiol.*, **33**, 405–417.
149. Benhamou, N., Gilboa-Garber, N., Trudel, J. and Asselin, A. (1988). A new lectin–gold complex for ultrastructural localization of galacturonic acids, *J. Histochem. Cytochem.*, **36**, 1403–1411.
150. Benhamou, N., Chamberland, H., Ouellette, G. B. and Pauze, F. J. (1988). Detection of galactose in two fungi causing wilt diseases and in their plant host tissues by means of gold-complexed *Ricinus communis* agglutinin I, *Physiol. Mol. Plant Pathol.*, **32**, 249–266.
151. Benhamou, N., Chamberland, H., Noel, S. and Ouellette, G. B. (1990). Ultrastructural localization of β-1,4-glucan-containing molecules in the cell walls of some fungi: a comparative study between spore and mycelium, *Can. J. Microbiol.*, **36**, 149–158.
152. Benhamou, N. (1992). Ultrastructural detection of β-1,3-glucans in tobacco root tissues infected by *Phytophthora parasitica* var. *nicotianae* using a gold-complexed tobacco β-1,3-glucanase, *Physiol. Mol. Plant Pathol.*, **41**, 351–370.
153. Dumasgaudot, E., Tahirialaoui, A. and Benhamou, N. (1992). Cytochemical localization of some polysaccharidic components in the cell-walls of *Chalara elegans* during its life-cycle, *Can. J. Microbiol.*, **38**, 828–837.
154. Horisberger, M. (1992). Applications of colloidal gold in cytochemistry. An overview, *Recent Adv. Cell. Mol. Biol.*, **4**, 263–269.
155. Horisberger, M. (1992). Colloidal gold and its application in cell biology, *Int. Rev. Cytol.*, **136**, 227–287.
156. Hayat, M. A. (1989). *Colloidal Gold: Principles, Methods, and Applications*, Vol. 1. Academic Press, San Diego, CA.
157. Hayat, M. A. (1989). *Colloidal Gold: Principles, Methods, and Applications*, Vol. 2. Academic Press, San Diego, CA.
158. Hayat, M. A. (1991). *Colloidal Gold: Principles, Methods, and Applications*, Vol. 3. Academic Press, San Diego, CA.
159. Rosch, J. and Caparon, M. (2004). A microdomain for protein secretion in Gram-positive bacteria, *Science*, **304**, 1513–1515.
160. Lawrence, J. R., Hitchcock, A. P., Leppard, G. G. and Neu, T. R. (2005). Mapping biopolymer distributions in microbial communities. In *Flocculation in Natural and Engineered Environmental Systems*, eds Leppard, G. G., Liss, S. N. and Milligan, T. G. CRC Press, Boca Raton, pp. 121–141.
161. Droppo, I. G., Flannigan, D. T., Leppard, G. G. and Liss, S. N. (1996). Microbial floc stabilization and preparation for structural analysis by correlative microscopy, *Water Sci. Technol.*, **34**, 155–162.
162. Droppo, I. G., Flannigan, D. T., Leppard, G. G., Jaskot, C. and Liss, S. N. (1996). Floc stabilization for multiple microscopic techniques, *Appl. Environ. Microbiol.*, **62**, 3508–3515.
163. Ghosh, K. and Schnitzer, M. (1981). Effect of pH and neutral electrolyte concentration on free radicals in humic substances, *Soil Sci. Soc. Am. J.*, **45**, 831.
164. Ghosh, K. and Schnitzer, M. (1980). Macromolecular structures of humic substances, *Soil Sci.*, **129**, 266–276.
165. Ghosh, K. and Schnitzer, M. (1982). A scanning electron microscopic study of effects of adding neutral electrolytes to solutions of humic substances, *Geoderma*, **28**, 53–56.
166. Stevenson, I. L. and Schnitzer, M. (1982). Transmission electron microscopy of extracted fulvic and humic acids, *Soil Sci.*, **133**, 179–185.
167. Stevenson, I. L. and Schnitzer, M. (1984). Energy-dispersive X-ray microanalysis of saturated fulvic acid–iron and–copper complexes, *Soil Sci.*, **138**, 123–126.
168. Atteia, O., Perret, D., Adatte, T., Kozel, R. and Rossi, P. (1998). Characterization of natural colloids from a river and spring in a karstic basin, *Environ. Geol.*, **34**, 257–269.
169. Couture-Mondi, C., Mavrocordatos, D., Perret, D. and Atteia, O. (1999). Interactions between iron and organic matter in a peaty zone. In *Structure et Ultrastructure des Sols et des*

Organismes Vivants, eds Elsass, F. and Jaunet, A. M. Colloques de l'INRA, Versailles, pp. 183–192.
170. Batson, P. E., Dellby, N. and Krivanek, O. L. (2002). Sub-Å resolution using aberration corrected electron optics, *Nature*, **419**, 94.
171. Krivanek, O. L., Dellby, N. and Lupini, A. R. (1999). Towards sub-Å electron beams, *Ultramicroscopy*, **78**, 1–11.
172. Krivanek, O. L., Nellist, P. D., Dellby, N., Murfitt, M. F. and Szilagyi, Z. (2003). Towards sub-0.5 Å electron beams, *Ultramicroscopy*, **96**, 229–237.
173. Bernard, P. C., Van Grieken, R. E. and Eisma, D. (1986). Classification of estuarine particles using automated electron-microprobe analysis and multivariate techniques, *Environ. Sci. Technol.*, **20**, 467–473.
174. Bruynseels, F., Storms, H., Van Grieken, R. and Vanderauwera, L. (1988). Characterization of North-Sea aerosols by individual particle analyses, *Atmos. Environ.*, **22**, 2593–2602.
175. Jambers, W., De Bock, L. and Van Grieken, R. (1996). Applications of microanalysis to individual environmental particles, *Fresenius' J. Anal. Chem.*, **355**, 521–527.
176. Jambers, W. and Van Grieken, R. (1996). Single particle characterization of inorganic North Sea suspension, *Bull. Soc. R. Sci. Liege*, **65**, 115–117.
177. Jambers, W., Smekens, A., Van Grieken, R., Shevchenko, V. and Gordeev, V. (1997). Characterization of particulate matter from the Kara Sea using electron probe X-ray micro analysis, *Colloids Surf. A*, **120**, 61–75.
178. Raeymaekers, B., Van Espen, P. and Adams, F. (1984). The morphological characterization of particles by automated scanning electron microscopy, *Mikrochim. Acta*, **2**, 437–454.
179. Raeymaekers, B., Van Espen, P., Adams, F. and Broekaert, J. A. C. (1988). A characterization of spark-produced aerosols by automated electron probe microanalysis, *Appl. Spectrosc.*, **42**, 142–150.
180. Raeymaekers, B. J., Liu, X., Janssens, K. H., Van Espen, P. J. and Adams, F. C. (1987). Determination of thickness of flat particles by automated electron microprobe analysis, *Anal. Chem.*, **59**, 930–937.
181. Raeymaekers, B. J. M. (1986). Characterization of particles by automated electron probe microanalysis. *Ph.D Thesis*, University of Antwerp.
182. Wouters, L., Bernard, P. and Van Grieken, R. (1988). Characterization of individual estuarine and marine particles by LAMMA and EPXMA, *Int. J. Environ. Anal. Chem.*, **34**, 17–29.
183. Lerman, A. (1979). *Geochemical Processes: Water and Sediment Environments*. John Wiley & Sons, Inc., New York.
184. Beddow, J. K. (1987). Size, shape, and texture analysis. In: *Particle Size Distribution: Assessment and Characterization* (Provder, T. ed). ACS Symp. Series 332. ACS, Washington. 2–29.
185. Beddow, J. K. (1987). Morphological analysis, *Adv. Ceram.*, **21**, 747–757.
186. Beddow, J. K. (1984). *Particle Characterization in Technology, Vol. 1: Applications and Microanalysis*. CRC Press, Boca Raton, FL.
187. Beddow, J. K. (1984). *Particle Characterization in Technology, Vol. 2: Morphological Analysis*. CRC Press, Boca Raton, FL.
188. Dougherty E. (1993). *Mathematical Morphology in Image Processing*. Marcel Dekker, New York.
189. Gonzalez, R., Woods, R. and Swain, W. (1986). Digital image processing: an introduction, *Digit. Des.*, **16**, 15–20.
190. Jain, A. K. (1983). Digital image processing: problems and practice, *KINAM Rev. Fis.*, **5**, 41–70.
191. Jain, A. K. (1981). Advances in mathematical models for image processing, *Proc. IEEE*, **69**, 502–528.
192. Jain, A. K. (1986). Image processing, *J. Opt. Soc. Am. A*, **3**, 4.
193. Kindratenko, V. V., Treiger, B. A. and Van Espen, P. J. M. (1996). Chemometrical approach to the determination of the fractal dimension(s) of real objects, *Chemom. Intell. Lab. Syst.*, **34**, 103–108.

194. Kindratenko, V. V., Van Espen, P. J. M., Treiger, B. A. and Van Grieken, R. E. (1996). Characterization of the shape of microparticles via fractal and fourier analyses of scanning electron microscope images, *Mikrochim. Acta*, **13**, 355–361.
195. Pitas, I. (1993). *Digital Image Processing Algorithms*. Prentice Hall, Englewood Cliffs, NJ.
196. Russ, J. C. and Russ, J. C. (1986). Shape and surface roughness characterization for particles and surfaces viewed in SEM, *Microbeam Anal.*, **21**, 509–512.
197. Russ, J. C. and Russ, J. C. (1986). Image processing for the location and isolation of features, *Microbeam Anal.*, **21**, 501–504.
198. Russ, J. C. (1988). Computers in stereology and image analysis, *Microbeam Anal.*, **23**, 14–17.
199. Russ, J. C. (1991). Computer-aided quantitative microscopy, *Mater. Charact.*, **27**, 185–197.
200. Russ, J. C. (1992). Imaging the three-dimensional microstructure of materials, *Adv. X-Ray Anal.*, **35B**, 1219–1226.
201. Serra, J. (1978). Quantitative analysis of images, *Recherche*, **9**, 247–256.
202. Serra, J. (1979). Biomedical image analysis by mathematical morphology, *Pathol. Biol.*, **27**, 205–207.
203. Serra, J. (1987). Morphological optics, *J. Microsc.*, **145**, 1–22.
204. Frey, J., Pinvidic, J. J., Botet, R. and Jullien, R. (1988). Light scattering by fractal aggregates: a numerical investigation, *J. Phys. (Paris)*, **49**, 1969–1976.
205. Lin, M. Y., Lindsay, H. M., Weitz, D. A., Ball, R. C., Klein, R. and Meakin, P. (1989). Universality of fractal aggregates as probed by light scattering, *Proc. R. Soc. London, Sen. A*, **423**, 71–87.
206. Lin, M. Y., Lindsay, H. M., Weitz, D. A., Ball, R. C., Klein, R. and Meakin, P. (1989). Universality in colloid aggregation, *Nature*, **339**, 360–362.
207. Lin, M. Y., Klein, R., Lindsay, H. M., Weitz, D. A., Ball, R. C. and Meakin, P. (1990). The structure of fractal colloidal aggregates of finite extent, *J. Colloid Interface Sci.*, **137**, 263–280.
208. Lin, M. Y., Lindsay, H. M., Weitz, D. A., Ball, R. C., Klein, R. and Meakin, P. (1990). Universal reaction-limited colloid aggregation, *Phys. Rev. A*, **41**, 2005–2020.
209. Meakin, P. (1984). Diffusion-limited aggregation in three dimensions: results from a new cluster–cluster aggregation model, *J. Colloid Interface Sci.*, **102**, 491–504.
210. Meakin, P. (1984). Computer simulation of cluster–cluster aggregation using linear trajectories: results from three-dimensional simulations and a comparison with aggregates formed using Brownian trajectories, *J. Colloid Interface Sci.*, **102**, 505–512.
211. Meakin, P. (1991). Fractal aggregates in chemistry, *Trends Chem. Phys.*, **1**, 303–347.
212. Meakin, P., Feder, J. and Joessang, T. (1991). Growth of adaptive networks in a modified diffusion-limited-aggregation model, *Phys. Rev. A*, **44**, 5104–5110.
213. Meakin, P., Feder, J. and Jossang, T. (1991). Radially biased diffusion-limited aggregation, *Phys. Rev. A*, **43**, 1952–1964.
214. Meakin, P. (1992). Aggregation kinetics, *Phys. Scr.*, **46**, 295–331.
215. Meakin, P. (1992). Simplified diffusion-limited aggregation models, *Physica A*, **187**, 1–17.
216. Meakin, P. (1994). What do we know about DLA?, *Heterocycl. Chem. Rev.*, **1**, 99–102.
217. Meakin, P. (1999). The diffusion-limited aggregation model and geological pattern formation. In *Proc. 11th Kongsberg Sem. Growth Dissol. Pattern Form. Geosyst.*, Kongsberg, Norway, pp. 177–188.
218. Albarede, F. (2003). *Geochemistry: an Introduction*. Cambridge University Press, Cambridge.
219. Leppard, G. G. and Arsenault, A. L. (2003). Quantification of individual native biocolloids in natural waters: assessing indicators of aquatic events, by using transmission electron microscopy with a modified approach to image analysis, *Arch. Hydrobiol.*, **156**, 565–573.
220. Couture, C., Lienemann, C. P., Mavrocordatos, D. and Perret, D. (1996). New directions towards the understanding of physico-chemical processes in aquatic systems, *Chimia*, **50**, 625–629.
221. Cheng, S., Lin, J., Wu, J. R. and Gentry, J. W. (1994). Test cases for examination of fractal dimension, *J. Aerosol Sci.*, **25**, S379–S380.

222. Chevalier, J. P., Colliex, C. and Tence, M. (1985). Annular dark-field imaging in a STEM: application to the calculation of the fractal dimension of aggregates of iron particles, *J. Microsc. Spectrosc. Electr.*, **10**, 417–424.
223. Clark, N. N., Diamond, H., Gelles, G., Bocoum, B. and Meloy, T. P. (1987). Polygonal harmonics of silhouettes: shape analysis, *Part. Charact.*, **4**, 38–43.
224. Orford, J. D. and Whalley, W. B. (1983). The use of the fractal dimension to quantify the morphology of irregular-shaped particles, *Sedimentology*, **30**, 655–668.
225. Jullien, R. (1990). The application of fractals to investigations of colloidal aggregation and random deposition, *New J. Chem.*, **14**, 239–253.
226. Fatin-Rouge, N., Toth, E., Perret, D., Backer, R. H., Merbach, A. E. and Buenzli, J. C. (2000). Lanthanide podates with programmed intermolecular interactions: luminescence enhancement through association with cyclodextrins and unusually large relaxivity of the gadolinium self-aggregates, *J. Am. Chem. Soc.*, **122**, 10810–10820.
227. Russ, J. C. (1973). Obtaining quantitative information from an SEM (scanning electron microscope) equipped with an energy-dispersive X-ray analyzer. In *Proc. Conf. Scanning Electr. Microsc. Syst. Appl.*, pp. 238–241.
228. Budd, P. M. and Goodhew, P. J. (1988). *Light-element Analysis in the Transmission Electron Microscope: WEDX and EELS*. Oxford Science Publications, Oxford.
229. Eberhart, J. P. (1991). *Structural and Chemical Analysis of Materials: X-ray, Electron and Neutron Diffraction, X-ray, Electron and Ion Spectrometry, Electron Microscopy*. John Wiley & Sons, Ltd, Chichester.
230. Goldstein, J. I., Newbury, D. E. and Echlin, P., Joy, D. C., Fiori, C. and Lifshin, E. (1984). *Scanning Electron Microscopy and X-Ray Microanalysis*. Plenum Press, New York.
231. Reimer, L. (1998). Energy-filtering imaging and diffraction, *Mater Trans.*, **39**, 873–882.
232. Reimer, L. (1995). *Introduction to Energy-filtering Transmission Electron Microscopy*. Springer, Berlin.
233. Reimer, L. (1997). *Transmission Electron Microscopy: Physics of Image Formation and Microanalysis*. Springer, Berlin.
234. Lienemann, C. P., Monnerat, M., Dominik, J. and Perret, D. (1999). Identification of stoichiometric iron–phosphorus colloids produced in a eutrophic lake, *Aquat. Sci.*, **61**, 133–149.
235. Egerton, R. F. (1980). An automated system for energy-loss microanalysis, In *Proc. 38th Annu. Meeting Electr. Microsc. Soc. Am.*, pp. 130–131.
236. Egerton, R. F. (1980). Instrumentation and software for energy-loss microanalysis, *Scanning Electron Microsc.*, pp. 41–52.
237. Egerton, R. F. (1980). Electron energy-loss analysis: theory and instrumentation, *Conf. Ser. Inst. Phys.*, **52**, 323–328.
238. Egerton, R. F. (1981). Applications of energy-loss microanalysis. In *Proc. Workshop Anal. Electron Microsc.*, pp. 154–160.
239. Egerton, R. F. (1981). Some general principles of EELS parallel detection. In *Proc. Workshop Anal. Electron Microsc.*, pp. 211–213.
240. Egerton, R. F. (1981). The range of validity of EELS microanalysis formulas, *Ultramicroscopy*, **6**, 297–300.
241. Egerton, R. F. (1981). Chemical analysis by energy-loss spectroscopy. In *Proc. 8th Microsc. Soc. Can.*, pp. 40–41.
242. Egerton, R. F. (1981). An introduction to EELS, *Bull. Microsc. Soc. Can.*, **9**, 4–8.
243. Egerton, R. F. (1982). Electron energy loss analysis in biology, *Pap. 10th Int. Congr. Elect Microsc.*, **1**, 151–158.
244. Egerton, R. F. (1982). Principles and practice of quantitative electron energy-loss spectroscopy, *Microbeam Anal.*, **17**, 43–53.
245. Egerton, R. F. (1982). Electron energy-loss spectroscopy for elemental analysis, *Philos. Trans. R. Soc. London, Sec. A*, **305**, 521–533.
246. Egerton, R. F. and Egerton, M. (1983). An electron energy-loss bibliography, *Scanning Electron Microsc.*, 119–142.
247. Egerton, R. F. (1984). Electron energy-loss spectroscopy. In *Proc. 25th Scottish Univ. Summer School Phys.*, pp. 273–304.

248. Egerton, R. F. (1984). Quantitative microanalysis by electron energy-loss spectroscopy: the current status, *Scanning Electron Microsc.*, 505–512.
249. Egerton, R. F., Crozier, P. A. and Rice, P. (1987). Electron energy-loss spectroscopy and chemical change, *Ultramicroscopy*, **23**, 305–312.
250. Egerton, R. F. (1989). Quantitative analysis of electron-energy-loss spectra, *Ultramicroscopy*, **28**, 215–225.
251. Egerton, R. F. (1993). Electron energy-loss spectroscopy (EELS). In *Proc. 40th Scottish Univ. Summer School Phys.*, pp. 145–168.
252. Egerton, R. F. (1996). *Electron Energy-loss Spectroscopy in the Electron Microscope*. Plenum Press, New York.
253. Egerton, R. F. (2003). New techniques in electron energy-loss spectroscopy and energy-filtered imaging, *Micron*, **34**, 127–139.
254. Egerton, R. F. and Malac, M. (2005). EELS in the TEM, *J. Electron Spectrosc. Relat. Phenom*, **143**, 43–50.
255. Reimer, L. (1992). Transmission electron microscopy. In *Proc. Int. Summer Sch. Diagn. Appl. Thin Films*, pp. 1–20.
256. Reimer, L., Fromm, I., Hirsch, P., Plate, U. and Rennekamp, R. (1992). Combination of EELS modes and electron spectroscopic imaging and diffraction in an energy-filtering electron microscope, *Ultramicroscopy*, **46**, 335–347.
257. Reimer, L. (1998). Energy-filtering imaging and diffraction, *Mater. Trans.*, **39**, 873–882.
258. Mavrocordatos, D. (1997). Développement de la microscopie électronique analytique pour la caractérisation physico-chimique de colloïdes aquatiques. *Ph.D Thesis*, University of Lausanne.
259. Perret, D., Lienemann, C.-P. and Mavrocordatos, D. (1995). EELS–ESI identification of heterogeneous suspensions of aquatic microparticles, *Microsc. Microanal. Microstruct.*, **6**, 41–51.
260. Leppard, G. G., Mavrocordatos, D. and Perret, D. (2004). Electron-optical characterization of nano- and micro-particles in raw and treated waters: an overview. *Water Sci. Technol.*, **50**, 1–8.
261. Lienemann, C.-P., Taillefert, M., Perret, D. and Gaillard, J.-F. (1997). Cobalt and manganese oxide (MnO_x) association at an oxic/anoxic interface, *Abstr. 213th ACS Nat. Meet.*, San Francisco, 13–17 April 1997, ENVR-040.
262. Couture, C., Mavrocordatos, D., Atteia, O. and Perret, D. (1998). The genesis and transformation of organo-mineral colloids in a drained peatland area, *Phys. Chem. Earth*, **23**, 153–157.
263. Myneni, S. C. B., Brown, J. T., Martinez, G. A. and Meyer-llse, W. (1999). Imaging of humic substance macromolecular structures in water and soils, *Science*, **286**, 1335–1337.
264. Myneni, S. C. B., Brown, J. T., Meyer-Ilse, W. and Martinez, G. A. (1999). Macromolecular structures of humic substances in water and soils under varying solution conditions, *Abstr. 217th ACS Nat. Meet.*, Anaheim, 21–25 March 1999, ENVR-078.
265. Myneni, S. C. B. (2002). Soft X-ray spectroscopy and spectromicroscopy studies of organic molecules in the environment, *Rev. Miner. Geochem.*, **49**, 485–579.
266. Leppard, G. G., West, M. M., Flannigan, D. T., Carson, J. and Lott, J. N. A. (1997). A classification scheme for marine organic colloids in the Adriatic Sea: colloid speciation by transmission electron microscopy, *Can. J. Fish. Aquat. Sci.*, **54**, 2334–2349.
267. Senesi, N. (1999). Aggregation patterns and macromolecular morphology of humic substances: a fractal approach, *Soil Sci.*, **164**, 841–856.
268. Leppard, G. G. (1995). The characterization of algal and microbial mucilages and their aggregates in aquatic ecosystems, *Sci. Total Environ.*, **165**, 103–131.
269. Leppard, G. G. (1997). Colloidal organic fibrils of acid polysaccharides in surface waters: electron-optical characteristics, activities and chemical estimates of abundance, *Colloids Surf. A*, **120**, 1–15.
270. Wilkinson, K. J., Stoll, S. and Buffle, J. (1995). Characterization of NOM–colloid aggregates in surface waters: coupling transmission electron microscopy staining techniques and mathematical modeling, *Fresenius' J. Anal. Chem.*, **351**, 54–61.

271. Wilkinson, K. J., Joz-Roland, A. and Buffle, J. (1997). Different roles of pedogenic fulvic acids and aquagenic biopolymers on colloid aggregation and stability in freshwaters, *Limnol. Oceanogr.*, **42**, 1714–1724.
272. Lienemann, C. P., Mavrocordatos, D. and Perret, D. (1997). Enhanced visualization of polysaccharides from aqueous suspensions, *Mikrochim. Acta*, **126**, 123–129.
273. Buffle, J., De Vitre, R. R., Perret, D. and Leppard, G. G. (1989). Physico-chemical characteristics of a colloidal iron phosphate species formed at the oxic–anoxic interface of a eutrophic lake, *Geochim. Cosmochim. Acta*, **53**, 399–408.
274. Leppard, G. G., Buffle, J., DeVitre, R. R. and Perret, D. (1988). The ultrastructure and physical characteristics of a distinctive colloidal iron particulate isolated from a small eutrophic lake, *Arch. Hydrobiol.*, **113**, 405–424.
275. Pizarro, J., Belzile, N., Filella, M., Leppard, G. G., Negre, J. C., Perret, D. and Buffle, J. (1995). Coagulation–sedimentation of submicron iron particles in a eutrophic lake, *Water Res.*, **29**, 617–632.
276. Borsheim, K. Y., Bratbak, G. and Heldal, M. (1990). Enumeration and biomass estimation of planktonic bacteria and viruses by transmission electron microscopy, *Appl. Environ. Microbiol.*, **56**, 352–356.
277. Proctor, L. M. and Fuhrman, J. A. (1990). Viral mortality of marine bacteria and cyanobacteria, *Nature*, **343**, 60–62.
278. Proctor, L. M. and Fuhrman, J. A. (1991). Roles of viral infection in organic particle flux, *Mar. Ecol. Prog. Ser.*, **69**, 133–142.
279. Proctor, L. M. and Fuhrman, J. A. (1992). Mortality of marine bacteria in response to enrichments of the virus size fraction from seawater, *Mar. Ecol. Prog. Ser.*, **87**, 283–293.
280. Weinbauer, M. G. and Peduzzi, P. (1994). Frequency, size and distribution of bacteriophages in different marine bacterial morphotypes, *Mar. Ecol. Prog. Ser.*, **108**, 11–20.
281. Weinbauer, M. G. and Peduzzi, P. (1995). Effect of virus-rich high molecular weight concentrates of seawater on the dynamics of dissolved amino acids and carbohydrates, *Mar. Ecol. Prog. Ser.*, **127**, 245–253.
282. Weinbauer, M. G. and Peduzzi, P. (1995). Significance of viruses versus heterotrophic nanoflagellates for controlling bacterial abundance in the Northern Adriatic Sea, *J. Plankt. Res.*, **17**, 1851–1856.
283. Danovaro, R., Dell'anno, A., Trucco, A., Serresi, M. and Vanucci, S. (2001). Determination of virus abundance in marine sediments, *Appl. Environ. Microbiol.*, **67**, 1384–1387.
284. Roberts, K. A., Santschi, P. H., Leppard, G. G. and West, M. M. (2004). Characterization of organic-rich colloids from surface and ground waters at the actinide-contaminated Rocky Flats Environmental Technology Site (RFETS), Colorado, USA, *Colloids Surf. A*, **244**, 105–111.
285. Ferris, F. G., Fyfe, W. S. and Beveridge, T. J. (1987). Bacteria as nucleation sites for authigenic minerals in a metal-contaminated lake sediment, *Chem. Geol.*, **63**, 225–232.
286. Fortin, D. and Beveridge, T. J. (2000). Mechanistic routes to biomineral surface development. In *Biomineralization*, Baeuerlein, E., ed., Wiley-VCH, Weinheim, 7–24.
287. Mavrocordatos, D. and Fortin, D. (2002). Quantitative characterization of biotic iron oxides by analytical electron microscopy, *Am. Mineral*, **87**, 940–946.
288. Heissenberger, A., Leppard, G. G. and Herndl, G. J. (1996). Ultrastructure of marine snow. II. Microbiological considerations. *Mar. Ecol. Prog. Ser.*, **135**, 299–308.
289. Kerner, M., Hohenberg, H., Ertl, S., Reckermann, M. and Spitzy, A. (2003). Self-organization of dissolved organic matter to micelle-like microparticles in river water, *Nature*, **422**, 150–154.
290. Liss, S. N., Liao, B. Q., Droppo, I. G., Allen, D. G. and Leppard, G. G. (2002). Effect of solids retention time on floc structure, *Water Sci. Technol.*, **46**, 431–438.
291. Verdugo, P., Alldredge, A. L., Azam, F., Kirchman, D. L., Passow, U. and Santschi, P. H. (2004). The oceanic gel phase: a bridge in the DOM–POM continuum, *Mar. Chem.*, **92**, 67–85.
292. Mavrocordatos, D., Pronk, W. and Boller, M. (2004). Analysis of environmental particles by atomic force microscopy, scanning and transmission electron microscopy, *Water Sci. Technol.*, **50**, 9–18.

293. Hitchcock, A. P., Morin, C., Tyliszczak, T., Koprinarov, I. N., Ikeura-Sekiguchi, H., Lawrence, J. R. and Leppard, G. G. (2002). Soft X-ray microscopy of soft matter–hard information from two softs, *Surf. Rev. Lett.*, **9**, 193–201.
294. Jacobsen, C., Wirick, S., Flynn, G. and Zimba, C. (2000). Soft X-ray spectroscopy from image sequences with sub-100 nm spatial resolution, *J. Microsc.*, **197**, 173–184.
295. Lerotic, M., Jacobsen, C., Schafer, T. and Vogt, S. (2004). Cluster analysis of soft X-ray spectromicroscopy data, *Ultramicroscopy*, **100**, 35–57.
296. Lerotic, M., Jacobsen, C., Gillow, J. B., Francis, A. J., Wirick, S., Vogt, S. and Maser, J. (2005). Cluster analysis in soft X-ray spectromicroscopy: finding the patterns in complex specimens, *J. Electron Spectrosc. Relat Phenom.*, **144–147**, 1137–1143.
297. Obst, M., Dittrich, M., Mavrocordatos, D. and Wehrli, B. (2002). Calcite formation by picoplankton, *Geochim. Cosmochim. Acta*, **66**, A566.
298. Obst, M., Dittrich, M., Mavrocordatos, D. and Gasser, P. (2003). Cyanobacterial calcite precipitation: laboratory study on different spatial scales, *EOS Trans. AGU, Fall Meeting 2003 Suppl.*, San Francisco, **84**, B12C-0799.
299. Obst, M., Gasser, P., Mavrocordatos, D. and Dittrich, M. (2005). TEM-specimen preparation of cell/mineral interfaces by focused ion beam milling, *Am. Mineral.*, **90**, 1270–1277.
300. Dittrich, M., Kurz, P. and Wehrli, B. (2004). The role of autotrophic picocyanobacteria in calcite precipitation in an oligotrophic lake, *Geomicrobiol. J.*, **21**, 45–53.
301. Mavrocordatos, D. and Wilkinson, K. J. (2003). Personal communication.
302. Mavrocordatos, D., Steiner, M. and Boller, M. (2003). Analytical electron microscopy and focused ion beam: complementary tool for the imaging of copper sorption onto iron oxide aggregates, *J. Microsc.*, **210**, 45–52.
303. Mavrocordatos, D., Leupin, O., Perret, D. and Gloter, A. (2003). Intimate interaction of Cu and hydrous ferric oxides determined by analytical electron microscopy, *Abstr. Pap. 225th ACS Nat. Meeting*, New Orleans, 23–27 March 2003, GEOC-198.
304. de Vries, J. and Waser, R. (1991). Grain boundary and lattice diffusion of Mn in $ATiO_3$ (A = Ba, Sr). In *7th IEEE Int. Symp. Appl. Ferroelectr.*, pp. 557–561.
305. Paterson, J. H. and Krivanek, O. L. (1990). ELNES of 3d transition-metal oxides. II. Variations with oxidation state and crystal structure, *Ultramicroscopy*, **32**, 319–325.
306. Ravikumar, V., Rodrigues, R. P. and Dravid, V. P. (1996). An investigation of acceptor-doped grain boundaries in $SrTiO_3$, *J. Phys. D*, **29**, 1799–1806.
307. Sparrow, T. G., Williams, B. G., Rao, C. N. R. and Thomas, J. M. (1984). L_3/L_2 white-line intensity ratios in the electron energy-loss spectra of 3d transition metal oxides, *Chem. Phys. Lett.*, **108**, 547–550.
308. Vollmann, M. and Waser, R. (1997). Grain boundary defect chemistry of acceptor-doped titanates: high field effects, *J. Electroceram.*, **1**, 51–64.
309. Daniels, J., Von Festenberg, C., Raether, H., and Zeppenfeld, K. (1970). Optical constants of solids by electron spectroscopy. *Springer Tracts in Modern Physics*, **54**, 77–135.